Doctoral Dissertation (Shinshu University)

Study on functional polymer microspheres for selective separation and release of halogen compounds

(高分子微粒子によるハロゲン化合物の選択的分離と放出に関する研究)

March 2018

Takuma Kureha

Graduate School of Textile Science & Technology

Table of Contents

1. Introductory remarks

1.1. Background

Separation processes play an important role in the chemical and pharmaceutical industries, where they account for 40−70% of the capital and the operating costs.[1] In particular, they are very important in the context of wastewater treatment, diagnostics, chemical and biological analyses, and food processing. In these areas, suitable separation materials have to fulfill several requirements, which include e.g. low cost, high efficiency, selectivity, and reusability.[2-6] One of the most used separation materials are "polymeric materials", such as membranes,[7,8] resins,[9,10] and gels,[11,12] because they can be synthesized on a large scale and easily modified by chemical reactions to meet the stipulated criteria for specific industrial applications, resulting in great advantages for the chemical industry. For example, starting in the late 1960s, membrane processes have been gradually introduced to industrial applications in order to provide feasible alternatives for, and to complement more traditional purification and separation processes such as distillation, evaporation, adsorptions, extraction, and chromatography.[13-17] This has been mostly motivated by the benefits that membrane technology offers relative to conventional techniques, specifically in terms of costs, environmental impact, and safety.

Apart from such bulk materials, "polymer microspheres" have also attracted much attention in material science.[18-24] Generally, polymer microspheres are dispersed in media such as water, and can move microscopically via Brownian motion. Their typical size is below ~ 10 μm, and they exhibit a large specific surface area, fast response, the potential to be used in mass production, high diffusibility, as well as ease of recovery and handling. In the context of this thesis, hydrogel microspheres (microgels) refer to polymer microspheres dispersed in aqueous solution that are composed of hydrophilic polymers. In contrast to microspheres composed of hydrophobic polymers (solid microspheres), these microgels exhibit a three-dimensional cross-linked structure that swells in water[25-35] and permits the controlled uptake/release of functional molecules. Indeed, target molecules can enter the inside of the microgels via diffusion, and exit the microgels upon applying an external stimulus,[36-40] whereby the response of the microgels is extremely rapid compared to that of bulk gels. Such swollen gels afford the microgels with high dispersion stability on account of the steric stabilization. Owing to the unique properties of these microspheres, they have been used as templates,[41-44] sensors,[45-50] catalysts,[51-55] and coatings[56-60], and they represent promising prospects for advanced chemical technologies such as drug carriers.[61-69] In particular, polymer microspheres could potentially be used as nanocarriers for chemical/biological separations.

One can envisage that polymer microspheres could be useful for drug/gene-delivery systems, i.e., for the adsorption, transportation, and release of drugs via the polymer microspheres. Indeed, the number of reported papers on polymer microspheres in drug-delivery systems accounts for most of the reports on molecular separation carriers (**Figure 1.1**).

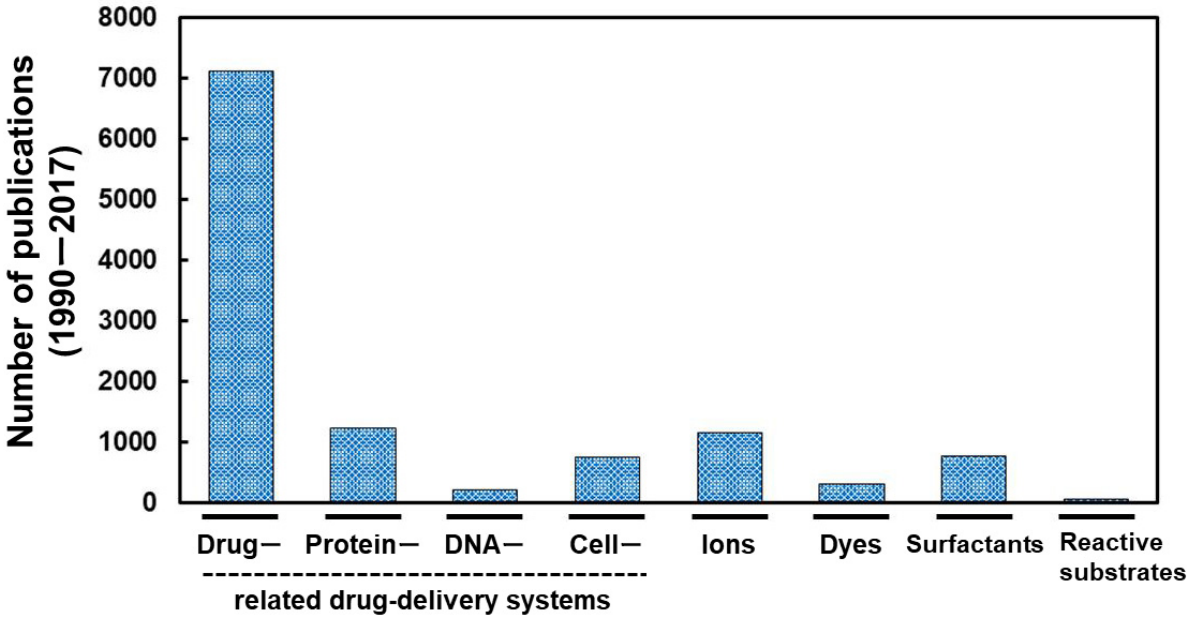

Figure 1.1 Number of publications on target molecules for polymer microspheres using the following search terms. **Drug**: polymer particles AND drug; **protein**: polymer particles AND protein; **DNA**: polymer particles AND DNA; **cell**: polymer particles AND cell; **ions**: Polymer particles AND ions; **dyes**: polymer particles AND dyes; **surfactant**: polymer particles AND surfactant; **reactive substrate**: polymer particles AND reactive substrate. These values were obtained from Web of Science (Clarivate Analytics Co., Ltd.).

In the 1960s, Speiser focused on developing nanoparticulate systems for vaccination processes.[70] Since then, marketed products based on nanotechnology have become available, while others are at the clinical trial stage. Nowadays, researchers focus on microspheres with a view to maintain chemical reactivity and to target specific compounds. The design of smart microspheres is subject to several requirements:[71] i) the targeted delivery of an active compound that may include the penetration of membranes and endocytosis in order to reach the target site; ii) the ability of the carrier to escape from biological protective mechanisms such as opsonization and the reticuloendothelial system clearance; iii) communication and recognition of environmental changes. Therefore, the modification and functionalization of the surface of microspheres with moieties that are responsive to a range of different

stimuli is beneficial. These stimuli can be endogenous (e.g., redox, enzyme, or pH value changes) or exogenous factors (e.g., light, ultra sound, or magnetic fields), as well as either endogenous or exogenous factors (temperature).[72-75]

In addition to drug and biomolecule carriers, polymer microspheres have been used as the absorbents to remove impurities from wastewater. Different organic, inorganic and biological impurities are added to water from anthropogenic and natural sources.[76] The presence of especially heavy metals in water inflicts serious harm to biological life. Moreover, organic impurities may include toxic dyes, antibiotics, herbicides, and aromatic compounds. Some of these pollutants can accumulate in the environment and become part of living organisms through the food chain.[77] Heavy metals may react with organic compounds and thus damage living organisms.[78,79] When microspheres are used to remove heavy metals from wastewater, coagulation and flocculation followed by sedimentation and filtration is usually employed. Coagulation is the destabilization of colloids by neutralizing the forces that keep them apart. Many coagulants that are widely used in conventional wastewater treatment processes, such as aluminum, effectively remove wastewater particulates and impurities by charge neutralization of polymer microspheres and by enmeshment of the impurities on the formed amorphous metal-hydroxide precipitates.[80]

Coagulation and flocculation of the microspheres are, however, undesirable in living bodies (e.g., in drug delivery systems) as the aggregation of these carriers in small spaces such as a blood vessels may cause thrombosis. Moreover, the aggregated microspheres suffer from poor reusability due to the decrease in their specific surface area and the increased number of process steps for re-dispersion.[81] Therefore, many researchers use swollen microgels to remove these impurities[82-86] because they exhibit high colloidal dispersion stability due to the sterically stabilized hydrogel networks as well as high stimuli-responsiveness for the controlled uptake/release of target molecules.

For example, Morris and Vincent *et al.* have reported the removal of Pb^{2+} from aqueous solutions using anionically charged poly(*N*-isopropyl acrylamide-*co*-acrylic acid) microgels, henceforth denoted as p(NIPAm-*co*-AAc) microgels. The deprotonated acrylic acid moieties in the microgels thereby strongly interact with the Pb^{2+} cations via attractive electrostatic forces.[87,88] It was demonstrated that in the swollen state at low temperature, where the pNIPAm chains adopt a coil structure in water, flocculation of the microgels does not occur due to the adsorption of Pb^{2+}. Conversely, above the lower critical solution temperature (LCST) of pNIPAm, where the pNIPAm chains undergo a coil-to-globule transition, the microgels aggregate. Thus, such temperature-induced flocculation could be used in a water clean-up system as a recovery mechanism for microgels

containing Pb^{2+}. For the removal of organic impurities, Parasuraman *et al.* have demonstrated the removal capacity of p(NIPAm-*co*-AAc) microgels for the organic dye Orange Ⅱ.[89,90] It was observed that the dye uptake capacity increases with increasing AAc content in the microgels, and the thermo- and pH-responsive behavior of the microgels allows controlling the uptake efficiency.

The adsorption/desorption mechanisms of surfactants on the polymer microspheres have been investigated from a viewpoint that is different from removal, because surfactants, including sodium dodecyl sulfate (SDS), 4-hexylphenylazosulfonate, reactive sodium dodecyl allyl sulfosuccinate, are sometimes used to control the size and size distribution of the microspheres when they are synthesized by polymerizations, such as emulsion polymerization and precipitation polymerization.[91-100] Pelton has reported thermo-responsive pNIPAm microgels for the first time in 1986[101] and investigated the effect of SDS adsorption on the structural changes in the pNIPAm microgels by dynamic light scattering (DLS), small-angle neutron scattering, and binding isotherm measurements.[102] It was proposed that SDS binds to the hydrophobic isopropyl groups on the pNIPAm microgels in units that contain a small number of SDS monomers. Furthermore, the uptake/release of functional surfactants as medical reagents has also been achieved. For example, Nerapusri *et al.* have demonstrated that the uptake/release of cetylpyridinium chloride, which is strongly bactericidal and antifungal, can be controlled by using thermo- and pH-responsive microgels.[103] This result may lead to applications such as the release of bactericides into food processing lines, or even to the release of bactericides from teeth and gum surfaces in the mouth.

Additionally, the molecular uptake/release behavior of microgels is an important phenomenon, especially for novel functional microgels, such as oscillating microgels[104-107] or organic/inorganic hybrid microgels that are used for catalysis,[108-110] as the diffusion and adsorption of reactive substrates into the microgels directly determines the oscillation properties and reaction rate. Recently, it has been accepted that water-immiscible monomers such as styrene and glycidyl methacrylate can diffuse into swollen microgels, resulting in the formation of solid polymer composite microgels by seeded emulsion polymerization (SEM).[111-114] In order to understand and improve the separation functions of microgels, the characterization of microgel networks at the molecular level is necessary as the target molecules interact and diffuse through these networks. In the context of this thesis, the relationship between the microscopic network structure was investigated, which was characterized by small-angle X-ray scattering, and the uptake behavior with respect to organic dyes.[35,115,116] For that purpose, pNIPAm-based microgels were selected as model microgels given their thermo-responsive behavior and considering that they can be obtained in uniform size. These results indicate that hydrophobic

interactions between the hydrophobic domains of the constituent isopropyl groups and rhodamine 6G or erythrosine, which are cationic and anionic organic dyes, respectively, affect the uptake behavior (**Figure 1.2**).

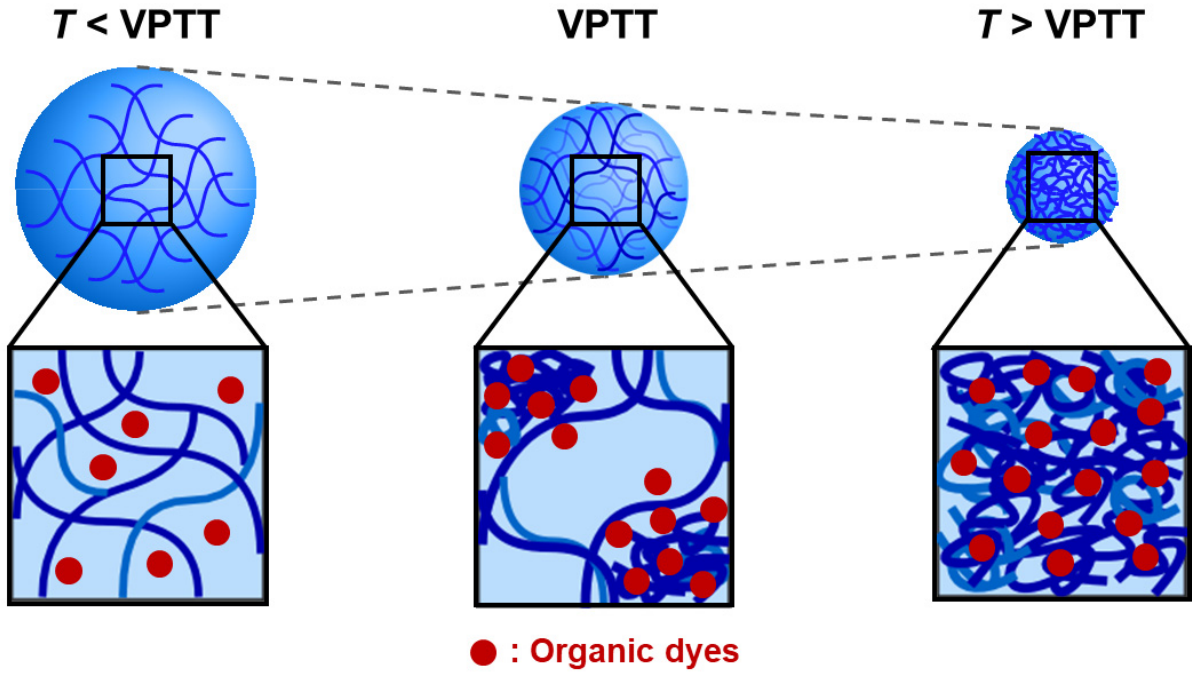

Figure 1.2 Illustration of the uptake behavior of thermo-responsive pNIPAm microgels with respect to organic dyes. Below the volume phase transition temperature (VPTT) of the pNIPAm microgels, the organic dyes are incorporated by the microgels, while above the VPTT, the dyes strongly interact with the deswollen pNIPAm microgels via hydrophobic interactions, which results in an increased uptake of dye quantities. Reprinted in part with permission from Kureha, T.; Sato, T.; Suzuki, D. Relationship between Temperature-Induced Changes in Internal Microscopic Structures of Poly(*N*-isopropylacrylamide) Microgels and Organic Dye Uptake Behavior. *Langmuir* **2014**, *30*, 8717−8725; copyright 2014, American Chemical Society.

In addition to the internal structure of the microgels, the stimuli-responsiveness of the microgels is also important to improve the separation functions, especially with respect to a controlled release of the guest molecules. However, it was discovered that in conventional thermo- and pH-responsive microgels such as p(NIPAm-*co*-AAc), the individual modes of response usually interfere with each other, which represents an intrinsic unsolved problem for such multi-responsive materials. Furthermore, in the presence of oppositely charged molecules, uncontrollable deswelling can occur due to adsorption.[116] In contrast to the hitherto reported microgels, we developed in the context of this

thesis mechanically cross-linked microgels, in which thermo-responsive polymers were cross-linked by rotaxane networks.[117] The aggregation/disaggregation between cyclodextrins in the rotaxane network, which can be controlled by the pH value, endows the microgels with a repeatable swelling/deswelling behavior. This mode of response does not interfere with the thermo-responsive behavior of the polymer backbone, both in the presence and absence of oppositely charged molecules. Therefore, these conceptually new microspheres may lead to the development of new design guidelines with applications that require a retention of their response even in environments that may contain foreign ions, for example, in *in vivo* experiments.

Against this background, it is feasible to assume that the polymer microspheres could be very useful as molecular separation carriers, and the development of the required separation functions is currently in progress. Except for the aforementioned target molecules, such as metal ions, proteins, and DNA, the selective separation of "halogen compounds" has, to the best of our knowledge, not yet been achieved although many halide compounds act as drugs and require delivery, or need to be removed from wastewater.[118-120]

Some anionic chlorine- and bromine-containing pollutants in industrial wastewater or natural water sources are of particular concern for safe drinking water due to their toxic, mutagenic, carcinogenic, or radioactive properties.[118,119,121] For example, bromate has been proven to be both toxic and mutagenic in both *in vitro* and *in vivo* studies, as well as carcinogenic in animal studies. Conversely, iodine is an essential element for the healthy development of the thyroid gland, and iodine compounds such as liothyronine sodium are accordingly required in a certain concentration in the blood. The average intake of iodine required for optimal health is 80-150 mg/day, but a significant number of people around the word currently suffer from iodine deficiency.[119] Thus far, the removal of anions of the halogen elements from aqueous solutions has been achieved predominantly using metallic materials, such as layered double hydroxides (LDHs).[120-122] However, the release of adsorbed halide anions from these LDHs is necessary in order to carry out their reduction,[121] which is usually accompanied by a release of chloride as a byproduct into solution, resulting in an increased number of reaction steps and hence removal costs.

A strategy that would allow a fast uptake and controlled release of halogen-containing compounds at low cost independent of time and place should be highly attractive for applications that include water treatment and medical technologies. With this objective in mind, we focused on the use of polymer microspheres, as they exhibit the aforementioned properties. The driving force for the adsorption of halogen compounds in the context of this thesis is halogen bonding, which occurs via

noncovalent interactions and results in anomalously short intermolecular distances, under concomitant formation of strong atomic interactions and high selectivity.

Halogen bonding is a noncovalent form of interaction that is in some ways analogous to hydrogen bonding. It has been known since the 19th century that Cl_2, Br_2, and I_2 can form complexes with Lewis bases such as ammonia and methylamines.[123,124] Such interactions have previously been described as "charge–transfer" or "electron donor–acceptor" interactions. Mulliken[125] and later Flurry[126,127] have developed theoretical formalisms to describe such interactions. Eventually, it was recognized that not only dihalogens and interhalogens, but also many organic halogen-containing compounds can form such complexes. An important advance in understanding the noncovalent interactions of halogen atoms came from the analysis of large numbers of crystal structures from the Cambridge Structural Database[128-130] by Murray-Rust *et al.*, who were looking for anomalously short intermolecular distances, i.e. less than the sum of the van der Waals radii, of the atoms involved. Such distances were used as an indicator for unusually strong atomic interactions. For halogens linked to carbons, certain characteristic trends were observed. Close contacts with electrophiles, such as metal ions, occurred largely at angles of 90°–120° with the carbon-halogen bond. However, with nucleophiles such as oxygen and nitrogen atoms, the preferred angles were between 160° and 180°. These generalizations apply to Cl, Br and I. The near-linear interactions with nucleophiles have since been labelled "halogen bonding".[131-134]

The working hypothesis of this thesis was thus based on the notion that polymer microspheres with electronegative methoxy groups should be suitable for the bonding of halogen-containing compounds, given that the electron-donating groups such as methoxy and amino groups, should play an important role for the halogen-bonding acceptor. Thus, hydrophobic poly(2-methoxyethyl acrylate) (pMEA) and analogue polymers were selected as the microsphere backbone. Moreover, the adsorption behavior toward halogen compounds was compared to several control microspheres (**Figure 1.3**).

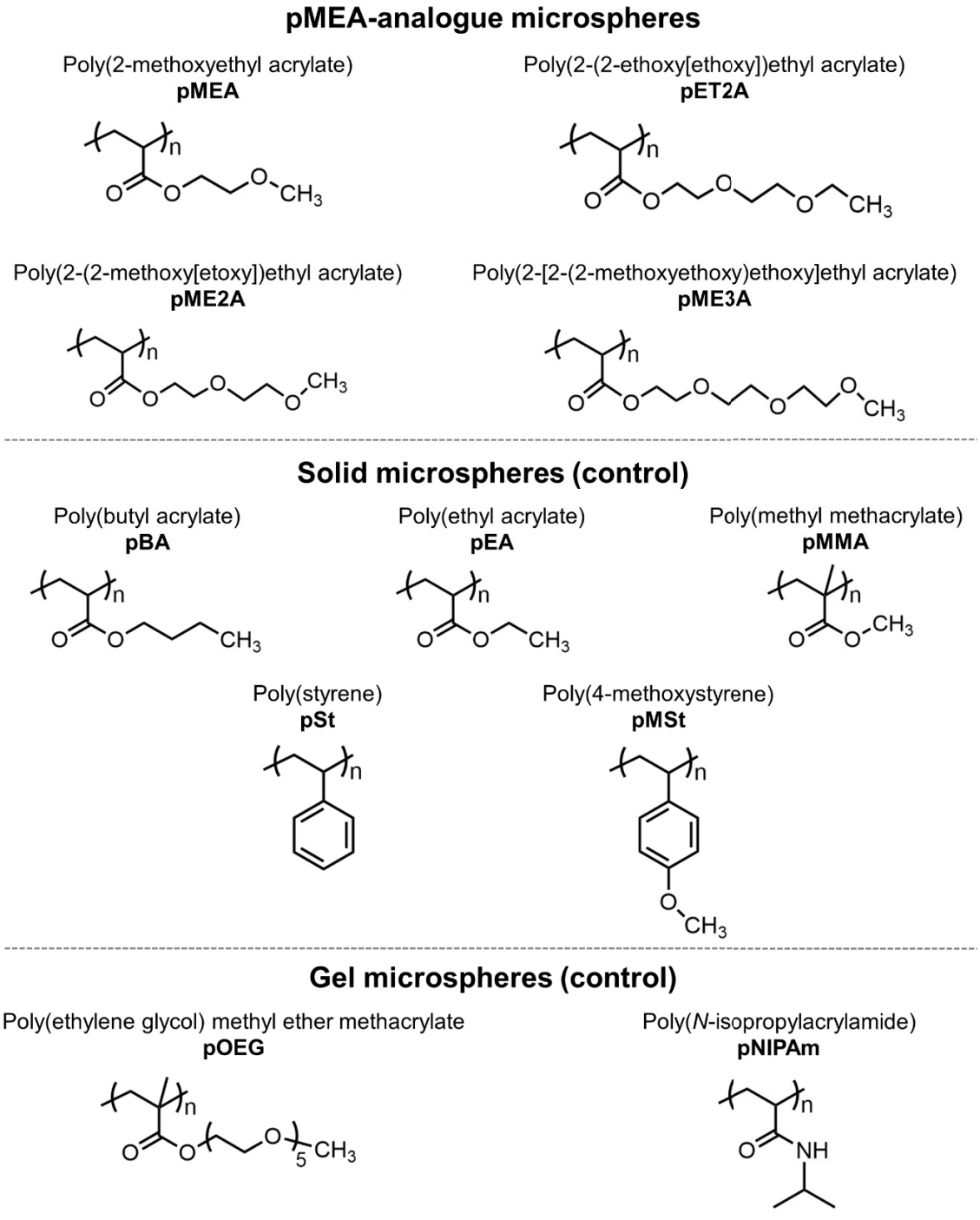

Figure 1.3. Chemical structures of the microspheres examined in this thesis.

In this thesis, the separation of halogen compounds by polymer microspheres was attempted (**Figure 1.4**) as outlined below.

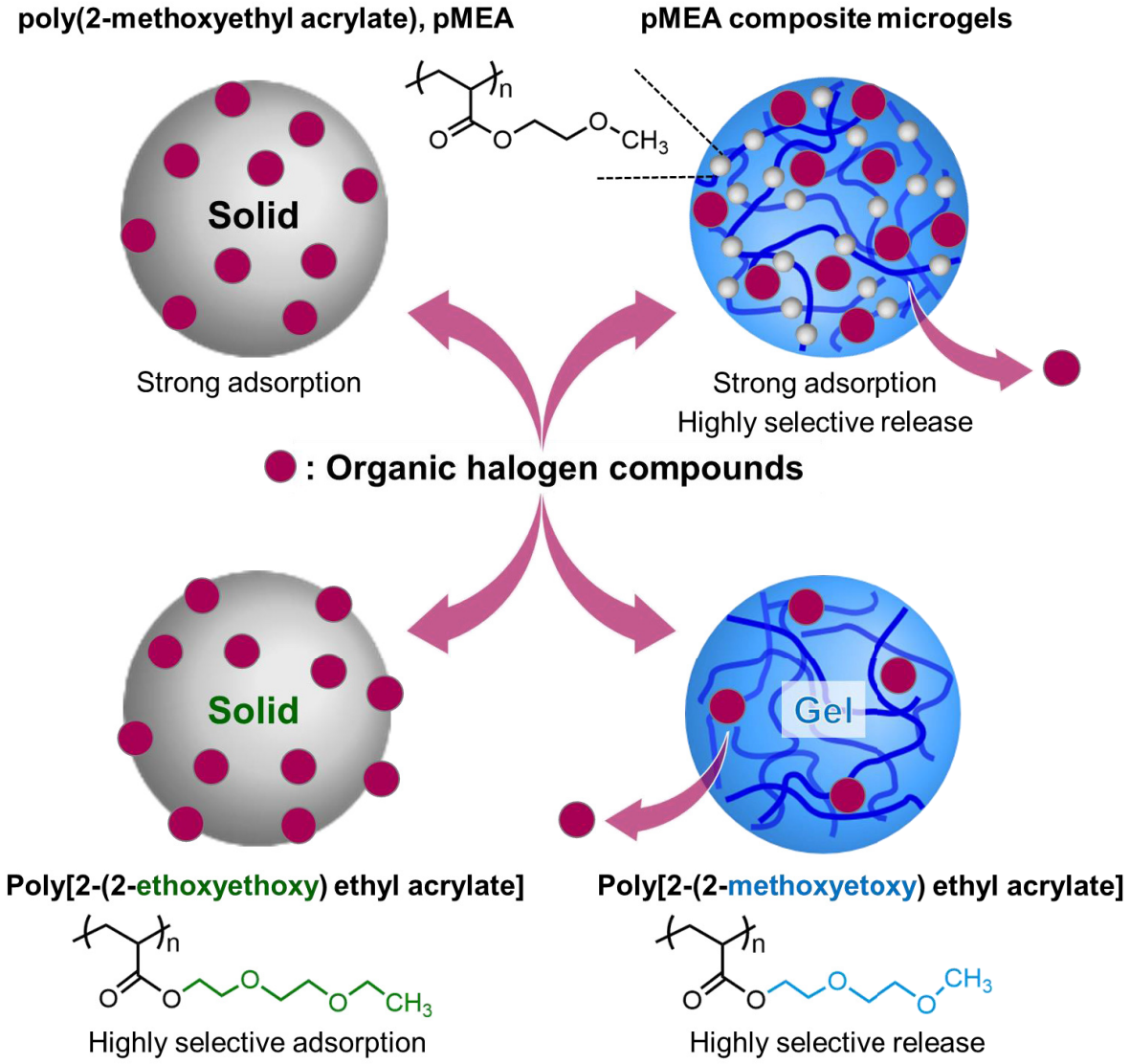

Figure 1.4. Summary of halogen-separating polymer microspheres in this thesis. Reproduced in part with permission from i) Kureha, T.; Suzuki, D. Nanocomposite Microgels for the Selective Separation of Halogen Compounds from Aqueous Solution. *Langmuir* **2017**, *in press*, DOI: 10.1021/acs.langmuir.7b01485; copyright 2017, American Chemical Society; and ii) Kureha, T.; Nishizawa, Y.; Suzuki, D. Controlled Separation and Release of Organoiodine Compounds using Poly(2-methoxyethyl acrylate)-analogue Microspheres. *ACS Omega* **2017**, *2*, 7686−7694; copyright 2017, American Chemical Society.

1.2. Outline

This thesis covers three research topics. In **Chapter I**, the synthesis and characterization of pMEA microspheres is presented as a basis to understand the adsorption behavior of halogen compounds. The pMEA microspheres can be synthesized via conventional radical polymerizations and exhibit properties suitable for biological applications and coatings. In **Chapter II**, the adsorption behavior of pMEA microspheres is discussed. The addition of a stimuli-responsive gel matrix is a key factor for the release of halogen compounds. **Chapter III** reports the effect of halogen-bonding strength on the adsorption capacity of the microspheres, and the development of pMEA-analogue microspheres that contain side-chains with the ability to engage in halogen bonding with iodine-containing compounds is discussed.

1.3. References

1. Adler, S.; Beaver, E.; Bryan, P.; Robinson, S.; Watson, J. *Vision 2020:2000 Separations Roadmap*; Center for Waste Reduction Technologies of the AIChE and Dept. of Energy of the United States of America, **2000**.
2. El-Ali, J.; Sorger, P. K.; Jensen, K. F. Cells on chips. *Nature* **2006**, *442*, 403-411.
3. Fent, K.; Weston, A. A.; Caminada, D. Ecotoxicology of human pharmaceuticals. *Aquatic Toxicology* **2006**, *76*, 122-159.
4. Hirneisen, K. A.; Black, E. P.; Cascarino, J. L.; Fino, V. R.; Hoover, D. G.; Kniel, K. E. Viral Inactivation in Foods: A Review of Traditional and Novel Food-Processing Technologies. *Comp. Rev. Food Sci. Saf.* **2010**, *9*, 3-20.
5. Karimi, K.; Taherzadeh, M. J. A critical review on analysis in pretreatment of lignocelluloses: Degree of polymerization, adsorption/desorption, and accessibility. *Bioresource Tech*. **2016**, *203*, 348-356.
6. Kandukuri, S. T.; Klausen, A.; Karimi, H. R.; Robbersmyr, K. G. A review of diagnostics and prognostics of low-speed machinery towards wind turbine farm-level health management. *Renewable Sustainable Energy Rev.* **2016**, *53*, 697-708.
7. Ulbricht, M. Advanced functional polymer membranes. *Polymer* **2006**, *47*, 2217-2262.
8. Dickhout, J. M.; Moreno, J.; Biesheuvel, P. M.; Boels, L.; Lammertink, R. G. H.; de Vos, W. M. Produced water treatment by membranes: A review from a colloidal perspective. *J. Colloid Inter. Sci.* **2017**, *487*, 523-534.
9. Nadkarni, R. A.; Morrison, G. H. Determination of molybdenum by neutron activation and Srafion NMRR ion exchange resin separation. *Anal. Chem*. **1978**, *50*, 294-296.
10. Jandera, P. Stationary and mobile phases in hydrophilic interaction chromatography: a review. *Anal. Chem. Acta* **2011**, *692*, 1-25.
11. Stayton, P. S.; Shimoboji, T.; Long, C.; Chilkoti, A.; Ghen, G.; Harris, J. M.; Hoffman, A. S. Control of protein–ligand recognition using a stimuli-responsive polymer. *Nature* **1995**, *378*, 472-474.
12. Tokarev, I.; Minko, S. Stimuli-Responsive Porous Hydrogels at Interfaces for Molecular Filtration,

Separation, Controlled Release, and Gating in Capsules and Membranes. *Adv. Mater*. **2010**, *22*, 3446–3462.
13. Bastani, D.; Esmaeili, N.; Asadollahi, M. Polymeric mixed matrix membranes containing zeolites as a filler for gas separation applications: A review. *J. Ind. Eng. Chem*. **2013**, *19*, 375-393.
14. Sanders, D. F.; Smith, Z. P.; Guo, R.; Robeson, L. M.; McGrath, J. E.; Paul, D. R.; Freeman, B. D. Energy-efficient polymeric gas separation membranes for a sustainable future: A review. *Polymer* **2013**, *54*, 4729-4761.
15. Wang, P.; Chung, T. S. Recent advances in membrane distillation processes: Membrane development, configuration design and application exploring. *J. Memb. Sci*. **2015**, *474*, 39-56.
16. Padaki, M.; Murali, R. S.; Abdullaha, M. S.; Misdan, N.; Moslehyani, A.; Kassim, M. A.; Hilal, N.; Ismail, A. F. Membrane technology enhancement in oil–water separation. A review. *Desalination* **2015**, *357*, 197-207.
17. Chu, Z.; Feng, Y.; Seeger, S. Oil/Water Separation with Selective Superantiwetting/Superwetting Surface Materials. *Angew. Chem. Int. Ed.* **2015**, *54*, 2328-2338.
18. Arshady, R. Suspension, emulsion, and dispersion polymerization: A methodological survey. *Colloid. Polym. Sci*. **1992**, *270*, 717-732.
19. Kawaguchi, H. Functional polymer microspheres. *Prog. Polym. Sci.* **2000**, *25*, 1171-1210.
20. Davis, M. E.; Chen, Z.; Shin, D. M. Nanoparticle therapeutics: an emerging treatment modality for cancer. *Nature Rev. Drug Discov.* **2000**, *7*, 771-782.
21. Torchilin, V. P. Micellar Nanocarriers: Pharmaceutical Perspectives. *Pharmaceutical Research* **2007**, *24*, 1-16.
22. Zetterlund, P. B.; Kagawa, Y.; Okubo, M. Controlled/Living Radical Polymerization in Dispersed Systems. *Chem. Rev*. **2008**, *108*, 3747-3794.
23. Grzelczak, M.; Vermant, J.; Furst, E. M.; Liz-Marzan, L. M. Directed Self-Assembly of Nanoparticles. *ACS Nano* **2010**, *4*, 3591-3605.
24. Shibuya, K.; Nagao, D.; Ishii, H.; Konno, M. Advanced soap-free emulsion polymerization for highly pure, micron-sized, monodisperse polymer particles. *Polymer* **2014**, *55*, 535-539.
25. Saunders, B. R.; Vincent, B. Microgel particles as model colloids: theory, properties and applications. *Adv. Colloid Inter. Sci.* **1999**, *80*, 1-25.
26. Pelton, R. Temperature-sensitive aqueous microgels. *Adv. Colloid Interface Sci*. **2000**, *85*, 1-33.
27. Nayak, S.; Lyon, L. A. Soft Nanotechnology with Soft Nanoparticles. *Angew. Chem. Int. Ed*. **2005**, *44*, 7686-7708.
28. Hoare, T.; Pelton, R. Characterizing charge and crosslinker distributions in polyelectrolyte microgels. *Curr. Opin. Colloid Interface Sci*. **2008**, *13*, 413-428.
29. Pich, A.; Richtering, W. Microgels by Precipitation Polymerization: Synthesis, Characterization, and Functionalization. *Adv. Polym. Sci*. **2010**, *234*, 1-37.
30. Lu, Y.; Ballauff, M. Thermosensitive core–shell microgels: From colloidal model systems to nanoreactors. *Prog. Polym. Sci*. **2011**, *36*, 767-792.
31. Hellweg, T. Responsive core–shell microgels: Synthesis, characterization, and possible applications. *J. Polym. Sci. B Polym. Phys.* **2013**, *51*, 1073-1083.
32. Musyanovych, A.; Landfester, K. Polymer Micro- and Nanocapsules as Biological Carriers with Multifunctional Properties. *Macromol. Biosci.* **2014**, *14*, 458-477.

33. Habicht, A.; Schmolke, W.; Goerigk, G.; Lange, F.; Saalwachter, K.; Ballauff, M.; Seiffert, S. Critical Fluctuations and Static Inhomogeneities in Polymer Gel Volume Phase Transitions. *J. Polym. Sci., Part B: Polym. Phys*. **2015**, *53*, 1112-1122.
34. Xing, X.; Hua, L.; Ngai, T. Depletion versus stabilization induced by polymers and nanoparticles: The state of the art. *Curr. Opin. Colloid Interface Sci.* **2015**, *20*, 54-59.
35. Suzuki, D.; Horigome, K.; Kureha, T.; Matsui, S.; Watanabe, T. Polymeric hydrogel microspheres: design, synthesis, characterization, assembly and applications. *Polym. J.* **2017**, *49*, 695-702.
36. Kiser, P. F.; Wilson, G.; Needham, D. Lipid-coated microgels for the triggered release of doxorubicin. *J. Cont. Rel.* **2000**, *68*, 9-22.
37. Nomura, Y.; Sasaki, Y.; Takagi, M.; Narita, T.; Aoyama, Y.; Akiyoshi, K. Thermoresponsive Controlled Association of Protein with a Dynamic Nanogel of Hydrophobized Polysaccharide and Cyclodextrin: Heat Shock Protein-Like Activity of Artificial Molecular Chaperone. *Biomacromolecules* **2005**, *6*, 447-452.
38. Kawamura, A.; Hata, Y.; Miyata, T.; Uragami, T. Synthesis of glucose-responsive bioconjugated gel particles using surfactant-free emulsion polymerization. *Colloid. Surf. B* **2012**, *99*, 74-81.
39. Schroeder, R.; Rudov, A. A.; Lyon, L. A.; Richtering, W.; Pich, A.; Potemkin, I. I. Electrostatic Interactions and Osmotic Pressure of Counterions Control the pH-Dependent Swelling and Collapse of Polyampholyte Microgels with Random Distribution of Ionizable Groups. *Macromolecules* **2015**, *48*, 5914-5927.
40. Walta, S.; Pergushov, D. V.; Oppermann, A.; Steinschulte, A. A.; Geisel, K.; Sigolaeva, L. V.; Plamper, F. A.; Wöll, D.; Richtering, W. Microgels enable capacious uptake and controlled release of architecturally complex macromolecular species. *Polymer* **2017**, *119*, 50-58.
41. Pérez-Moral, N.; Mayes, A. G. Comparative study of imprinted polymer particles prepared by different polymerisation methods. *Anal. Chem. Acta* **2004**, *504*, 15-21.
42. Nie, Z.; Xu, S.; Seo, M.; Lewis, P. C.; Kumacheva, E. Polymer Particles with Various Shapes and Morphologies Produced in Continuous Microfluidic Reactors. *J. Am. Chem. Soc*. **2005**, *127*, 8058-8063.
43. Parakhonskiy, B. V.; Yashchenok, A. M.; Konrad, M.; Skirtach, A. G. Colloidal micro- and nano-particles as templates for polyelectrolyte multilayer capsules. *Adv. Colloid. Int. Sci*. **2014**, *207*, 253-264.
44. Björnmalm, M.; Cui, J.; Bertleff-Zieschang, N.; Song, D.; Faria, M.; Rahim, M. A.; Caruso, F. Nanoengineering Particles through Template Assembly. *Chem. Mater*. **2017**, *29*, 289−306.
45. Holtz, J. H.; Asher, S. A. Polymerized colloidal crystal hydrogel films as intelligent chemical sensing materials. *Nature* **1997**, *389*, 829-832.
46. Haupt, K.; Mosbach, K. Molecularly Imprinted Polymers and Their Use in Biomimetic Sensors. *Chem. Rev.* **2000**, *100*, 2495-2504.
47. Shipway, A. N.; Katz, E.; Willner, I. Nanoparticle Arrays on Surfaces for Electronic, Optical, and Sensor Applications. *Chem. Phys. Chem*. **2000**, *1*, 18-52.
48. Wu, C.; Bull, B.; Christensen, K.; McNeill, J. Ratiometric Single-Nanoparticle Oxygen Sensors for Biological Imaging. *Angew. Chem. Int. Ed*. **2009**, *48*, 2741–2745.
49. Wackerlig, J.; Lieberzeit, P. A. Molecularly imprinted polymer nanoparticles in chemical sensing

–Synthesis, characterisation and application. *Sens. Actuators, B* **2015**, *207*, 144-157.
50. Kamra, T.; Chaudhary, S.; Xu, C.; Montelius, L.; Schnadt, J.; Ye, L. Covalent immobilization of molecularly imprinted polymer nanoparticles on a gold surface using carbodiimide coupling for chemical sensing. *J. Colloid. Int. Sci*. **2016**, *461*, 1-8.
51. Jia, H.; Zhu, G.; Wang, P. Catalytic Behaviors of Enzymes Attached to Nanoparticles: The Effect of Particle Mobility. *Biotech. Bioeng*. **2003**, *84*, 406-414.
52. Demir, M. M.; Gulgun, M. A.; Menceloglu, Y. Z.; Erman, B.; Abramchuk, S. S.; Makhaeva, E. E.; Khokhlov, A. R.; Matveeva, V. G.; Sulman, M. G. Palladium Nanoparticles by Electrospinning from Poly(acrylonitrile-*co*-acrylic acid)-$PdCl_2$ Solutions. Relations between Preparation Conditions, Particle Size, and Catalytic Activity. *Macromolecules* **2004**, *37*, 1787-1792.
53. Lu, Y.; Mei, Y.; Drechsler, M.; Ballauff, M. Thermosensitive Core–Shell Particles as Carriers for Ag Nanoparticles: Modulating the Catalytic Activity by a Phase Transition in Networks. *Angew. Chem. Int. Ed*. **2006**, *45*, 813-816.
54. Mei, Y.; Lu, Y.; Polzer, F.; Ballauff, M. Catalytic Activity of Palladium Nanoparticles Encapsulated in Spherical Polyelectrolyte Brushes and Core-Shell Microgels. *Chem. Mater*. **2007**, *19*, 1062-1069.
55. Cai, H.; Liu, L.; Chen, Q.; Lu, P.; Dong, J. Ni-polymer nanogel hybrid particles: A new strategy for hydrogen production from the hydrolysis of dimethylamine-borane and sodium borohydride. *Energy* **2016**, *99*, 129-135.
56. Kreuter, J.; Alyautdin, R. N.; Kharkevich, D. A.; Ivanov, A. A. Passage of peptides through the blood-brain barrier with colloidal polymer particles (nanoparticles). *Brain Res.* **1995**, *674*, 171-174.
57. Van Steenkiste, T. H.; Smith, J. R.; Teets, R. E. Aluminum coatings via kinetic spray with relatively large powder particles. *Surf. Coat. Tech*. **2002**, *154*, 237-252.
58. Xu, X.; Asher, S. A. Synthesis and Utilization of Monodisperse Hollow Polymeric Particles in Photonic Crystals. *J. Am. Chem. Soc*. **2004**, *126*, 7940-7945.
59. Win, K. Y.; Feng, S. S. Effects of particle size and surface coating on cellular uptake of polymeric nanoparticles for oral delivery of anticancer drugs. *Biomaterials* **2005**, *26*, 2713-2722.
60. Hiroshige, S.; Kureha, T.; Aoki, D.; Sawada, J.; Aoki, D.; Takata, T.; Suzuki, D. Formation of Tough Films via the Evaporation of Water from Dispersions of Elastomer Microspheres Crosslinked with Rotaxane Supramolecules. *Chem.-Eur. J*. **2017**, *23*, 8405-8408.
61. Ugelstad, J.; Berge, A.; Ellingsen, T.; Schmid, R.; Nilsen, T. N.; Mork, P. C.; Stenstad, P.; Hornes, E.; Olsvik, O. PREPARATION AND APPLICATION OF NEW MONOSIZED POLYMER PARTICLES. *Prog. Polym. Sci*. **1992**, *17*, 87-161.
62. Harada, A.; Kataoka, K. Supramolecular assemblies of block copolymers in aqueous media as nanocontainers relevant to biological applications. *Prog. Polym. Sci*. **2006**, *31*, 949-982.
63. Oh, J. K.; Drumright, R.; Siegwart, D. J.; Matyjaszewski, K. The development of microgels/nanogels for drug delivery applications. *Prog. Polym. Sci*. **2008**, *33*, 448-477.
64. Kumari, A.; Yadav, S. K.; Yadav, S. C. Biodegradable polymeric nanoparticles based drug delivery systems. *Colloid. Surf., B* **2010**, *75*, 1-18.
65. Esser-Kahn, A. P.; Odom, S. A.; Sottos, N. R.; White, S. R.; Moore, J. S. Triggered Release from Polymer Capsules. *Macromolecules* **2011**, *44*, 5539–5553.

66. Hoshino, Y.; Lee, H.; Miura, Y. Interaction between synthetic particles and biomacromolecules: fundamental study of nonspecific interaction and design of nanoparticles that recognize target molecules. *Polym. J.* **2014**, *46*, 537-545.
67. Tahara, Y.; Akiyoshi, K. Current advances in self-assembled nanogel delivery systems for immunotherapy. *Adv. Drug Del. Rev*. **2015**, *95*, 65-76.
68. Cui, J.; Richardson, J. J.; Björnmalm, M.; Faria, M.; Caruso, F. Nanoengineered Templated Polymer Particles: Navigating the Biological Realm. *Acc. Chem. Res*. **2016**, *49*, 1139-1148.
69. Pelaz, B.; Alexiou, C.; Alvarez-Puebla, R. A.; Alves, F.; Andrews, A. M.; Ashraf, S.; Balogh, L. P.; Ballerini, L.; Bestetti, A.; Brendel, C.; Bosi, S.; Carril, M.; Chan, W. C. W.; Chen, C.; Chen, X.; Chen, X.; Cheng, Z.; Cui, D.; Du, J.; Dullin, C.; Escudero, A.; Feliu, N.; Gao, M.; George, M.; Gogotsi, Y.; Grünweller, A.; Gu, Z.; Halas, N. J.; Hampp, N.; Hartmann, R. K.; Hersam, M. C.; Hunziker, P.; Jian, J.; Jiang, X.; Jungebluth, P.; Kadhiresan, P.; Kataoka, K.; Khademhosseini, A.; Kopeček, J.; Kotov, N. A.; Krug, H. F.; Lee, D. S.; Lehr, C. M.; Leong, K. W.; Liang, X. J.; Lim, M. L.; Liz-Marzán, L. M.; Ma, X.; Macchiarini, P.; Meng, H.; Möhwald, H.; Mulvaney, P.; Nel, A. E.; Nie, S.; Nordlander, P.; Okano, T.; Oliveira, J.; Park, T. H.; Penner, R. M.; Prato, M.; Puntes, V.; Rotello, V. M.; Samarakoon, A.; Schaak, R. E.; Youqing Shen, Y.; Sjöqvist, S.; Skirtach, A. G.; Soliman, M. G.; Stevens, M. M.; Sung, H. W.; Tang, B. Z.; Tietze, R.; Udugama, B. N.; VanEpps, J. S.; Weil, T.; Weiss, P. S.; Willner, I.; Wu, Y.; Yang, L.; Yue, Z.; Zhang, Q.; Zhang, Q.; Zhang, X. E.; Zhao, Y.; Zhou, X.; Parak, W. J. Diverse Applications of Nanomedicine. *ACS Nano* **2017**, *11*, 2313-2381.
70. Kreuter, J. Nanoparticles - A historical perspective. *Int. J. Pharm*. **2007**, *331*, 1–10.
71. Kim, H. J.; Kim, A.; Miyata, K.; Kataoka, K. Recent progress in development of siRNA delivery vehicles for cancer therapy. *Adv. Drug Del. Rev*. **2016**, *104*, 61-77.
72. Molina, M.; Asadian-Birjand, M.; Balach, J.; Bergueiro, J.; Miceliac, E.; Calderon, M. Stimuli-responsive nanogel composites and their application in nanomedicine. *Chem. Soc. Rev*. **2015**, *44*, 6161-6186.
73. Karimi, M.; Mirshekari, H.; Aliakbari, M.; Sahandi-Zangabad, P.; Hamblin, M. R. Smart mesoporous silica nanoparticles for controlled-release drug delivery. *Nanotechnol. Rev*. **2016**, *5*, 195–207.
74. Chassenieux, C.; Tsitsilianis, C. Recent trends in pH/thermo-responsive self-assembling hydrogels: from polyions to peptide-based polymeric gelators. *Soft Matter* **2016**, *12*, 1344-1359.
75. Kocak, G.; Tuncer, C.; Butun, V. pH-Responsive polymers. *Polym. Chem*. **2017**, *8*, 144-176.
76. Parasuraman, D.; Sarker, A. K.; Serpe, M. J. Recyclability of poly (*N*-isopropylacrylamide) microgel based assemblies for organic dye removal from water. *Colloid. Polym. Sci.* **2013**, *291*, 1795-1802.
77. Naseem, K.; Begum, R.; Farooqi, Z. H. Catalytic reduction of 2-nitroaniline: a review. *Environ. Sci. Pollut. Res*. **2017**, *24*, 6446-6460.
78. Crini, G. Non-conventional low-cost adsorbents for dye removal: A review. *Bioresource Tech*. **2006**, *97*, 1061-1085.
79. Mohan, D.; Pittman Jr., C. U. Arsenic removal from water/wastewater using adsorbents—A critical review. *J. Hazard. Mater.* **2007**, *142*, 1-53.
80. Fu, F.; Wang, Q. Removal of heavy metal ions from wastewaters: A review. *J. Environ. Manage.*

2011, *92*, 407-418.
81. Szilagyi, I.; Trefalt, G.; Tiraferri, A.; Maroni, P.; Borkovec, M. Polyelectrolyte adsorption, interparticle forces, and colloidal aggregation. *Soft Matter* **2014**, *10*, 2479−2502.
82. Murray, M. J.; Snowden, M. J. The preparation, characterisation and applications of colloidal microgels. *Adv. Colloid. Int. Sci.* **1995**, *54*, 73-91.
83. Bradley, M.; Ramos, J.; Vincent, B. Equilibrium and Kinetic Aspects of the Uptake of Poly(ethylene oxide) by Copolymer Microgel Particles of *N*-Isopropylacrylamide and Acrylic Acid. *Langmuir* **2005**, *21*, 1209-1215.
84. Jin, L.; Sun, Q.; Xu, Q.; Xu, Y. Adsorptive removal of anionic dyes from aqueous solutions using microgel based on nanocellulose and polyvinylamine. *Bioresour. Technol*. **2015**, *197*, 348-355.
85. Pan, S.; Torres, J. M. G. T.; Hoare, T.; Ghosh, R. Transmission behavior of pNIPAM microgel particles through porous membranes. *J. Memb. Sci*. **2015**, *479*, 141-147.
86. Bibi, F.; Ajmal, M.; Naseer, F.; Farooqi, Z. H.; Siddiq, M. Preparation of magnetic microgels for catalytic reduction of 4-nitrophenol and removal of methylene blue from aqueous medium. *Int. J. Environ. Sci. Technol*. **2017**, 14, 1-12.
87. Snowden, M. J.; Thomas, D.; Vincent, B. Use of colloidal microgels for the absorption of heavy metal and other ions from aqueous solution. *Analyst* **1993**, *118*, 1367-1369.
88. Morris, G. E.; Vincent, B.; Snowden, M. J. Adsorption of Lead Ions onto N-Isopropylacrylamide and Acrylic Acid Copolymer Microgels. *J. Colloid Interface Sci.* **1997**, *190*, 198−205.
89. Parasuraman, D.; Serpe, M. J. Poly(*N*-Isopropylacrylamide) Microgels for Organic Dye Removal from Water. *ACS Appl. Mater. Interfaces* **2011**, *3*, 2732−2737.
90. Parasuraman, D.; Serpe, M. J. Poly(N-Isopropylacrylamide) Microgel-Based Assemblies for Organic Dye Removal from Water. *ACS Appl. Mater. Interfaces* **2011**, *3*, 4714−4721.
91. Bovey, F. A.; Kolthoff, I. M.; Medalia, A. I.; Meehan, E. J.; Emulsion polymerization. New York: *Inter. Sci. Publishers*, **1965**.
92. Okubo, M.; Yamada, A.; Matsumoto, T. Estimation of morphology of composite polymer emulsion particles by the soap titration method. *J. Polym. Sci. Polym. Chem. Ed.* **1980**, *18*, 3219–3228.
93. Chevalier, Y.; Pichot, C.; Graillat, C.; Joanicot, M.; Wong, K.; Maquest, J.; Lindner, P.; Cabane, B. Film formation with latex particles. *Colloid. Polym. Sci.* **1992**, *270*, 806-821.
94. Canelas, D. A.; Betts, D. E.; DeSimone, J. M. Dispersion Polymerization of Styrene in Supercritical Carbon Dioxide: Importance of Effective Surfactants. *Macromolecules* **1996**, *29*, 2818-2821.
95. Kim, B. J.; Oh, S. G.; Han, M. G.; Im, S. S. Preparation of Polyaniline Nanoparticles in Micellar Solutions as Polymerization Medium. *Langmuir* **2000**, *16*, 5841-5845.
96. Asua, J. Miniemulsion polymerization. *Prog. Polym. Sci*. **2002**, *27*, 1283-1346.
97. Chern, C. S. Emulsion polymerization mechanisms and kinetics. *Prog. Polym. Sci*. **2006**, *31*, 443-486.
98. Bradley, M.; Vincent, B.; Warren, N.; Eastoe, J.; Vesperinas, A. Photoresponsive Surfactants in Microgel Dispersions. *Langmuir* **2006**, *22*, 101-105.
99. Rao, J. P.; Geckeler, K. E. Polymer nanoparticles: Preparation techniques and size-control parameters. *Prog. Polym. Sci*. **2011**, *36*, 887-913.

100. Wedel, B.; Brandel, T.; Bookhold, J.; Hellweg, T. Role of Anionic Surfactants in the Synthesis of Smart Microgels Based on Different Acrylamides. *ACS Omega* **2017**, *2*, 84−90.
101. Pelton, R.; Chibante, P. Preparation of aqueous latices with N-isopropylacrylamide. *Colloids Surf.* **1986**, *20*, 247-256.
102. Mears, S. J.; Deng, Y.; Cosgrove, T.; Pelton, R. Structure of Sodium Dodecyl Sulfate Bound to a Poly(NIPAM) Microgel Particle. *Langmuir* **1997**, *13*, 1901-1906.
103. Nerapusri, V.; Keddie, J. L.; Vincent, B.; Bushnak, I. A. The Absorption of Cetylpyridinium Chloride into PolyNIPAM-based Microgel Particles, in Dispersion and as Surface-Deposited Monolayers. *Langmuir* **2007**, *23*, 9572-9577.
104. Suzuki, D.; Sakai, T.; Yoshida, R. Self-Flocculating/Self-Dispersing Oscillation of Microgels. *Angew. Chem., Int. Ed*. **2008**, *47*, 917-920.
105. Suzuki, D.; Taniguchi, H.; Yoshida, R. Autonomously Oscillating Viscosity in Microgel Dispersions. *J. Am. Chem. Soc*. **2009**, *131*, 12058-12059.
106. Suzuki, D.; Kobayashi, T.; Yoshida, R.; Hirai, T. Soft Actuators of Organized Self-Oscillating Microgels. *Soft Matter* **2012**, *8*, 11447-11449.
107. Matsui, S.; Kureha, T.; Nagase, Y.; Okeyoshi, K.; Yoshida, R.; Sato, T.; Suzuki, D. Small-angle X-ray scattering study on internal microscopic structures of poly(*N*-isopropylacrylamide-*co*-tris(2,2-bipyridyl))ruthenium(II) complex microgels. *Langmuir* **2015**, *31*, 7228–7237.
108. Lu, Y.; Mei, Y.; Ballauff, M.; Drechsler, M. Thermosensitive Core-Shell Particles as Carrier Systems for Metallic Nanoparticles. *J. Phys. Chem. B* **2006**, *110*, 3930−3937.
109. Carregal-Romero, S.; Buurma, N. J.; Pérez-Juste, J.; Liz-Marzán, L. M.; Hervés, P. Catalysis by Au@pNIPAM Nanocomposites: Effect of the Cross-Linking Density. *Chem. Mater*. **2010**, *22*, 3051−3059.
110. Hervés, P.; Pérez-Lorenzo, M.; Liz-Marzán, L. M.; Dzubiella, J.; Lu, Y.; Ballauff, M. Catalysis by Metallic Nanoparticles in Aqueous Solution: Model Reactions. *Chem. Soc. Rev*. **2012**, *41*, 5577−5587.
111. Suzuki, D.; Yamagata, T.; Murai, M. Multilayered Composite Microgels Synthesized by Surfactant-Free Seeded Polymerization. *Langmuir* **2013**, *29*, 10579-10585.
112. Suzuki, D.; Kobayashi, C. Raspberry-shaped Composite Microgel Synthesis by Seeded Emulsion Polymerization with Hydrogel Particles. *Langmuir* **2014**, *30*, 7085-7092.
113. Kobayashi, C.; Watanabe, T.; Murata, K.; Kureha, T.; Suzuki, D. Localization of Polystyrene Particles on the Surface of Poly(*N*-isopropylacrylamide-*co*-methacrylic acid) Microgels Prepared by Seeded Emulsion Polymerization of Styrene. *Langmuir* **2016**, *32*, 1429−1439.
114. Watanabe, T.; Kobayashi, C.; Song, C.; Murata, K.; Kureha, T.; Suzuki, D. Impact of Spatial Distribution of Charged Groups in Core Poly(*N*-isopropylacrylamide)-Based Microgels on the Resultant Composite Structures Prepared by Seeded Emulsion Polymerization of Styrene. *Langmuir* **2016**, *32*, 12760−12773.
115. Kureha, T.; Sato, T.; Suzuki, D. Relationship between Temperature-Induced Changes in Internal Microscopic Structures of Poly(*N*-isopropylacrylamide) Microgels and Organic Dye Uptake Behavior. *Langmuir* **2014**, *30*, 8717−8725.
116. Kureha, T.; Shibamoto, T.; Matsui, S.; Sato, T.; Suzuki, D. Investigation of Changes in the Microscopic Structure of Anionic Poly(*N*-isopropylacrylamide-*co*-Acrylic acid) Microgels in the

Presence of Cationic Organic Dyes toward Precisely Controlled Uptake/Release of Low-Molecular-Weight Chemical Compound. *Langmuir* **2016**, *32*, 4575−4585.
117. Kureha, T.; Aoki, D.; Hiroshige, S.; Iijima, K.; Aoki, D.; Takata, T.; Suzuki, D. Decoupled Thermo- and pH-responsive Hydrogel Microspheres Cross-linked by Rotaxane Networks. *Angew. Chem. Int. Ed.* **2017**, *56*, 15393-15396.
118. Bathija, A. Bromate in Drinking-water, Background document for development of WHO Guidelines for Drinking-water Quality, Springer, Berlin, **2004**.
119. Guidelines for Drinking-water Quality, 4th ed. WHO Press, *World Health Organization*: Geneva, Switzerland, **2011**.
120. Theiss, F. L.; Couperthwaite, S. J.; Ayoko, G. A.; Frost, R. L. A review of the removal of anions and oxyanions of the halogen elements from aqueous solution by layered double hydroxides. *J. Colloid. Inter. Sci.* **2014**, *417*, 356-368.
121. Chitrakar, R.; Sonoda, A.; Makita, Y.; Hirotsu, T. Calcined Mg–Al Layered Double Hydroxides for Uptake of Trace Levels of Bromate from Aqueous Solution. *Ind. Eng. Chem. Res*. **2011**, *50*, 9280-9285.
122. Chitrakar, R.; Makita, Y.; Sonoda, A.; Hirotsu, T. Fe–Al layered double hydroxides in bromate reduction: Synthesis and reactivity. *J. Colloid. Inter. Sci*. **2011**, *354*, 798-803.
123. Guthrie, F. XXVIII.—On the iodide of iodammonium. *J. Chem. Soc*. **1863**, *16*, 239-244.
124. Remsen, I.; Norris, J. F. Action of the Halogens on the Methylamines. *Am. Chem. J*. **1896**, *18*, 90-96.
125. Mulliken, R. S. Molecular Compounds and Their Spectra. 3. The Interaction of Electron Donors and Acceptors. *J. Am. Chem. Soc*. **1952**, *74*, 811–824.
126. Flurry, R. L. Jr. Molecular Orbital Theory of Electron DonorAcceptor Complexes. I. A Simple Semiempirical Treatment. *J. Phys. Chem*. **1969**, *69*, 1927–1933.
127. Flurry, R. L. Jr. Molecular orbital theory of electron donor-acceptor complexes. II. Charged donors and acceptors. *J. Phys. Chem.* **1969**, *73*, 2111–2117.
128. Murray-Rust, P.; Motherwell, W. D. S. Computer retrieval and analysis of molecular geometry. 4. Intermolecular interactions. *J. Am. Chem. Soc*. **1979**, *101*, 4374-4376.
129. Murray-Rust, P.; Stallings, W. C.; Monti, C. T.; Preston, R. K.; Glusker, J. P. Intermolecular interactions of the carbon-fluorine bond: the crystallographic environment of fluorinated carboxylic acids and related structures. *J. Am. Chem. Soc*. **1983**, *105*, 3206–3214.
130. Ramasubbu, N.; Parthasarathy, R.; Murray-Rust, P. Angular preferences of intermolecular forces around halogen centers: preferred directions of approach of electrophiles and nucleophiles around carbon-halogen bond. *J. Am. Chem. Soc*. **1986**, *108*, 4308–4314.
131. Politzer, P.; Lane, P.; Concha, M. C.; Ma, Y.; Murray, J. S. An overview of halogen bonding. *J. Mol. Model*. **2007**, *13*, 305-311.
132. Legon, A. C. The halogen bond: an interim perspective. *Phys. Chem. Chem. Phys.* **2010**, *12*, 7736-7747.
133. Erdélyi, M. Halogen bonding in solution. *Chem. Soc. Rev*. **2012**, *41*, 3547-3557.
134. Beale, T. M.; Chudzinski, M. G.; Sarwar, M. G.; Taylor, M. S. Halogen bonding in solution: thermodynamics and applications. *Chem. Soc. Rev*. **2013**, *42*, 1667-1680.

2. Chapter I

"Synthesis of poly(2-methoxyethyl acrylate) (pMEA) Microspheres"

*Part of this work was published in *Colloids and Surfaces B: Biointerfaces*. Reprinted with permission from Kureha, T.; Hiroshige, S.; Matsui, S.; Suzuki, D. Water-immiscible bioinert coatings and film formation from aqueous dispersions of poly(2-methoxyethyl acrylate) microspheres. *Colloids and Surfaces B: Biointerfaces*, 2017, 155, 166-172; copyright 2017, Elsevier B. V.

2.1. Introduction

To achieve the controlled separation of halogen compounds, the pMEA microspheres were prepared and characterized. So far, it is widely accepted that the pMEA is a new-generation bioinert polymer exhibiting poor water solubility.[1] Tanaka *et al.* classified the structure of water adsorbed onto pMEA through differential scanning calorimetry into three types: nonfreezing water (nonfreezing bound water), intermediate water (freezing bound water), and free water (freezing water).[2] They concluded that the intermediate water interacts with the methoxy moiety in the pMEA side-chain terminal with a small water cluster and it plays an important role in the bioinertness of pMEA.[3] Intermediate water also exists in poly(ethylene glycol) (PEG) and poly(methacryloyloxyethyl phosphorylcholine) (pMPC).[2,4] Furthermore, pMEA chains have a glass transition temperature (T_g) of ~ −50°C,[1] resulting in a rubber-like state under body environment. Thus far, linear pMEA chains dissolved in organic solvents have been used as bio- and antifouling-coating agents for artificial heart/lung fabrication and metal products manufacturing.[5]

Therefore, the author hypothesize that pMEA microspheres also show excellent biocompatibility and are suitable for applications such as bioseparation, sensors, and films' formation. In addition, the revelation of the surface properties of pMEA microsphere helps me to understand the adsorption behavior of halogen compounds afterward.

Here, the syntheses of pMEA-based microspheres have been achieved through various methods, as reported in previous literature. For example, microspheres with a size of less than 100 nm composed of pMEA and poly(poly(ethylene glycol) methyl ether methacrylate) (PPEGMA), which is used as a macromolecular chain transfer agent, were prepared by dispersion polymerization of MEA in water using a redox initiator, resulting in the formation of core–shell microspheres with a pMEA-rich core and a PPEGMA-rich shell owing to the amphiphilic character of poly(MEA-*b*-PPEGMA).[6] In addition, (poly(MEA-*co*-poly(ethylene glycol)methyl ethyl acrylate))/poly(*N,N'*-dimethyl

acrylamide)) core–shell microspheres were prepared through reversible addition–fragmentation chain transfer (RAFT)-mediated dispersion polymerization, and their volume transition temperatures were controllable by tuning the monomer ratio.[7]

Although, pMEA-based microspheres have been synthesized and considered as promising colloidal carriers, very few studies have been reported about their biocompatibility.[26] Since the pMEA chains in these microspheres are usually copolymerized with other water soluble polymers such as PEG-based[6,7] and poly(*N*-vinylcaprolactam),[8] checking their resistance to non-specific protein adsorption and the potential capacity of pure (or non-cross-linked and non-functionalized) pMEA microspheres is important to obtain the design concept for pMEA-based microspheres for future bioapplications.

Moreover, to the best of my knowledge, the rubber properties of pMEA-based microspheres have not been discussed with respect to film formation despite the fact that polymer microspheres are suitable for the formation of tailorable films.[9,10] This is an important research area as a majority of commercially produced latex polymers are typically being cast into films or are being used as binders. Particularly, rubber-state (i.e., low T_g) microspheres are soft and deformable, resulting in an easy fusion between them through the evaporation of water without the impurities such as surfactants, other polymers, and organic solvents.[11] In addition, free-standing films have recently been researched extensively; it was observed that they are required to sustain their shape and maintain their properties after they are detached from the substrates and subsequently transferred to other surfaces.[12,13] Indeed, in this chapter, an adhesive, flexible, and transferable free-standing film composed of soft pMEA microspheres is formed and characterized under mild and biocompatible conditions for applications in biomedical engineering. Previously, pMEA coatings were prepared by casting organic solvents such as 1,4-dioxane, toluene, and methanol and dissolving pMEA chains prepared through conventional solution polymerization.[1-3] A large amount of organic solvents are expected to be required to synthesize pMEA chains and form free-standing films composed of these pMEA chains. Furthermore, although the pMEA chains prepared by living radical polymerization in water have been studied, the copolymer such as poly(2-hydroxyethyl acrylate) is necessary to dissolve the pMEA chains in water.[14-16]

Therefore, this chapter primarily aims at clarifying the properties of pure pMEA microspheres in terms of protein adsorption resistance and film formation. First, monodisperse pMEA microspheres are synthesized via aqueous free-radical precipitation or emulsion polymerization without any dispersion stabilizers such as surfactants and other polymers. The plasma protein adsorption behavior of the pMEA and other typical polymer microspheres is characterized in terms of the amounts of

plasma proteins adsorbed by the dispersed pMEA microspheres in a bulk solution. Moreover, a substrate coated with pMEA microspheres and a free-standing film is formed through water evaporation in the pMEA dispersion.

2.2. Experimental Section

Materials

2-methoxyethyl acrylate (MEA, purity 98%), styrene (St, 99%), methyl methacrylate (MMA, 98%), ethyl acrylate (EA, 99%), butyl acrylate (BA, 99%), potassium peroxodisulfate (KPS, 95%), 2,2'-azobis(2-methylpropionamidine) dihydrochloride (V-50, 98%), disodium hydrogenphosphate (99%), human serum albumin (HSA, 95%), fibrinogen from human plasma (FIB, 90%), and immunoglobulin G (IgG, 90%) were purchased from Wako Pure Chemical Industries and used as received. The water used for microsphere preparations was distilled and then ion-exchanged (EYELA, SA-2100E1), and Milli-Q water (Merck Millipore, LCMQ96001) was used for the polymer purifications, characterizations, and protein-adsorption experiments.

Synthesis of pMEA and Control Microspheres

The pMEA and other microspheres were prepared via aqueous soap-free precipitation or emulsion polymerization using the water-soluble anionic initiator KPS. Polymerizations were performed in a 300-mL three-neck, round-bottom flask equipped with a mechanical stirrer, condenser, and nitrogen gas inlet. The initial total concentrations of each monomer are listed in **Table 1**. Monomer solutions were dissolved in 95 mL water in the round-bottom flask and heated to 70°C under a stream of nitrogen with constant stirring at 250 rpm. The solutions were allowed to stabilize for at least 30 min prior to initiation to purge oxygen. Free-radical polymerizations were then initiated using KPS (0.054 g) dissolved in water (5 mL). The solutions were stirred and allowed to react for 24 h. After the completion of the polymerizations, these dispersions were cooled to room temperature. Each microsphere was purified via centrifugation/redispersion with water twice using a relative centrifugal force (RCF) of 20000 × g followed by dialysis for a week with daily water changes.

Characterization of the microspheres

The hydrodynamic diameter (D_h) of the microspheres was determined through dynamic light scattering (DLS, Malvern Instruments Ltd., Zetasizer Nano S). The time-dependent scattering intensity was detected at a total scattering angle of 173°, corresponding to a scattering vector (q) of 0.0264 nm^{-1} in

aqueous media. The microspheres' D_h was calculated from the measured diffusion coefficient using the Stokes–Einstein equation (Zetasizer software v6.12). The DLS experiments were conducted at a microsphere concentration of 0.001 wt%. The samples were allowed to thermally equilibrate at 25°C for 10 min prior to each measurement. The autocorrelation functions were an average of 15 measurements with an intensity acquisition time of 30 s.

The electrophoretic mobility of the microspheres was measured using a Zetasizer Nano ZS instrument (Malvern). The samples were allowed to thermally equilibrate at 25°C for 10 min prior to measurement. The electrophoretic mobility was measured at a microsphere concentration of 0.001 wt%, and NaCl was used to adjust the total salt concentration to 1 mM. The zeta potential was calculated from the measured mobility using the Smoluchowski equation (Zetasizer software ver. 4.20), which was applied when the radius of the microspheres was much larger than the thickness of the diffused electric double layer.

Atomic force microscopy (AFM) images under ambient conditions were recorded using SPM-9500J3 (Shimadzu, Kyoto, Japan) to visualize the microspheres deposited on the circular mica substrates (radius = 1.5 mm) operating in the contact mode. For sample preparation, the microsphere dispersion (0.5 μL) at the required concentration was applied on the freshly prepared mica and dried for 60 min. AFM imaging was performed using a Si_3N_4 probe (Olympus, OMCL-AC240FS). The scanning speed was 0.2 Hz and the operating voltage was 0.3 V. The scanning area was 30 μm × 30 μm, which is the full scale of this equipment. For the film preparation, a silicone template (10 mm × 10 mm × 1 mm, AS ONE corporation) was used. The microsphere dispersion (100 μL) was injected into the template and was dried for 12 h at room temperature.

Protein adsorption experiment.

HSA, FIB, and IgG were used as model plasma proteins and dissolved in sodium phosphate buffer (SPB, pH 7.0). The tested microsphere dispersions in SPB were poured into a vial. The final microsphere concentrations were 0.1 wt% for all experiments. The microsphere dispersions were allowed to thermally equilibrate at 25°C for 1 h with constant stirring at 300 rpm in an incubator (CN-25C, Mitsubishi Electric Engineering Co., Ltd.). After the solution was stabilized in the incubator, the appropriate protein stock solution was injected into the vial. The final concentration of the tested proteins was adjusted appropriately for the individual conditions (50–2000 μg/mL). After exposure for 60 min, the mixture was divided into three centrifuge tubes (SC-0200, Ina-Optika Co., Ltd.). The mixtures were centrifuged at an RCF of 20000 g to accumulate the microspheres at the bottom of each

tube. The three supernatants were carefully removed from the centrifuge tubes without disturbing the microsphere pellet at the bottom. The amount of proteins in the aqueous medium was determined using the bicinchonic acid (BCA) method, in which proteins reduce Cu^{2+} to Cu^{+} in the alkaline condition and the Cu^{+} forms a complex with BCA.[17] These reactions proceed quantitatively. Therefore, the absorbance at 562 nm, which is characteristic of the complex, provides the protein amount.

2.3. Results and Discussion

2.3.1. Synthesis of pMEA Microspheres in Aqueous Solution

The pMEA and other polymer microspheres were synthesized via precipitation or soap-free emulsion polymerization in water (**Table 2.1**).

Table 2.1 Summary of synthetic conditions and characterization for anionic polymer microspheres.

code	Monomer concentration (mM)	MEA	St	MMA	EA	BA	KPS	[a] yield	[b] D_h	[b] ζ
				(g)			(mM)	(%)	(nm)	(mV)
pMEA214	100	1.30					2	87	214	-31.2
pMEA450	500	6.51					2	91	450	-35.2
pMEA1050	1000	13.0					2	88	1050	-48.9
pSt	500		5.21				2	92	251	-37.8
pMMA	1000			10.1			2	93	463	-47.5
pEA	500				5.01		2	87	257	-51.3
pBA	500					6.41	2	85	414	-47.2

[a] The yield was calculated using a dry-weight method of microsphere dispersions after purification.

[b] The data were measured when the microspheres were dispersed in a pH 7.0 SPB (80 mM).

When the concentration of MEA monomer was 100 mM, MEA was completely dissolved in water because the solubility of MEA is ~290 mM (37.7 g/L at 25°C) and pMEA was insoluble in water. Therefore, MEA is a potential candidate for meeting the requirements for demonstrating aqueous precipitation polymerization. Furthermore, in the case of 500 mM and 1000 mM, the MEA monomer was not completely soluble in water, and the polymerization followed the soap-free emulsion polymerization mechanism and not the precipitation polymerization mechanism. The difference in the polymerization mechanisms did not influence the resultant pMEA microspheres adversely because the yields of the series of pMEA microspheres obtained were approximately 90%, which is similar to that

observed in other control polymer microspheres, i.e., pSt, pMMA, pEA, and pBA (**Table 2.1**), and the resultant microspheres were uniform size, as determined from the AFM images (**Figure 2.1**).

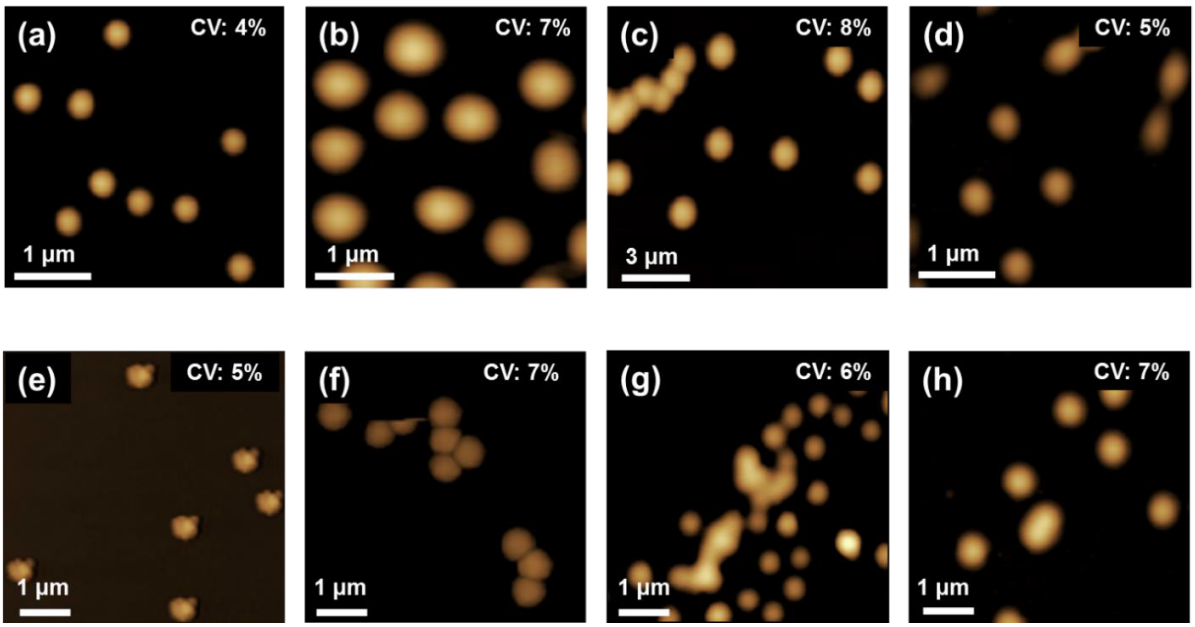

Figure 2.1 AFM images of polymer microspheres; (a) pMEA214, (b) pMEA450, (c) pMEA1050, (d) pMEA+, (e) pSt, (f) pMMA, (g) pEA, and (h) pBA. The coefficient of variation (CV) of each microsphere is also shown ($N = 50$), indicating that the size these microspheres is uniform.

In addition, the size of the pMEA microspheres can be controlled from ~200 nm to ~1 μm by tuning the monomer concentration (100–1000 mM), which is similar to that of a typical microsphere synthesis, for instance, polystyrene[18] and poly(methyl methacrylate).[19] In addition, the dispersion stability of these microspheres was provided by the electrostatic repulsion originating from the sulfate groups introduced by the initiator, which caused a negatively charged surface as evidenced by the zeta potential, ζ (**Table 1**). Thus, the microspheres were stable even though other polymers or surfactants did not exist on the surface. As mentioned above, pMEA-based microspheres with well-defined structures have been synthesized by RAFT dispersion polymerization through a complicated process, which requires the use of a synthesized macromolecular chain transfer agent and organic solvents such as dioxane and *N,N*'-dimethylformamide.[6,7] In contrast to these pMEA-based microspheres, the resultant pMEA microspheres in this study were prepared through simple and green methods using only a monomer, an initiator, and water. In addition, the pMEA microspheres have clean surfaces and a uniform size. Therefore, it is easy to conduct theoretical experiments for the characterization of the microsphere surface, including film formation and adsorption behavior of proteins as described below.

2.3.2. Characterization of Plasma Protein Adsorption Behavior of pMEA Microspheres

To characterize the plasma protein adsorption resistance of dispersed pMEA microspheres in bulk solution, adsorption studies were conducted using HSA, FIB and IgG, which are the major components of plasma proteins, in a pH 7.0 SPB. At pH 7.0, HSA and FIB were negatively charged and IgG was positively charged, because the isoelectric points of HSA,[20] FIB,[21] and IgG[22] are 5.3, 5.5, and 9.0, respectively. The anionic pMEA microsphere with the size of ~200 nm (pMEA214, **Table 1**) was selected mainly for the adsorption experiments because it had the largest specific surface area among the microspheres studied here. **Figure 2.2** shows the adsorption isotherm of the HSA, FIB, and IgG proteins onto the tested anionic microspheres as a function of the protein concentration. Here, the adsorbed amounts of the proteins were normalized against the total surface area of each microsphere at 0.1 wt% because the size of the tested microspheres was different for each chemical species (**Table 1**). Except for pMEA, HSA, FIB and IgG exhibit significant non-specific adsorption despite the fact that the net charge of HSA, FIB, and the tested microspheres was negative at pH 7.0 (**Fig. 2.2a,b**). This may be because of the occurrence of the two interactions, a hydrophobic interaction between the hydrophobic surface of the microspheres and the proteins, and an electrostatic attractive force as the uneven distribution of the charges on the surface of the proteins leads to a dipole moment of appreciable magnitude. Therefore, the adsorption of HSA and FIB was induced by the electrostatic attractive force between the protein and the microspheres, which is similar to that of cationic IgG.

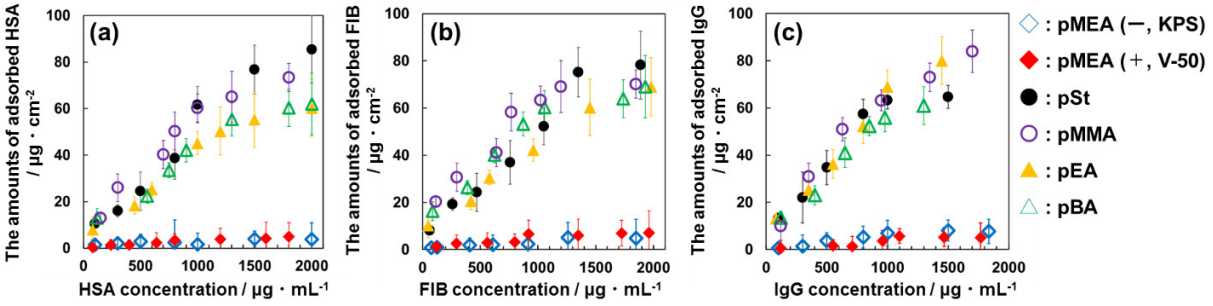

Figure 2.2 The adsorbed amounts of plasma proteins per unit surface area of anionic pMEA (open diamonds), pSt (solid circles), pMMA (open circles), pEA (solid triangles), pBA (open triangles), and cationic pMEA microspheres (solid diamonds) at 0.1 wt% in a pH 7.0 sodium phosphate buffer as a function of protein concentration; anionic human serum albumin (a, HSA), anionic fibrinogen (b, FIB), and cationic immunoglobulin G (c, IgG).

In contrast, the adsorbed amounts of the plasma proteins per unit surface area of the anionic pMEA microspheres were much lower than those of the other polymer microspheres, and the plasma

protein adsorption onto the negatively charged pMEA microspheres was suppressed even when the protein concentrations increased to 2000 μg/mL (i.e., ~3.8 μg/cm^2 for pMEA and ~85.5 μg/cm^2 for pSt in the case of HSA, **Figure 2.2**), suggesting that the energy required for the dehydration of the sulfate group and the ionic group of the proteins surpasses the electrostatic attractive force, which removes the water localized at the surface and causes the adsorption of proteins.[23]

In many studies of pMEA chains, the surface potential of the pMEA coated surface was approximately 0 mV because the pMEA chains were usually prepared through free radical polymerization using a nonionic initiator, 2,2'-azobis-isobutyronitrile.[1-3] Thus, the effect of the charge on the protein adsorption behavior of pMEA has not been discussed. In the present study, the amount of cationic IgG adsorbed by the anionic pMEA microspheres was slightly higher than that adsorbed by anionic HSA and FIB (e.g., ~3.8 μg/cm^2 of HSA and 7.6 μg/cm^2 of IgG at 2000 μg/mL, **Figure 2.2a,c**). Thus, to confirm the effect of the charged state of the pMEA microspheres on the protein adsorption, cationic pMEA microspheres (pMEA+) were synthesized through precipitation polymerization with the cationic initiator V-50 (2 mM) at a monomer concentration of 100 mM. The polymerization was conducted under the same conditions as in the case of anionic pMEA214 microspheres. As a result, the hydrodynamic diameter D_h and the zeta potential ζ of pMEA+ dispersed in pH 7.0 SPB were found to be 243 nm and 21.3 mV, respectively. Furthermore, they were uniform, as evidenced from the AFM image (**Figure 2.1**). The amounts of the tested plasma proteins adsorbed by cationic pMEA+ are also shown in **Figure 2.2**, indicating that the amounts of proteins adsorbed per unit surface area are close to those for the anionic pMEA microspheres. Especially, the amounts of IgG are slightly smaller than that of anionic pMEA microspheres, but this difference is within the error range (~ 3 μg / cm^2). It seems reasonable to interpret that intermediate water, which is bound to the bioinert polymer, including uncharged pMEA chains,[1] PEG, [1] and pMPC,[4] also exists at the surface of the charged pMEA microspheres synthesized in this chapter. Therefore, it is assumed that similar to the uncharged pMEA linear chain, the oxygen atom of the methoxy group in the pMEA microsphere also interacts with the intermediate water, and plays an important role for bioinertness. Notably, the pMEA microsphere size does not affect the amounts of plasma proteins adsorbed, i.e., the pMEA microspheres (pMEA450 and 1050) are able to suppress non-specific protein adsorption (**Figure 2.3**).

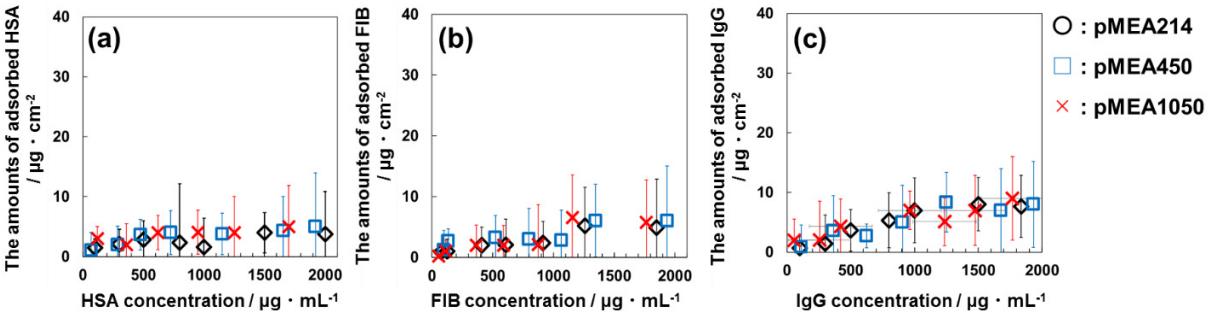

Figure 2.3 The amounts of plasma proteins (a; HSA, b; FIB, and c; IgG) adsorbed by pMEA microspheres with different sizes as a function of the protein concentration.

2.3.3. Coating and Formation of Films of pMEA Microspheres

In this chapter, pMEA microspheres are obtained in a batch through aqueous free radical polymerization and they exhibit a suppression of non-specific adsorption of proteins, suggesting that the easy film formation by these microspheres can have many bioapplications, such as that in implant devices and protein adsorption-preventing barriers. Therefore, to form a pMEA microsphere film by depositing a pMEA dispersion and evaporating water, the author investigated the effect of the pMEA concentration on the substrate surface coverage. **Figure 2.4** shows the AFM images of the adsorbed pMEA microspheres with different concentrations (wt%) measured under ambient conditions. The analysis of the AFM images presented in **Figure 2.4** provides the coverage of the substrate by adsorbed pMEA microspheres with different sizes, and the average coverage is plotted as a function of the microsphere concentration in **Figure 2.5**. Note that, the pMEA microspheres are adsorbed on the substrate without spin-coating and precoating, which results in the variable arrangement of the microspheres on the substrate when the film thickness is nearly equal to the microsphere diameter because the immersion capillary forces between the microspheres can be operative and responsible for the experimentally observed two-dimensional microsphere aggregation and ordering during evaporation in a thin liquid layer.[24,25] Indeed, the white turbid part and the transparent part are observed for the same pMEA microsphere thin films, for instance, 3 wt% for pMEA450, and the coverage differs depending on the location of the substrate when the pMEA concentration is low (e.g., 0.1 and 1 wt% for pMEA1050, as shown in **Figure 2.8**). Thus, the average coverage is determined from the ten images, as shown in the **Figures 2.6, 2.7, and 2.8**, and the typical images are shown in **Figure 2.4**.

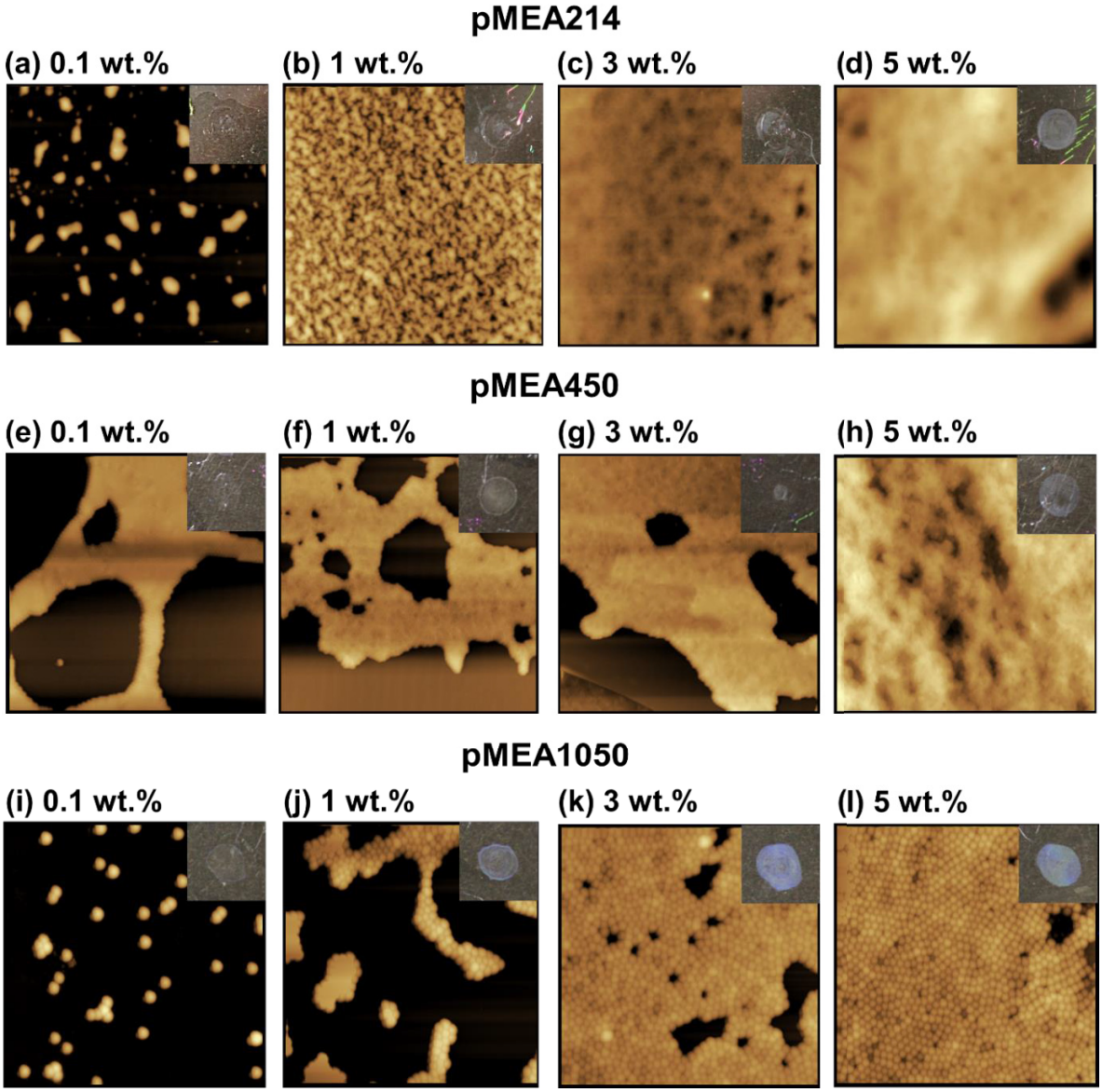

Figure 2.4 Typical AFM images (scan size: 30 × 30 μm^2) of the adsorbed pMEA microspheres with different sizes at each concentration (0.1–5 wt%); pMEA214 (a-d), pMEA450 (e-h), and pMEA1050 (i-l). The insets show photographs of pMEA microsphere thin films formed after drying the microsphere dispersions. 0.5 μL of pMEA dispersions were dried on fresh mica substrates at room temperature (25 ± 2°C). Humidity was less than 30% in all cases.

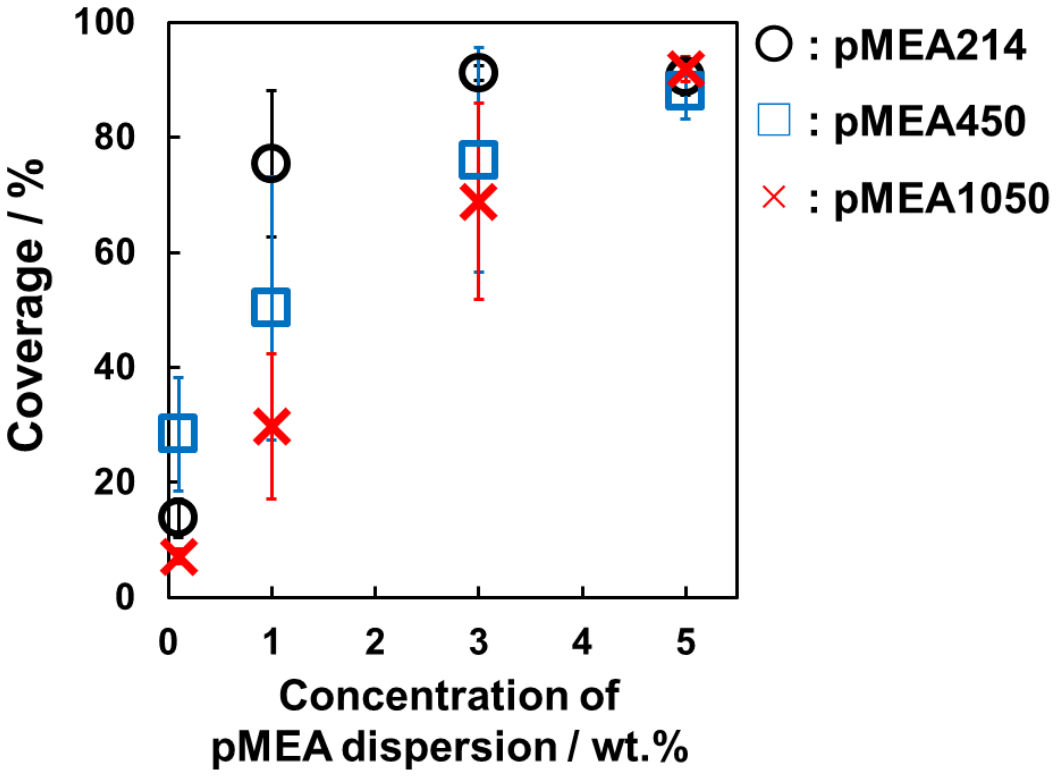

Figure 2.5 Mean coverage of adsorbed pMEA microspheres with different sizes against the concentration obtained from the AFM images with a scan size of 30 × 30 μm^2 (N = 10), as shown in Figures 2.4, 2.6, 2.7, and 2.8.

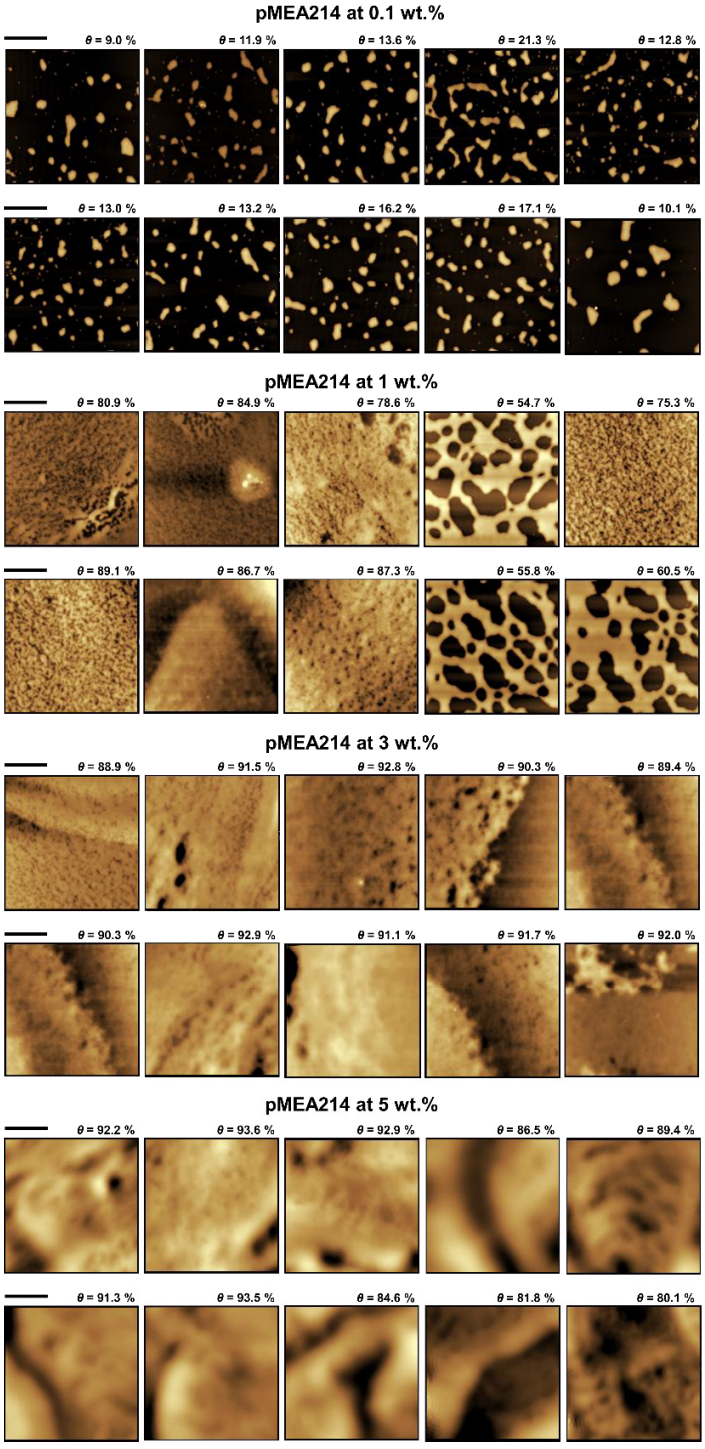

Figure 2.6 AFM images (scan size: 30 × 30 μm^2) of pMEA214 microspheres with different concentrations (0.1–5 wt%). Scale bars are 10 μm. The coverage (θ) of adsorbed pMEA microspheres on the substrate is shown at each image, and the average coverage is calculated and displayed in Figure 2.5.

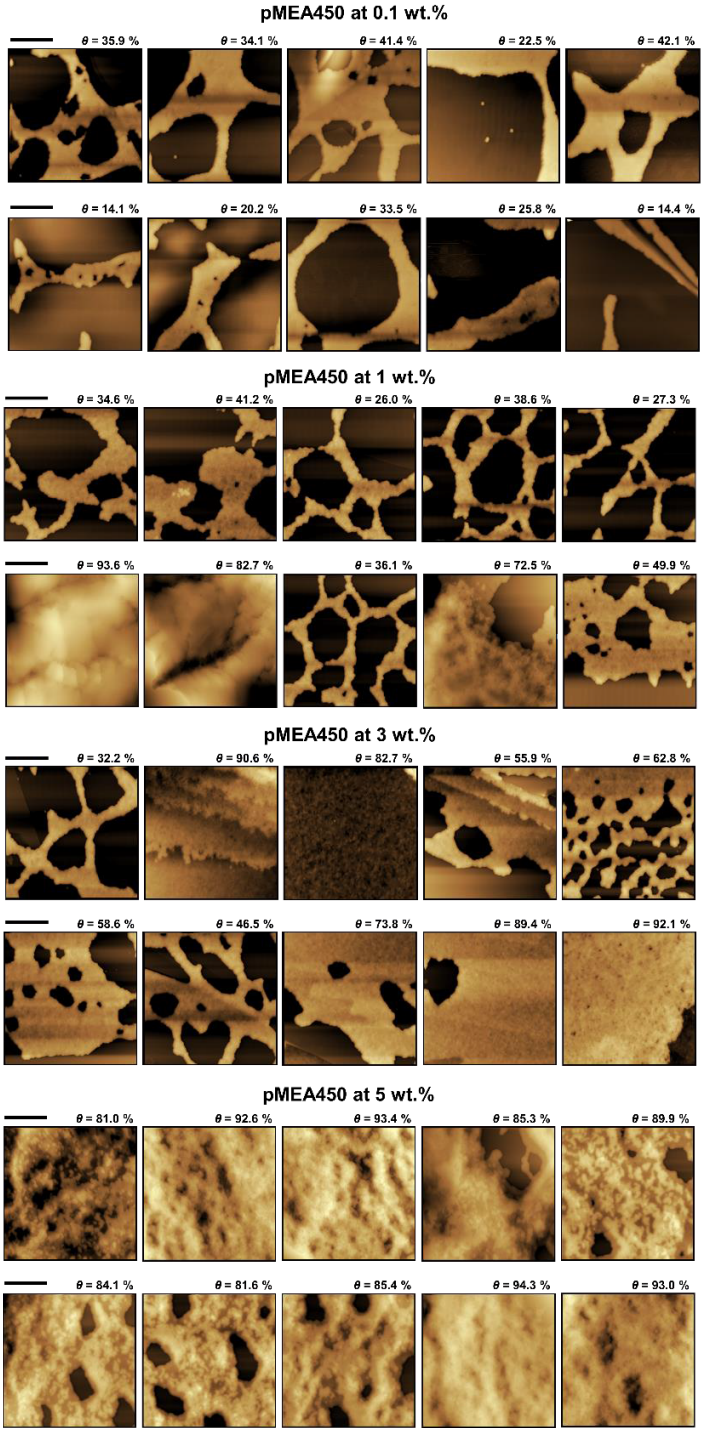

Figure 2.7 AFM images (scan size: 30 × 30 μm^2) of pMEA450 microspheres with different concentrations (0.1–5 wt%). Scale bars are 10 μm. The coverage (θ) of adsorbed pMEA microspheres on the substrate is shown at each image, and the average coverage is calculated and displayed in Figure 2.5.

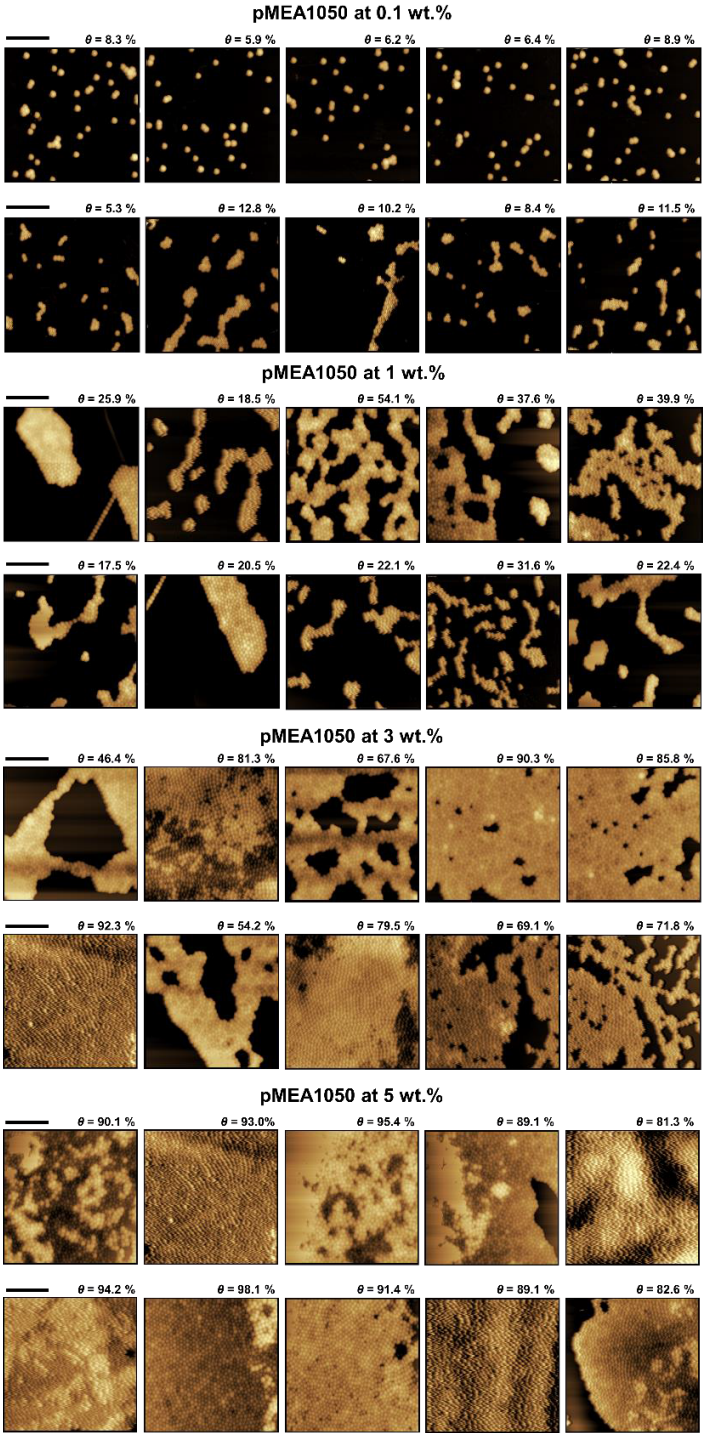

Figure 2.8 AFM images (scan size: 30 × 30 μm^2) of pMEA1050 microspheres with different concentrations (0.1–5 wt%). Scale bars are 10 μm. The coverage (θ) of adsorbed pMEA microspheres on the substrate is shown at each image, and the average coverage is calculated and displayed in Figure 2.5.

Here, as indicated from the results of the AFM cross-sectional analysis (**Figure 2.9**), the adsorbed pMEA microspheres on the substrate are deformed at the dried state. The formation of a dry, homogeneous film from a polymer microsphere dispersion in water is described as a series of three sequential processes: (1) water evaporation to concentrate the microspheres and overcome the repulsion that maintains colloidal stability,[26] (2) microsphere deformation into space-filling polyhedra,[27-29] and (3) interdiffusion of the polymer chains to blur the microsphere boundaries and build cohesive strength.[30-32] Thus, the deformation of pMEA microspheres is the key factor for the film formation and substrate coverage. Here, the deformation degree (D_d) is defined as the value obtained by dividing the hydrodynamic diameter by the height (h) of the pMEA microsphere adsorbed on the substrate, which are obtained by DLS and AFM measurements, respectively. The average values of h and D_d are shown in **Table 2.2**. By increasing the hydrodynamic diameter of pMEA microsphere from 214 nm to 1050 nm, D_d of the pMEA microspheres is found to decrease (e.g., $D_d \sim 4.0$ for pMEA214, $D_d \sim 2.4$ for pMEA450, and $D_d \sim 1.8$ for pMEA1050) when the average value of h is calculated from that of the individual microspheres on the substrate (i.e., the aggregation height of microspheres is not measured).

Table 2.2. Summary of pMEA microsphere deformation data.

code	D_h	[a] Height, h	[b] Deformation degree, D_d
	nm	nm	
pMEA214	214±4	54±8	4
pMEA450	450±3	186±13	2.4
pMEA1050	1050±12	583±25	1.8

[a] The height of the adsorbed microspheres was calculated from the AFM images ($N = 50$).
[b] The deformation degree D_d was defined as D_h (dispersed state)/h (dried state).

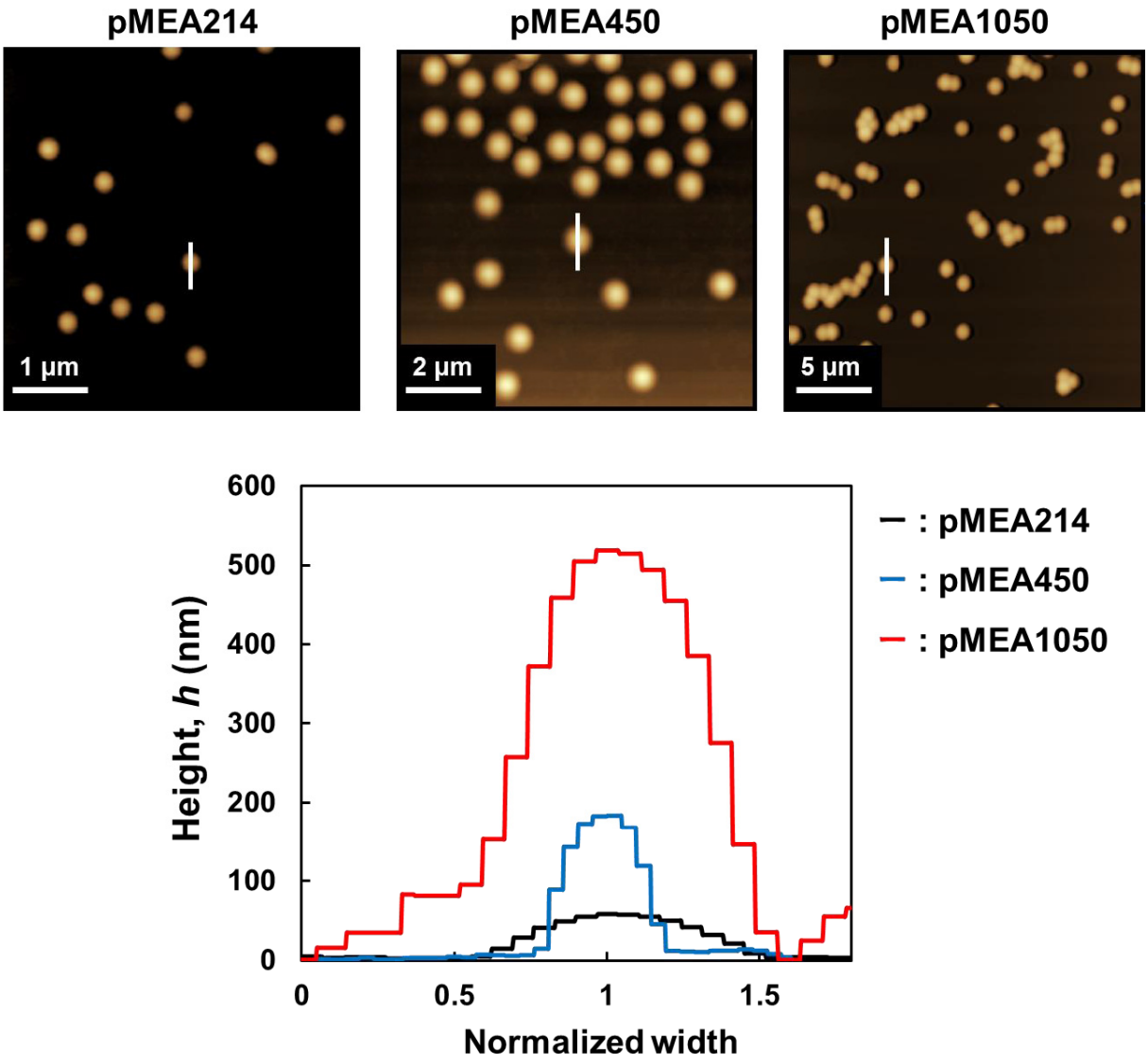

Figure 2.9 AFM images of pMEA microspheres (top) and the cross-sectional analysis (bottom). The displayed cross-sectional data reflect the results of the microspheres drawn using white lines in the top panels.

The modern approach to adhesion between elastic bodies, including microspheres, in a contact is based on the classical work by Johnson, Kendal, and Roberts (JKR)[33] that extended the Hertz theory[34] of the elastic contact by accounting for the effect of adhesion in the contact area. According to this model, the height of the deformed microsphere is defined as $\Delta h \propto R_p(W/KR_p)^{2/3}$. R_p is the radius of an elastic sphere, W is the work of adhesion, and K is rigidity of microsphere ($= 2G / (1 - v)$), where G is the sphere shear modulus and v is the Poisson ratio. This means that the microspheres are more deformed (i.e., the changes in height become pronounced) when the size of the pMEA

microsphere increases, assuming that the pMEA microspheres have the same rigidity. However, as can be seen from the D_d values, a series of pMEA microspheres shows the opposite tendency; smaller microspheres are deformed more than the larger microspheres. Indeed, the sphere shape of pMEA214 aggregation and the boundary between them cannot be clearly observed when the aggregation of the pMEA microspheres is observed using enlarged AFM images (**Figure 2.10a**). In contrast, the sphere shape of pMEA1050 aggregation is maintained (**Figure 2.10c**) compared with that of pMEA214. The pMEA microspheres do not contain the chemical cross-linking, indicating that the sphere shape is maintained by physical cross-linking, such as entanglement and interpenetration between pMEA chains. Therefore, the author infers that the synthetic method affects the rigidity of the resultant pMEA microspheres, but this is unclear in the present study and it will be clarified in our following studies. Moreover, a higher microsphere weight leads to an increase of the average coverage. Particularly, the coverages of pMEA microspheres are close to ~90% for the same concentration (5 wt%), even when the size of the pMEA microspheres is different (**Figure 2.5**). With decreasing pMEA microsphere size, the concentration of pMEA dispersion in which the coverage is close to above 80% decreases (e.g., 1 wt% for pMEA214 and 5 wt% for pMEA1050). This may be because of the fact that the number and D_d of pMEA214 is larger than that of pMEA450 and 1050 for the same concentration.

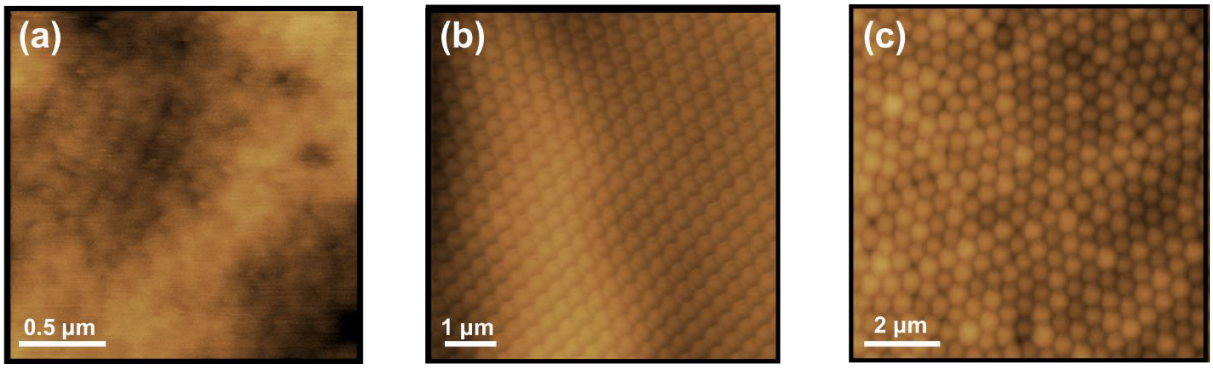

Figure 2.10 The enlarged AFM images of adsorbed pMEA microspheres; (a) pMEA214, (b) pMEA450, and (c) pMEA1050. The concentration of deposited pMEA dispersions at each image is 5 wt%.

In addition to the formation of pMEA coating, the free-standing film, which is strong enough not to be deformed even when it is removed from the template, can be formed by simply injecting the pMEA dispersion into the template without an additive, such as a precoating layer, and a microsphere cross-linker. **Figure 2.11a** shows the film composed of pMEA1050 microspheres with different concentrations. The concentration of pMEA microspheres is an important factor for obtaining a useful

film, because films are found to be deformed by removing the template when the injecting weight to the template is low (e.g., 5 and 10 mg in **Figure 2.11a**). Therefore, the interdiffusion between the soft and deformable microspheres serves as a physical cross-linking point of the whole film, resulting in an increase in the strength and thickness to maintain the film's shape. If the strength of the microspheres increases and/or the interdiffusion between the surfaces of the microspheres is linked by chemical cross-linking, stable films will be formed even at low concentrations.[11,35] However, there is a possibility that the biocompatibility of pMEA microspheres may decrease when the cross-linking agent is added to the microsphere system. This may be because flexibility and mobility are important factors for the pMEA chains' bioinertness,[36] as characterized by ^{13}C dipolar decoupled magic-angle spinning and cross-polarization magic-angle spinning NMR methods, besides the intermediate water on the polymer surface, allowing me to infer that the flexibility of polymer chains may be decreased by chemical cross-linking.

Here, the free-standing pMEA film was successfully transferred from a silicone substrate to a glass substrate and it adhered to the substrate strongly (**Figure 2.11b**). The adsorbed film was stable when soaked in pH 7.0 SPB for a week and disintegration of the film was not observed (**Figure 2.11c**). After the film was transferred and it adhered onto a flexible silicone substrate, it covered the desired location of the substrate (**Figure 2.11d**). These results suggest that the pMEA microsphere film may be used to modify body surfaces like human skin or organs that cannot be accomplished through direct self-assembling.[12] As mentioned above, it is expected that it may be necessary to form and case organic solvents dissolving pMEA linear chains to develop a free-standing film. In addition, the free-standing pMEA film can probably be made through bulk polymerization. However, it is necessary to perform polymerization each time for the preparation of many films and remove both the residual monomer and heat of polymerization. In this chapter, pMEA microspheres are suitable for the formation of clean and sustainable coatings or free-standing films because the organic solvents are not used for the preparation of pMEA microspheres and their applications, and the tailorable film cannot be formed by only injecting pMEA aqueous dispersion and evaporating the aqueous medium. Indeed, the required shape film is obtained by tuning the template shape (**Figure 2.11e**).

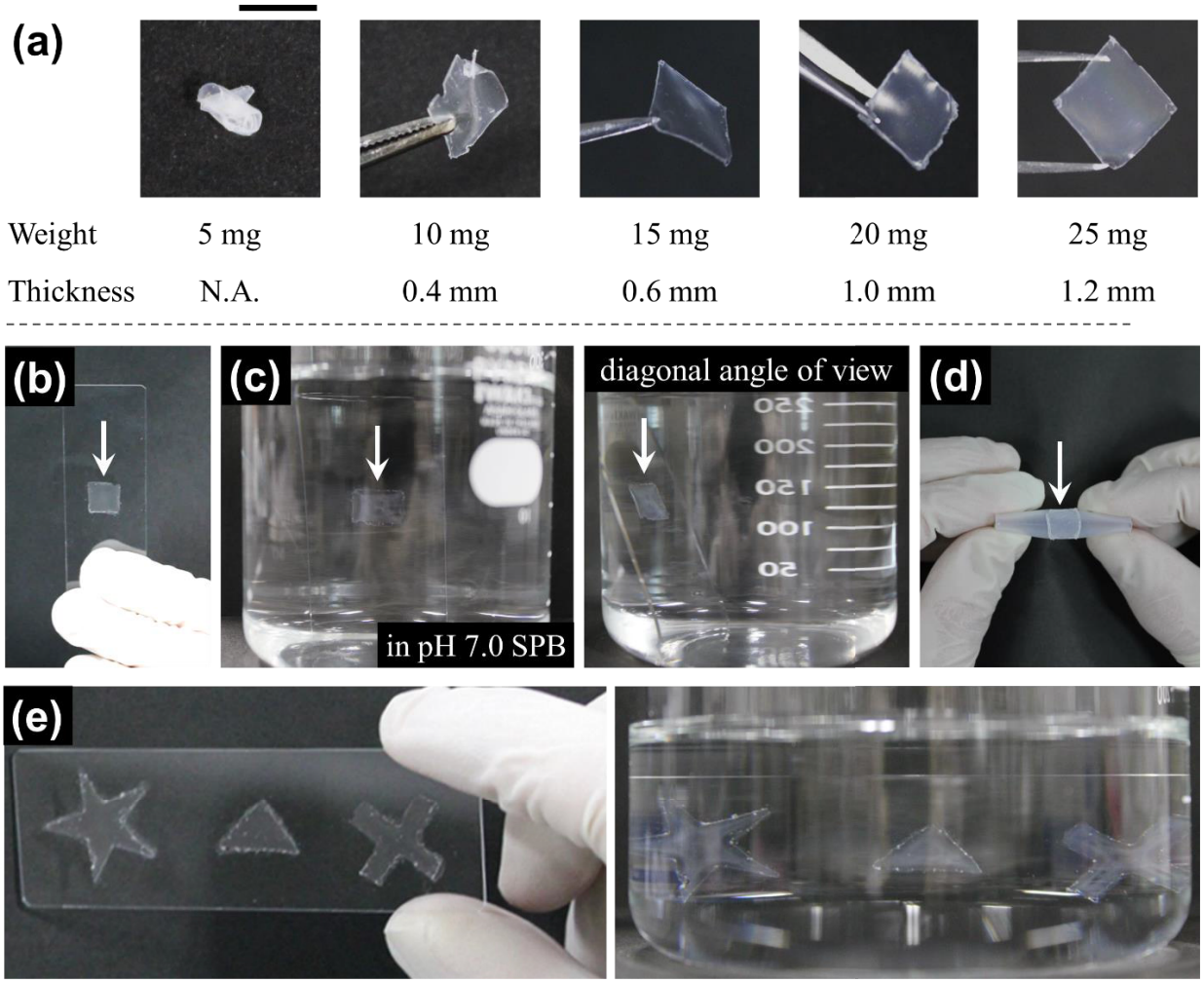

Figure 2.11 (a) Photographs of pMEA microsphere films with different injecting weights (5–25 mg) to the template (10 mm × 10 mm × 1 mm) after removal from the template, except for the left panel at 5 mg. Scale bars are 10 mm. (b) the transferred pMEA1050 film (15 mg) from a silicone substrate to a glass substrate, (c) the soaked film in pH 7.0 SPB after a week, (d) the adsorbed film on the flexible silicone substrate, and (e) the different shapes of the pMEA1050 (15 mg) films adsorbed on the glass substrate. The films are indicated by the arrows.

2.4. Conclusions

The author found that non-functionalized and non-cross-linking pMEA microspheres could be obtained by aqueous soap-free precipitation and emulsion polymerization in water. These pMEA microspheres showed a suppression of non-specific protein adsorption, which was confirmed through a plasma protein adsorption experiment; the adsorption amounts of the HSA, FIB, and IgG were much lower than those on other surfaces of the polymer microspheres in bulk solution, regardless of the charged state of the pMEA microspheres. Moreover, the injectable pMEA dispersion could be applied

to form the pMEA coated substrate and the adhesive and transferable free-standing film owing to the rubber property of the pMEA microspheres without any impurities and organic solvents, which are usually used to form the pMEA chains and their applications.

2.5. References

1. Tanaka, M.; Motomura, T.; Kawada, M.; Anzai, T.; Kasori, Y.; Shiroya, T.; Shimura, K.; Onishi, M.; Mochizuki, A. Blood compatible aspects of poly(2-methoxyethylacrylate) (PMEA)—relationship between protein adsorption and platelet adhesion on PMEA surface. *Biomaterials* **2000**, *21*, 1471-1481.
2. Tanaka, M.; Mochizuki, A. Clarification of the Blood Compatibility Mechanism by Controlling the Water Structure at the Blood–Poly(meth)acrylate Interface. *J. Biomater. Sci. Polym. Ed*. **2010**, *21*, 1849-1863.
3. Morita, S.; Tanaka, M.; Ozaki, Y. Time-Resolved In Situ ATR-IR Observations of the Process of Sorption of Water into a Poly(2-methoxyethyl acrylate) Film. *Langmuir* **2007**, *23*, 3750-3761.
4. Tanaka, M.; Hayashi, T.; Morita, S. The roles of water molecules at the biointerface of medical polymers. *Polym. J.* **2013**, *45*, 701-710.
5. Mueller, X. M.; Jegger, D.; Augstburger, M.; Horisberger, J.; von Segesser, L. K. Poly2-methoxyethylacrylate (PMEA) Coated Oxygenator: An Ex Vivo Study. *Int. J. Artif. Organs*. **2002**, *25*, 223–229.
6. Liu, G.; Qiu, Q.; Shen, W.; An, Z. Aqueous Dispersion Polymerization of 2-Methoxyethyl Acrylate for the Synthesis of Biocompatible Nanoparticles Using a Hydrophilic RAFT Polymer and a Redox Initiator. *Macromolecules* **2011**, *44*, 5237–5245
7. Liu, G.; Qiu, Q.; An, Z. Development of Thermosensitive Copolymers of Poly(2-methoxyethyl acrylate-co-Poly(ethylene glycol) Methyl Ether Acrylate) and Their Nanogels Synthesized by RAFT Dispersion Polymerization in Water. *Polym. Chem*. **2012**, *3*, 504-513.
8. Melle, A.; Balaceanu, A.; Wu, Y.; Kather, M.; Gau, E.; Sun, W.; Huang, X.; Shi, X.; Karperiend, M.; Pich, A. Stimuli-responsive Poly(*N*-vinylcaprolactam-*co*-2-methoxyethyl acrylate) Core–shell Microgels: Facile Synthesis, Modulation of Surface Properties and Controlled Internalisation into Cells. *J. Mater. Chem. B*. **2016**, *4*, 5127-5137.
9. Stewarda, P. A.; Hearn, J.; Wilkinson, M. C. An Overview of Polymer Latex Film Formation and Properties. *Adv. Colloid. Inter. Sci*. **2000**, *86*, 195-267.
10. Carter, F. T.; Kowalczyk, R. M.; Millichamp, I.; Chainey, M.; Keddie, J. L. Correlating Particle Deformation with Water Concentration Profiles during Latex Film Formation: Reasons That Softer Latex Films Take Longer to Dry. *Langmuir* **2014**, *30*, 9672−9681.
11. Taylor, J. W.; Winnik, M. A. Functional Latex and Thermoset Latex Films. *J. Coatings Tech. Res*. **2004**, *1*, 163-190.

12. Han, La.; Wang, Z.; Lu, X.; Dong, L.; Xie, C.; Wang, K.; Chen, X.; Ding, Y.; Weng, L. Mussel-inspired Adhesive and Transferable Free-standing Films by Self-assembling Dexamethasone Encapsulated BSA Nanoparticles and Vancomycin Immobilized Oxidized Alginate. *Colloid. Surf., B* **2015**, *126*, 452-458.
13. Palivan, C. G.; Goers, R.; Najer, A.; Zhang, X.; Car, A.; Meier, W. Bioinspired Polymer Vesicles and Membranes for Biological and Medical Applications. *Chem. Soc. Rev*. **2016**, *45*, 377-411.
14. Steinhauer, W.; Hoogenboom, R.; Keul, H.; Moeller, M. Copolymerization of 2-Hydroxyethyl Acrylate and 2-Methoxyethyl Acrylate via RAFT: Kinetics and Thermoresponsive Properties. *Macromolecules* **2010**, *43*, 7041–7047.
15. Steinhauer, W.; Hoogenboom, R.; Keul, H.; Moeller, M. Block and Gradient Copolymers of 2-Hydroxyethyl Acrylate and 2-Methoxyethyl Acrylate via RAFT: Polymerization Kinetics, Thermoresponsive Properties, and Micellization. *Macromolecules* **2013**, *46*, 1447−1460.
16. Warren, N. J.; Armes, S. P. Polymerization-Induced Self-Assembly of Block Copolymer Nanoobjects via RAFT Aqueous Dispersion Polymerization. *J. Am. Chem. Soc*. **2014**, *136*, 10174−10185.
17. Stoscheck, C. M. Quantitation of protein. *Methods in Enzymology* **1990**, *182*, 50–68.
18. Goodall, A. R.; Wilkinson, M. C.; Hearn, J. Mechanism of Emulsion Polymerization of Styrene in Soap-free Systems. *J. Polym. Sci. Polym. Chem*. **1977**, *15*, 2193-2218.
19. Arai M, Arai K, Saito S. On the Rate of Soapless Emulsion Polymerization of Methyl Methacrylate. *J. Polym. Sci.* **1980**, *18*, 2811-2821.
20. Fanali, G.; di Masi, A.; Trezza, V.; Marino, M.; Fasano, M.; Ascenzi, P. Human Serum Albumin: From Bench to Bedside. *Molecular Aspects of Medicine* **2012**, *33*, 209–290.
21. Jerrold H. Levy, J. H.; Welsby, I.; Goodnough, L. T. Fibrinogen as A Therapeutic Target for Bleeding: A Review of Critical Levels and Replacement Therapy. *Transfusion* **2014**, *54*, 1389-1450.
22. Brezski, R. J.; Georgiou, G. Immunoglobulin Isotype Knowledge and Application to Fc Engineering. *Current Opinion in Immunology* **2016**, *40*, 62–69.
23. Kitano, H. Characterization of Polymer Mmaterials Based on Structure Analyses of Vicinal Water. *Polymer J.* **2016**, *48*, 15–24.
24. Kralchevsky, P. A.; Nagayama, K. Capillary Interactions between Particles Bound to Interfaces, Liquid Films and Biomembranes. *Adv. Colloid. Inter. Sci*. **2000**, *85*, 145-192.
25. Nguyen, V. X.; Stebe, K. J. Patterning of Small Particles by a Surfactant-Enhanced Marangoni-Bénard Instability. *Phys. Rev. Lett*. **2002**, *88*, 164501.
26. Routh, A. F. Drying of Thin Colloidal Films. *Rep. Prog. Phys*. **2013**, *76*, 46603.
27. Crowley, T.; Sanderson, A.; Morrison, J. Formation of Bilayers and Plateau Borders during the Drying of Film-Forming Latexes as Investigated by Small-Angle Neutron Scattering. *Langmuir* **1992**, *8*, 2110−2123.
28. Rharbi, Y.; Boué, F.; Joanicot, M.; Cabane, B. Deformation of Cellular Polymeric Films. *Macromolecules* **1996**, *29*, 4346−4359.

29. Gonzalez, E.; Tollan, C.; Chuvilin, A.; Barandiaran, M. J.; Paulis, M. Determination of the Coalescence Temperature of Latexes by Environmental Scanning Electron Microscopy. *ACS Appl. Mater. Interfaces* **2012**, *29*, 4276−4282.
30. Wang, Y.; Winnik, M. A. Polymer Diffusion across Interfaces in Latex Films. *J. Phys. Chem*. **1993**, *97*, 2507−2515.
31. Kim, K. D.; Sperling, L. H.; Klein, A.; Hammouda, B. Reptation Time, Temperature, and Cosurfactant Effects on the Molecular Interdiffusion Rate during Polystyrene Latex Film Formation. *Macromolecules* **1994**, *27*, 6841−6850.
32. Arda, E.; Özer, F.; Pişkin, E.; Pekcan, Ö. Film Formation from Nanosized Copolymeric Latex Particles: A Photon Transmission Study. *J. Colloid Interface Sci*. **2001**, *233*, 271−279.
33. Johnson, K. L.; Kendall, K.; Roberts, A. D. *Proc. R. Soc. London A* **1971**, *324*, 301–313.
34. Johnson, K. L. *Contact Mechanics, 9th ed.; Cambridge University Press: New York*, **2003**.
35. Iyer, B. V. S.; Yashin, V. V.; Hamer, M. J.; Kowalewski, T.; Matyjaszewski, K.; Balazs, A. C. Ductility, Toughness and Strain Recovery in Self-healing Dualcross-linked Nanoparticle Networks Studied by Computersimulations. *Prog. Polym. Sci*. **2015**, *40*, 121-137.
36. Miwa, Y.; Ishida, H.; Saito, H.; Tanaka, M.; Mochizuki, A. Network Structures and Dynamics of Dry and Swollen Poly(acrylate)s. Characterization of High- and Low-frequency Motions as Revealed by Suppressed or Recovered Intensities (SRI) Analysis of ^{13}C NMR. *Polymer* **2009**, *50*, 6091-6099.

3. Chapter II

"Characterization of the Halogen Compound Separation Capacity of pMEA Microspheres and pMEA Composite Hydrogel Microspheres"

*Part of this work was published in *Langmuir*. Reprinted with permission from Kureha, T.; Suzuki, D. Nanocomposite Microgels for the Selective Separation of Halogen Compounds from Aqueous Solution. *Langmuir* **2018**, 34, 837-846; copyright 2018, American Chemical Society.

3.1. Introduction

In **Chapter I**, the non-functionalyzed pMEA microspheres can be synthesized easily and characterized in terms of bioinertness and coating ability. Thus, in this chapter, the adsorption capacity for the halogen compounds of pMEA microspheres is investigated. Moreover, the author designs nanocomposite microgels, wherein the solid pMEA components are distributed and dissolved in the entire swollen microgel at the molecular level because the gel network permit the controlled uptake/release of functional molecules. This should afford a high specific adsorption volume, high dispersion stability, and the ability to release the target molecules from the solid pMEA domains. In this chapter, the pMEA components were incorporated in swollen microgels and their functions, such as selective separation, controlled release, and usability are also discussed.

3.2. Experimental Section

Materials

2-methoxyethyl acrylate (MEA, purity 98%), styrene (St, 99%), methyl methacrylate (MMA, 98%), ethyl acrylate (EA, 99%), butyl acrylate (BA, 99%), potassium peroxodisulfate (KPS, 95%), disodium hydrogenphosphate (99%), eosin Y (EoY, 95%), phloxine B (PhB, 98%), erythrosine (Ery, 95%), rose bengal (RB, 95%), orange II (OrII, 98%), tartrazine (Ttz, 98%), and sea sand (methanol washed, 425-850 μm, 20-35 mesh) were purchased from Wako Pure Chemical Industries and used as received. Poly(ethylene glycol) methyl ether methacrylate (OEG, av. M_n = 300 g/mol) and ethylene glycol dimethacrylate (EGDMA, 98%) were purchased from Sigma-Aldrich and used as received. Water used for microsphere preparations was distilled and then ion-exchanged (EYELA, SA-2100E1).

Synthesis of pMEA, control, and pMEA composite microspheres

All microspheres were prepared via aqueous soap-free precipitation or emulsion polymerization using potassium peroxodisulfate (KPS). Polymerizations were performed in a three-necked round-bottom

flask (300 mL) equipped with a mechanical stirrer, condenser, and nitrogen gas inlet. For p(MEA-*co*-NIPAm) and p(MEA-*co*-AAm) microgels, the initial total monomer concentration was held constant at 100 mM. Mixtures of NIPAm (0.555 g, 49 mol%) or AAm (0.348 g, 49 mol%), MEA (0.651 g, 50 mol%), and BIS (0.015 g, 1 mol%) were prepared as the monomer solution. For highly cross-linked pMEA composite microgels (**pM6O4E5**), the initial total monomer concentration was held constant at 100 mM. Mixtures of MEA (0.781 g, 60 mol%), OEG (1.050 g, 35 mol%), and EGDMA (0.099 g, 5 mol%) were prepared as the monomer solution. All monomer solutions were dissolved in water (95 mL) in the round-bottom flask and heated to 70 °C under constant stirring (250 rpm) and a stream of nitrogen. The solutions were allowed to stabilize for at least 30 min prior to initiation. Free-radical polymerizations were subsequently initiated using KPS (0.054 g) in water (5 mL). The solutions were stirred for 24 h, and after the completion of the polymerizations, the obtained dispersions were cooled to room temperature. Each microsphere was purified via two cycles of centrifugation/re-dispersion in water using a relative centrifugal force (RCF) of 20000 × *g*, followed by dialysis for a week with daily water changes.

Characterization of the microspheres

The hydrodynamic diameter (D_h) of the microspheres was determined by DLS (Malvern Instruments Ltd., Zetasizer Nano S). The time-dependent scattering intensity was detected at a total scattering angle of 173° in aqueous solution. D_h values of the microspheres were calculated from the measured diffusion coefficient using the Stokes–Einstein equation (Zetasizer software v6.12). The DLS experiments were conducted at a microsphere concentration of 0.001 wt%. The samples were allowed to thermally equilibrate at the desired temperature for 10 min prior to each measurement. The autocorrelation functions used an average of 15 intensity measurements (acquisition time: 30 s). The electrophoretic mobility of the microspheres was measured using a Zetasizer Nano ZS instrument (Malvern) at a microsphere concentration of 0.001 wt%. Samples were allowed to thermally equilibrate at 25 °C for 10 min prior to each measurement. The zeta potential of the solid microspheres was calculated from the measured mobility using the Smoluchowski equation (Zetasizer software ver. 4.20). Atomic force microscopy (AFM) images were recorded under ambient conditions using an SPM-9500J3 microscope (Shimadzu, Kyoto, Japan) operating in contact mode to visualize the microspheres deposited on circular mica substrates. For the sample preparation, microsphere dispersions (0.5 μL) at the required concentration were applied on freshly prepared mica substrates and dried for 60 min. AFM

images were recorded using an Si_3N_4 probe (Olympus, OMCL-AC240FS; scanning speed = 0.2 Hz; operating voltage = 0.3 V).

Dye adsorption experiments

Stock solutions of anionic dyes (20 mM) in a sodium phosphate buffer (SPB; 80 mM, pH = 7.0) were prepared. The tested microsphere dispersions were poured into a vial. The final concentration of the microsphere was 0.1 wt% for all experiments. The microgel dispersions were allowed to thermally equilibrate at the desired temperature for 1 h under constant stirring (300 rpm) in an incubator (CN-25C, Mitsubishi Electric Engineering Co., Ltd.). After the solutions had stabilized in the incubator, the appropriate dye stock solutions were injected into the vials. The final dye concentrations were adjusted appropriately for the required conditions (0.1-2 mM). After 1 h of exposure, the mixtures were divided into three centrifuge tubes (SC-0200, Ina-Optika Co., Ltd). The mixtures were centrifuged (RCF; 20000 × *g*) to pack the microspheres at the bottom of each tube. The supernatants were carefully removed from the centrifuge tubes without disturbing the microsphere pellets at the bottom and the absorbance of each supernatant was measured using a UV–vis spectrophotometer (JASCO, V-630iRM).

Analysis of the adsorption isotherms. The Langmuir model is based on the assumption that maximum adsorption corresponds to monolayer formation of the adsorbate layer on the adsorbent surface. The energy of adsorption is constant and no transmigration of adsorbate occurs on the surface.[1] The mathematical form of Langmuir equation is

$$\frac{C_e}{Q_e} = \frac{C_e}{Q_m} + \frac{1}{Q_m b} \quad \ldots (1)$$

where C_e (mg L^{-1}) represents the equilibrium dye concentration in solution, Q_e (mg g^{-1}) the amount of adsorbed dyes by the microspheres, Q_m (mg g^{-1}) the adsorption capacity, i.e., the amount of dye that can be absorbed by a unit mass of the adsorbent for the formation of monolayer on the surface, and b (L mg^{-1}) the Langmuir constant, which is related to the affinity between the dyes and microspheres. A dimensionless equilibrium parameter (R_L), known as the separation factor can be calculated using the following equation:[2]

$$R_L = \frac{1}{(1 + bC_0)} \quad \ldots (2)$$

where C_0 (mg L^{-1}) is the initial dye concentration in solution.

The Freundlich isotherm can be used to describe the adsorption on both homogeneous and

heterogeneous surfaces.[3] The linearized form of Freundlich isotherm is:

$$\log Q_e = \log K_F + \frac{1}{n} \log C_e \ldots (3)$$

where K_F and n represent the Freundlich constants that describe the adsorption capacity at unit concentration and intensity of adsorption, respectively.

Dye release experiments

The optimal conditions for the adsorption of dyes were used to prepare a mixture of the microspheres and dyes. After the supernatant was removed from each centrifuge tube, each microsphere pellet was re-dispersed in a different buffer solution at 25, 40, or 70 °C, and placed in the centrifuge tubes at the same concentration used in the adsorption experiment. Each dispersion was subsequently mixed for 1 h using a thermomixer (Thermomixer R, Eppendorf) at 25, 40, or 70 °C. This period was selected for all microspheres, as complete re-dispersion occurred under all conditions used for the release experiments. Each mixture was then centrifuged (RCF; 20000 × *g*) and the supernatants were removed from the centrifuge tubes. The absorbance of each supernatant was measured using a UV–vis spectrophotometer.

Preparation of the microsphere films and columns

For the preparation of the free-standing film, a silicone template (10 × 10 × 1 mm^3; AS ONE corporation) was used. A microsphere dispersion (50 mg, 100 μL) was injected into the template and dried for 12 h at room temperature. For the preparation of the microsphere-packed column, microsphere powder was obtained by freeze drying (FDU-1200, Tokyo Rikakikai Co., LTD.). Cotton wool was packed on the inside bottom of a Pasteur pipette (IWAKI IK-PAS-5P, IWAKI&CO., LTD.), followed by sea sand (0.10 g) in order to prevent the pMEA microspheres (0.05 g) or microgels (0.05 g) from escaping the pipette with the dye solution. Prior to the injection of the dye solutions, the columns were washed by injecting pure water.

3.3. Results and Discussion

3.3.1. Adsorption Behavior of Halogen Compounds on pMEA Microspheres

First, hydrophobic pMEA was selected as the solid component, as i) pMEA can be easily obtained by free-radical polymerization,[4-8] and ii) pMEA chains exhibit good compatibility with human blood,[4-7] which may be beneficial for the development of biological applications. Pure, i.e.,

non-fractionalized and non-cross-linked pMEA microspheres with uniform size were synthesized via precipitation and soap-free emulsion polymerization in water (**Table 3.1** and **Figure 3.1**).[8] In addition, given the low glass-transition temperature of the pMEA chains (T_g ~ −50 °C),[4] polystyrene (pSt), poly(methyl methacrylate) (pMMA), poly(ethyl acrylate) (pEA), and poly(butyl acrylate) (pBA) were selected as solid control microspheres that cover a wide T_g range. These solid microspheres exhibit negatively charged surfaces on account of the sulfate groups introduced by the initiator, which is reflected in the zeta potential, ζ (**Table 3.1**), allowing us to ignore the effect of electrostatic attraction between the microspheres and the tested anionic dyes on the halogen-bonding intensity.

The chemical structures of the tested dye are shown in **Figure 3.2**, and their visible absorption spectra are shown in **Figure 3.3**. The anionic halide xanthene dyes, eosin Y (EoY), erythrosine (Ery), phloxine B (PhB), and rose bengal (RB) were selected as model halogen-containing compounds to examine the origin of the halogen bonding, since it is generally accepted that the strength of the donor-acceptor interaction depends on the polarizability of the halogen atom, which decreases in the order I > Br > Cl.[9-11] In order to compare the halogen bonding with other, e.g. hydrophobic interactions, other anionic dyes that do not contain halogen atoms such as orange II (OrII) and tartrazine (Ttz) were also examined.

Table 3.1 Summary of the synthetic conditions for the generation of solid anionic microspheres and their characterization.

Microsphere	Monomer concentration (mM)	MEA	St	MMA	EA	BA	KPS	[a] D_h	[a] ζ	T_g
				(g)			(mM)	(nm)	(mV)	(°C)
pMEA	100	1.30					2	214	-31.2	-50[b]
pSt	500		5.21				2	251	-37.8	104[c]
pMMA	1000			10.1			2	463	-47.5	103[c]
pEA	500				5.01		2	257	-51.3	-21[c]
pBA	500					6.41	2	414	-47.2	-40[c]

[a]Data were measured on dispersions of the microspheres in sodium phosphate buffer (80 mM) at pH = 7.0.
[b]T_g value of pMEA was from reference 4 in this chapter.
[c]T_g values were from reference 19.

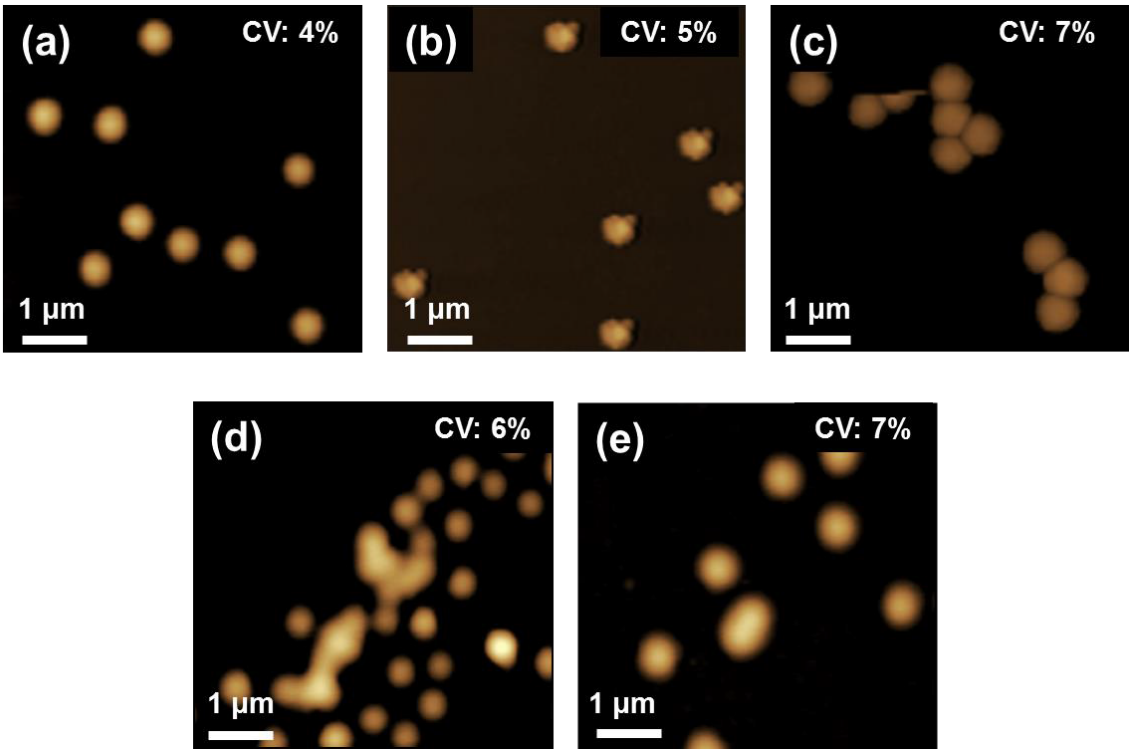

Figure 3.1 AFM images of polymer microspheres: (a) pMEA, (b) pSt, (c) pMMA, (d) pEA, and (e) pBA. The coefficient of variation (CV) for each microsphere is also shown (N = 50), indicating that the shape of these microspheres is uniform.

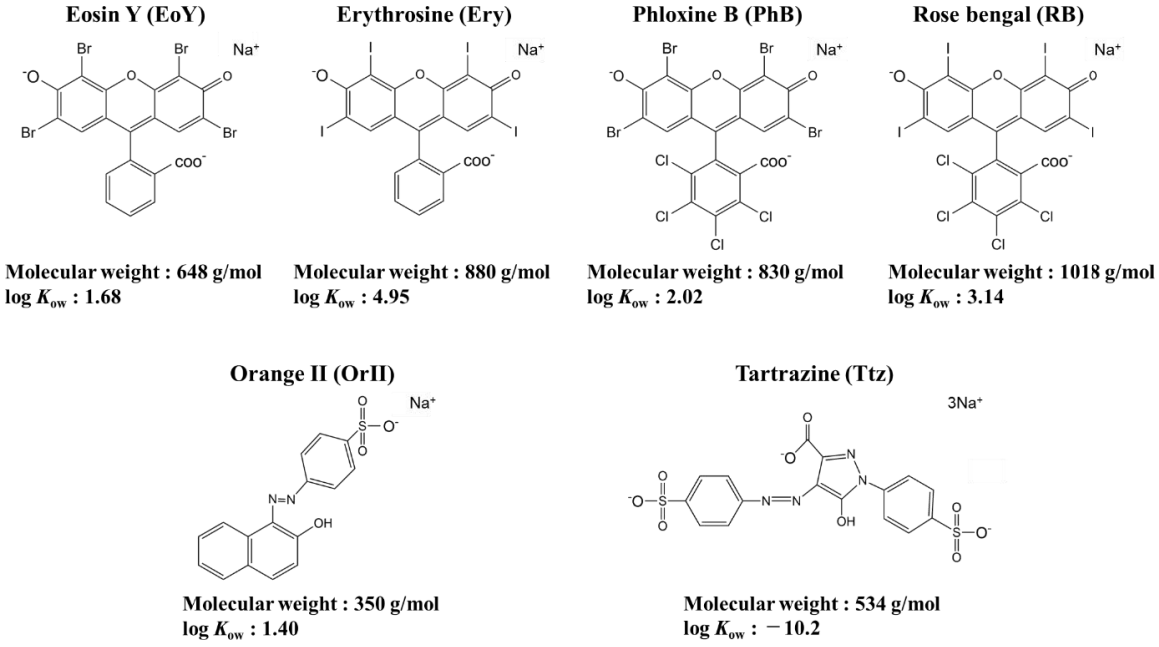

Figure 3.2 Chemical structures of the anionic dyes tested. The molecular weight and octanol/water partition coefficient of each dye is shown under each structure.

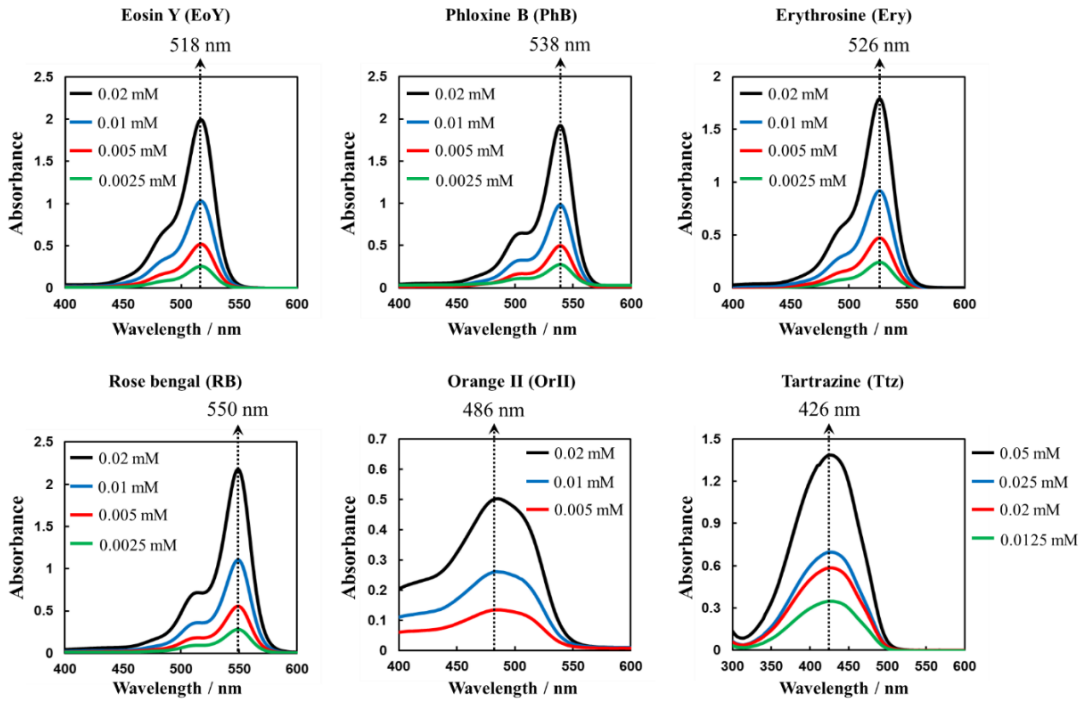

Figure 3.3 UV-vis spectra of the tested dyes in SPB buffer (pH = 7.0) at several concentrations (25 °C). Arrows represent the maximum wavelength for each dye.

Figure 3.4a shows the adsorption isotherm for each dye for the tested microspheres at 25 °C. Langmuir (equation 1) and Freundlich (equation 3) models were applied in order to analyze the adsorption equilibrium data. These isotherms are shown in **Figure 3.5**. The adsorption capacity (Q_m), Langmuir constant (b), intensity of adsorption (n), and Freundlich constant (K_F) can be determined from the two isotherms. In all cases, the correlation coefficient (R^2) of the Langmuir model was close to 1 and much larger than that of the Freundlich model, indicating a good fit of the Langmuir model. **Table 3.2** shows the values of the Langmuir isotherm parameters and all values are summarized in **Table 3.3**. Here, the Q_m values determined by the Langmuir model were normalized as moles of dye per total surface area of tested microsphere ($N_{m/s}$, μmol/m^2) in order to compare the adsorption behavior considering the different size of these microspheres and the different molecular weight of each dye. Furthermore, the essential characteristics of the Langmuir isotherm can be described by a separation factor (R_L), which is defined by equation 2 (**Tables 3.2** and **3.3**). The value of R_L indicates the shape of the Langmuir isotherm and the nature of the adsorption process: irreversible ($R_L = 0$), favorable ($0 < R_L < 1$), linear ($R_L = 1$), or unfavorable ($R_L > 1$).[2]

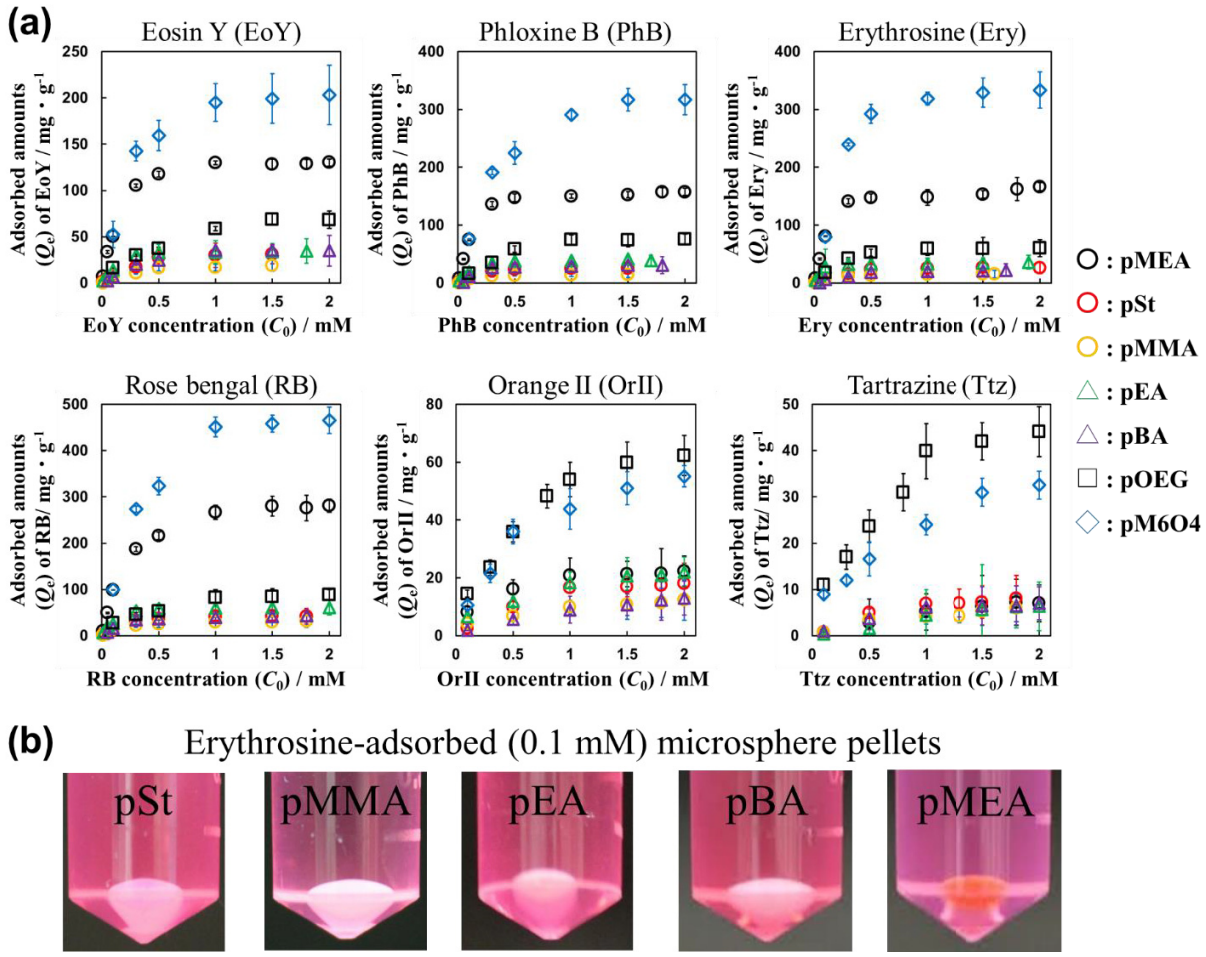

Figure 3.4 (a) Adsorption isotherms for the tested dyes on each microsphere at 25 °C. Each point represents an average of three replicate uptake experiments, and the error bars denote the standard deviations. (b) Photographs of pellets of each microsphere (0.1 wt%) after centrifugation in the presence of erythrosine (0.1 mM).

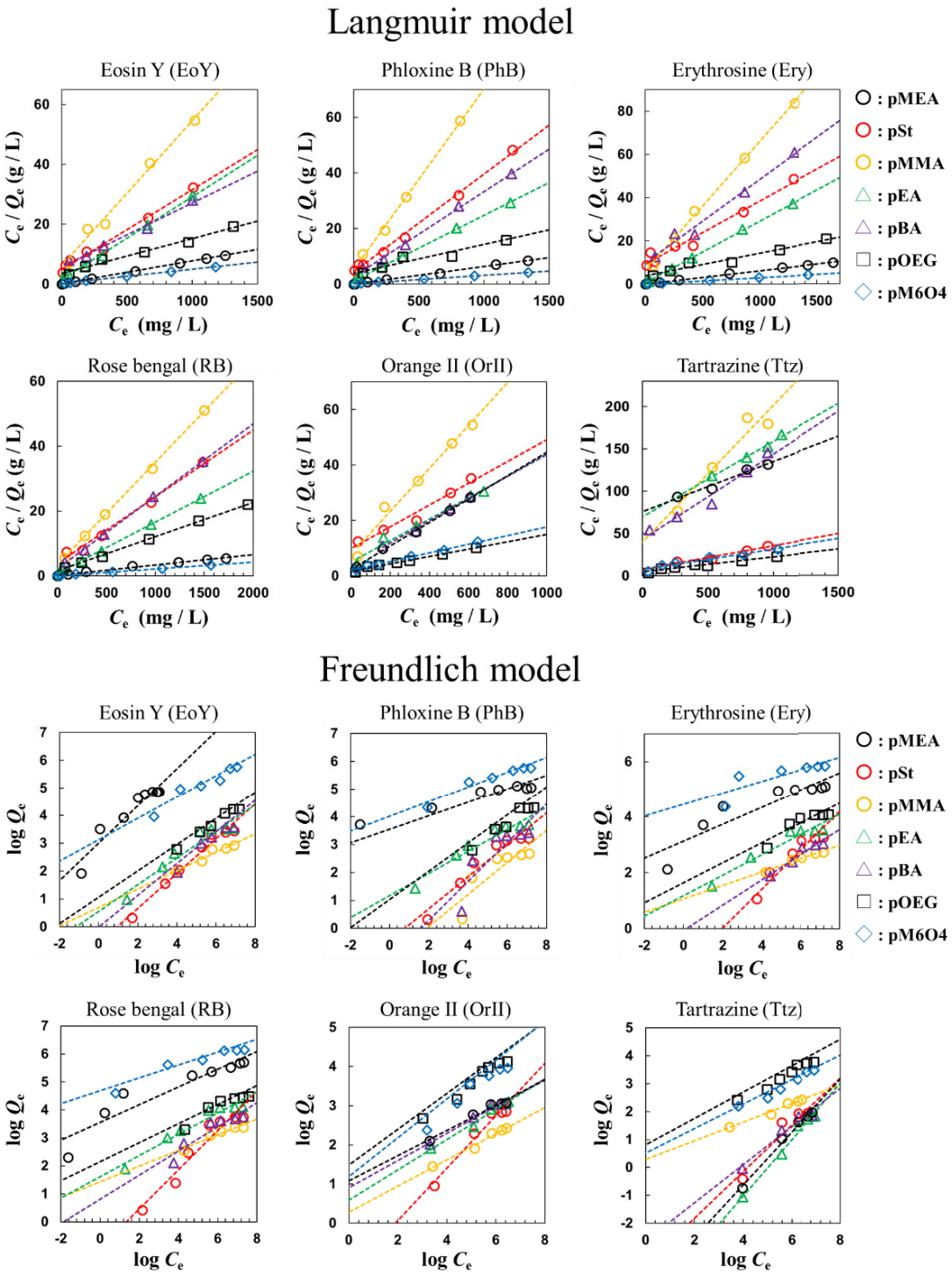

Figure 3.5 Langmuir (top) and Freundlich (bottom) isotherms for the adsorption of the tested dyes onto different microspheres (0.1 wt%) at different initial dye concentrations (25 °C, pH = 7.0).

Table 3.2 Langmuir isotherm parameters for the adsorption of the tested anionic dyes on the solid microspheres at 25 °C.

Dye	Adsorbent[a]	Langmuir				
		Q_m mg / g	$N_{m/s}$[b] μmol / m^2	b L / mg	R_L at 0.1mM	R^2
Rose bengal	pMEA	310	10.9	0.050	0.08	0.9928
	pSt	48.6	2.09	0.008	0.76	0.9888
	pMMA	32.8	2.35	0.007	0.82	0.9964
	pEA	64.3	3.00	0.017	0.59	0.9967
	pBA	47.4	3.42	0.011	0.70	0.9972
Phloxine B	pMEA	157	6.76	0.041	0.13	0.9989
	pSt	30.1	1.58	0.007	0.82	0.9937
Erythrosine	pMEA	163	6.61	0.031	0.21	0.9994
	pSt	32.2	1.60	0.004	0.95	0.9865
Eosin Y	pMEA	131	6.06	0.025	0.28	0.9991
	pSt	29.8	1.88	0.005	0.94	0.9864
Orange II	pMEA	23.7	2.42	0.008	0.76	0.9976
	pSt	25.5	3.18	0.004	0.95	0.9660
Tartrazine	pMEA	15.9	1.03	0.002	0.99	0.9872
	pSt	8.56	0.71	0.006	0.80	0.9937

[a][microspheres] = 0.1 wt%.

[b]$N_{m/s}$ represents the adsorbed moles of dye per total surface area of the tested microspheres.

Table 3.3. Langmuir and Freundlich isotherm parameters for the adsorption (25 °C) of the tested anionic dyes on all microspheres synthesized in this chapter.

		Langmuir						Freundlich		
Dye	Adsorbent[a]	Q_m mg/g	$N_{m/s}$[b] µmol / m^2	$N_{m/v}$[d] µmol / m^3	b L/mg	R_L at 0.1mM	R^2	K_F L/mg	n	R^2
Eosin Y	pMEA	131.2	6.06	21.0	0.025	0.28	0.9991	20.1	3.38	0.9219
	pSt	29.8	1.88	4.78	0.005	0.94	0.9864	0.47	1.48	0.9862
	pMMA	20.7	2.18	3.32	0.008	0.76	0.9883	0.85	1.76	0.9369
	pEA	36.2	2.49	5.81	0.007	0.82	0.9970	1.45	1.87	0.9491
	pBA	39.7	4.21	6.37	0.003	0.98	0.9811	0.16	1.15	0.9297
	pOEG	80.4	N.A.[c]	25.2	0.005	0.94	0.9960	2.55	2.12	0.9860
	pM6O4	211.9	N.A.[c]	66.4	0.028	0.26	0.9966	20.8	2.56	0.9283
Phloxine B	pMEA	157.1	6.76	21.1	0.041	0.13	0.9989	32.9	0.18	0.8810
	pSt	30.1	1.58	4.03	0.007	0.82	0.9937	0.51	1.58	0.9511
	pMMA	14.7	1.29	1.96	0.013	0.66	0.9997	0.29	1.61	0.9338
	pEA	40.7	2.39	5.45	0.011	0.70	0.9839	2.86	2.31	0.9539
	pBA	32.5	2.88	4.35	0.012	0.68	0.9996	0.27	1.40	0.7264
	pOEG	91.9	N.A.[c]	24.0	0.003	0.98	0.9888	2.11	1.98	0.9492
	pM6O4	328.8	N.A.[c]	86.0	0.034	0.18	0.9980	53.0	3.77	0.9410
Erythrosine	pMEA	163.5	6.61	20.6	0.031	0.21	0.9994	23.4	3.40	0.8222
	pSt	32.2	1.6	4.06	0.004	0.95	0.9865	0.21	1.32	0.9719
	pMMA	15.6	1.38	1.97	0.013	0.66	0.9981	0.04	2.20	0.9692
	pEA	35.1	1.9	4.43	0.016	0.61	0.9989	2.90	2.50	0.9507
	pBA	27.3	2.27	3.45	0.008	0.76	0.9989	0.67	2.19	0.9873
	pOEG	65.7	N.A.[c]	16.2	0.008	0.76	0.9973	4.96	2.79	0.8311
	pM6O4	337.2	N.A.[c]	83.1	0.03	0.21	0.9998	83.5	4.78	0.6624
Rose bengal	pMEA	310.7	10.9	33.9	0.05	0.08	0.9928	35.1	3.21	0.8881
	pSt	48.6	2.09	5.30	0.008	0.76	0.9888	0.11	1.43	0.9273
	pMMA	32.8	2.35	3.58	0.007	0.82	0.9964	3.78	3.02	0.8473
	pEA	64.3	3.00	7.02	0.017	0.59	0.9967	4.51	2.42	0.9665
	pBA	47.4	3.42	5.17	0.011	0.70	0.9972	1.62	2.05	0.9353
	pOEG	95.1	N.A.[c]	20.2	0.006	0.80	0.9987	7.71	2.94	0.8572
	pM6O4	475.1	N.A.[c]	101.3	0.039	0.14	0.9982	97.1	4.35	0.9397
Orange II	pMEA	23.7	2.42	7.51	0.008	0.76	0.9976	8.54	3.11	0.9720
	pSt	25.5	3.18	8.08	0.004	0.95	0.9660	0.05	1.47	0.9607
	pMMA	13.0	2.70	4.12	0.009	0.71	0.9815	1.93	3.01	0.9807
	pEA	25.9	3.52	8.21	0.008	0.76	0.9845	3.88	2.59	0.9788
	pBA	23.9	4.02	7.58	0.011	0.70	0.9952	7.98	2.88	0.9780
	pOEG	75.8	N.A.[c]	46.9	0.007	0.82	0.9825	19.2	2.18	0.9732
	pM6O4	64.2	N.A.[c]	39.7	0.008	0.76	0.9937	7.73	2.01	0.9602
Tartrazine	pMEA	15.9	1.03	3.30	0.002	0.99	0.9872	0.01	1.06	0.9601
	pSt	8.56	0.71	1.77	0.006	0.80	0.9937	0.03	1.19	0.9110
	pMMA	6.18	0.84	1.28	0.004	0.95	0.9351	0.04	1.32	0.9203
	pEA	11.2	1.01	2.32	0.001	0.99	0.9905	0.08	0.99	0.9879
	pBA	9.94	1.31	2.06	0.002	0.99	0.9642	0.21	1.46	0.9620
	pOEG	56.6	N.A.[c]	22.9	0.004	0.95	0.9825	19.2	2.12	0.9732
	pM6O4	64.2	N.A.[c]	26.0	0.008	0.76	0.9937	7.73	2.01	0.9602

[a][microspheres] = 0.1 wt%.
[b]$N_{m/s}$ represents the adsorbed moles of dye per total surface area of the tested microspheres.
[c]$N_{m/s}$ could not be determined, as it is difficult to determine the surface area of the microgels.
[d]$N_{m/v}$ represents the adsorbed moles of dye per total volume of the tested microsphere. The specific volume of the pOEG and pM6O4 microgels was calculated based on the assumption that the fully swollen microgels contain ~80% water.

In this chapter, all R_L values of the tested microspheres for halide-containing dyes at 0.1 mM were < 1, suggesting a favorable adsorption (**Tables 3.2** and **3.3**). The author found that the hydrophobic interactions between the anionic Ery and the hydrophobic domain that is composed of isopropyl groups in the anionic pNIPAm microgels are affected by the uptake of Ery at high temperature, where the microgels exhibit a volume transition.[12] Similar to the present case, hydrophobic interactions should occur between the tested dyes and the microspheres, which consist of hydrophobic polymers. In this case, the anionic dye Ttz was used for the adsorption experiment, as Ttz exhibits the lowest octanol-water partition coefficient (log K_{ow}), which is a measure of the hydrophobicity, (log K_{ow} Ttz ~ -10.2; log K_{ow} RB ~ 3.14; **Figure 3.2**). At the same concentration, the quantity of Ttz adsorbed by the solid microspheres was smaller than those of the other halide dyes (**Figure 3.4a**). A similar behavior was also observed for OrII.

Conversely, pure pMEA microspheres adsorbed much higher quantities of halide dyes than other solid microspheres at the same dye concentration (**Figure 3.4a**), resulting in facile staining of the pMEA paste with e.g. the red color of Ery after centrifugation (**Figure 3.4b**). Although the R_L values of the pMEA microspheres for the halide dyes were close to 0 (e.g. R_L ~ 0.08 for pMEA at 0.1 mM RB, R_L ~ 0.76 for pSt at 0.1 mM RB; **Table 3.2**), the quantities of anionic OrII and Ttz, which do not contain halogen atoms, adsorbed by pMEA were almost identical to those adsorbed by the other solid microspheres (**Figure 3.4a**). Additionally, the $N_{m/s}$ of the pMEA for the halide dyes was three to four times higher than those of the other solid microspheres (**Table 3.2**). These results suggest that the specific adsorption, i.e., the halogen bonding, occurred between the surface of the pMEA microspheres and the halide dyes.

Metrangolo and Resnati *et al.* have investigated the driving force for formation of supramolecular architectures that are caused by hydrogen or halogen bonding.[13] They found that the ability of halogen bonding may overpower hydrogen bonding in a cooperative hydrogen-bonded network of non-covalent copolymers in aqueous solution, and that oxygen atoms can form strong halogen bonds that successfully rival the hydrogen bonds in controlling the self-assembly of organic compounds. Based on these results, the author speculated that the oxygen atom of the methoxy group in pMEA may be able to interact with the halogen atoms of the halide dyes in aqueous solution by replacing the intermediate water with hydrogen bonds.[4-6] Moreover, as expected, the R_L values of the halide dyes (0.1 mM) for pMEA microspheres followed the ordered EoY (~ 0.24) > Ery (~ 0.21) > PhB (~ 0.13) > RB (~ 0.08) (**Table 3.2**). This order is consistent with the reported characteristics of the halogen bonding[9-11] and supports our hypothesis, i.e., the reversibility of the adsorption of RB is

lower than in other halide dyes on account of i) the higher number of halogen atoms in RB compared to those in EoY and Ery, and ii) the strength of the halogen bonding of the iodine atoms in RB should be higher than that of the bromine atoms of e.g. PhB (**Figure 3.2**).

The strong halogen bonding between pMEA and the halide dyes was also confirmed by the desorption behavior. As maximum adsorption was observed at 25 °C in the presence of 1 mM of dyes, pMEA microspheres (0.1 wt%) were subjected to these conditions prior to evaluating the desorption behavior of the dyes. **Figure 3.6a** shows the quantities of released halide dyes from the surface of the pMEA microspheres as a function of temperature, indicating that the halide dyes remained strongly attached to the pMEA surface, even at 70 °C. This result supports the fact that R_L is close to 0, i.e., that the adsorption should be irreversible (**Table 3.2**).

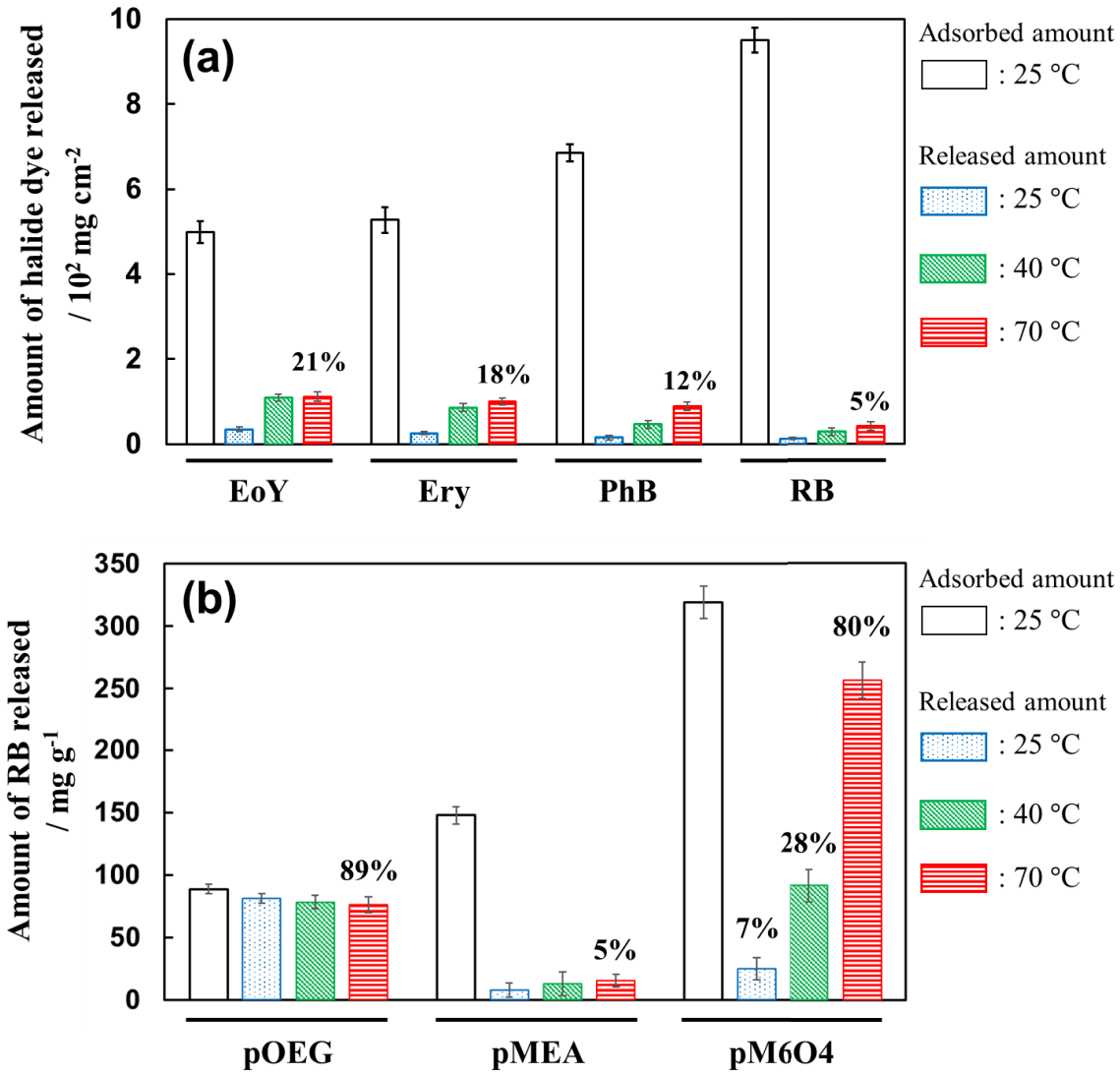

Figure 3.6 (a) Released amounts of halide dyes per unit surface area of pMEA microspheres as a function of temperature. (b) Released amounts of RB per unit gram of pOEG, pMEA, and **pM6O4** microgels as a function of temperature. The white bars at the left of each dye and microsphere represent the adsorbed amounts of dye at 25 °C.

3.3.2. Synthesis of pMEA Nanocomposite Hydrogel Microspheres

In order to increase the release efficiency by temperature induced dehydration of the gel components, pMEA domains were incorporated into thermo-responsive microgels. The author focused on the use of the PEG-analogue poly(oligo ethylene glycol methacrylate) (pOEG) as the microgel backbone, as pOEG displays a lower critical solution temperature (LCST) in water,[14] and as pOEG-based bulk materials and microgels display all the advantageous non-immunogenic, noncytotoxic, and protein-repellent properties of PEG,[15,16] which should offer the possibility to use such microgels *in*

vivo. These nanocomposite microgels were synthesized by precipitation copolymerization. For this purpose, OEG with an ethylene oxide chain length of 5 or 6 was selected as a comonomer, as the LCST of pOEGs is ~ 64 °C,[14,17] and the volume transition temperature of p(MEA-*co*-OEG) can be tuned by changing the monomer ratio (mol%) of OEG and MEA. The synthetic protocols for the preparation of various pMEA composite microgels are listed in **Table 3.4** (denoted as pMXOY, whereby M and O represent MEA and OEG, respectively, while X and Y refer to the molar feed ratios of MEA and OEG during the polymerization.).

Table 3.4 Synthesis conditions used and properties of the resulting p(MEA-*co*-OEG) microgels

Microgels	Monomer concentration (mM)	MEA	OEG (mol%)	EGDMA	KPS (mM)	D_h at 25 °C [a]	D_h at 40 °C [a]	D_h at 70 °C [a]	D_h at 85 °C [a]	Swelling ratio, α [b]	Yield [c] (%)
						(nm)					
pOEG	150	0	99	1	2	332	314	218	131	16.5	87
pM5O5	100	50	49	1	2	1121	1098	458	358	31.4	79
pM6O4	100	60	39	1	2	840	698	250	248	38.1	88
pM7O3	100	70	29	1	2	564	485	197	195	23.8	90
pM8O2	100	80	19	1	2	238	178	107	106	11.2	86
pM9O1	100	90	9	1	2	113	95	93	92	1.89	85

[a]Measured for microspheres dispersed in sodium phosphate buffer (80 mM) at pH = 7.0.
[b]The swelling ratio is defined by: $\alpha = R_h^3$ at 25 °C / R_h^3 at 85 °C, where the tested composite microgels were deswollen completely.
[c]The yield was calculated using a dry-weight method of microsphere dispersions after purification.

As evident from the AFM images (**Figure 3.7**), p(MEA-*co*-OEG) microgels were successfully prepared for all monomer ratios using ethylene glycol dimethacrylate (EGDMA) (1 mol%) as the cross-linker. However, different morphologies were observed for the ratios. Especially substrate-adsorbed **pM6O4** microgels dried at 25 °C formed dotted nanospheres in the entire microspheres (**Figure 3.8a, left**), which suggests that the MEA segments initially copolymerized randomly, before they subsequently aggregated locally in **pM6O4** microgels after removal of the water. Moreover, the dotted nanospheres were surely incorporated in the microgels, which was confirmed by drying the sample at 70 °C, where the composite microgels were highly deswollen (**Figure 3.8a, right**). As a result, the shape of microgels was became spherical, suggesting that the pMEA domain were taken into the whole microgels. Therefore, the author concluded that these dotted nanospheres (**Figure 3.8a, left**) were composed of hydrophobic pMEA, and were incorporated in pOEG gel networks.

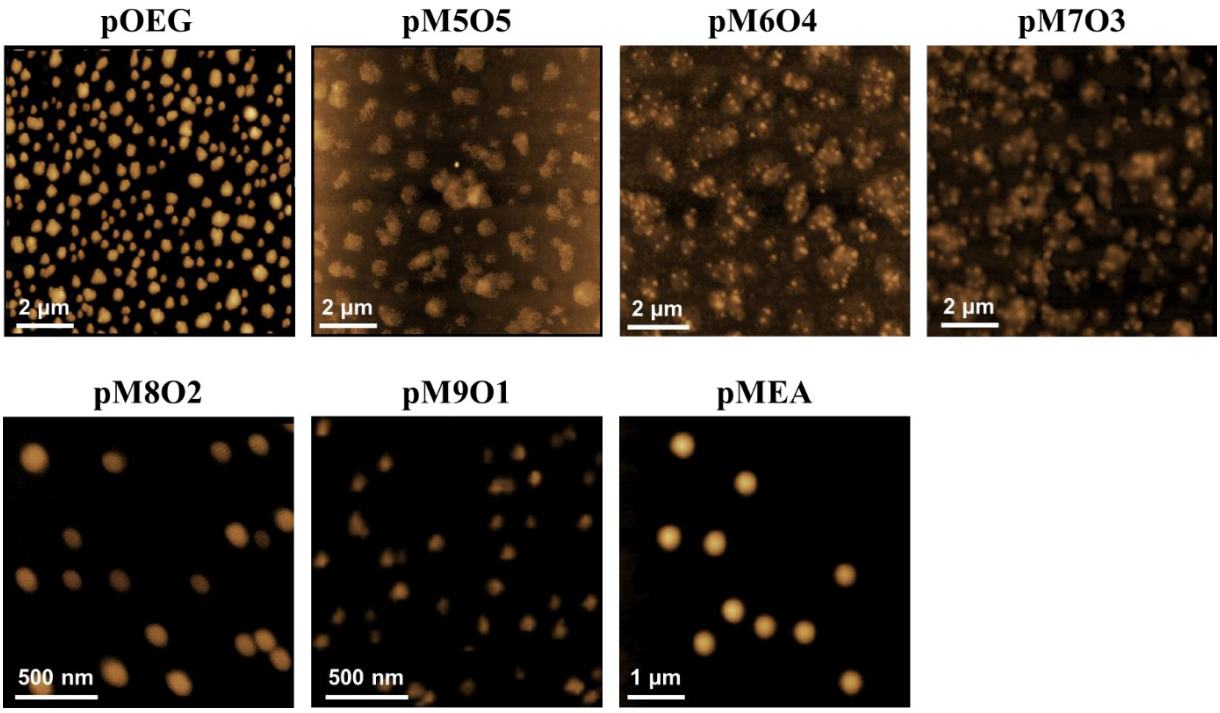

Figure 3.7. AFM images of p(MEA-*co*-OEG) microgels obtained from different monomer feed ratios (mol%) of MEA and OEG during the copolymerization.

This stands in contrast to the behavior of other dried p(MEA-*co*-OEG) microgels, which afford homogenous spherical shapes similar to pure pMEA or pOEG microgels such as **pM5O5** or **pM8O2** (**Figure 3.7**). Moreover, upon increasing the feeding monomer ratio of MEA, the thermo-responsiveness of the p(MEA-*co*-OEG) microgels was almost lost according to the results of DLS measurements (e.g. **pM9O1**: D_h ~ 114 nm at 25 °C and D_h ~ 91 nm at 85 °C; **Figure 3.8b**), under concomitant decrease of the swelling ratio ($\alpha = R_h^3$ at 25 °C / R_h^3 at 85 °C; **Table 3.4**). Notably, *N*-isopropyl acrylamide (NIPAm) and acrylamide (AAm), which are the most typical monomers as gel components, were also selected as the comonomer. However, the synthesis of the corresponding microgels was unsuccessful when MEA and NIPAm or AAm were used in a ratio of 1:1 (**Figure 3.9**). This may be due to the fact that the LCST of p(MEA-*co*-NIPAm) and p(MEA-*co*-AAm) is lower or higher, respectively, compared to that of p(MEA-*co*-OEG). Accordingly, the critical chain length for the globule state should be too short or too long to form stable nuclei for the formation of the microspheres during the copolymerization of NIPAm or AAm with MEA.

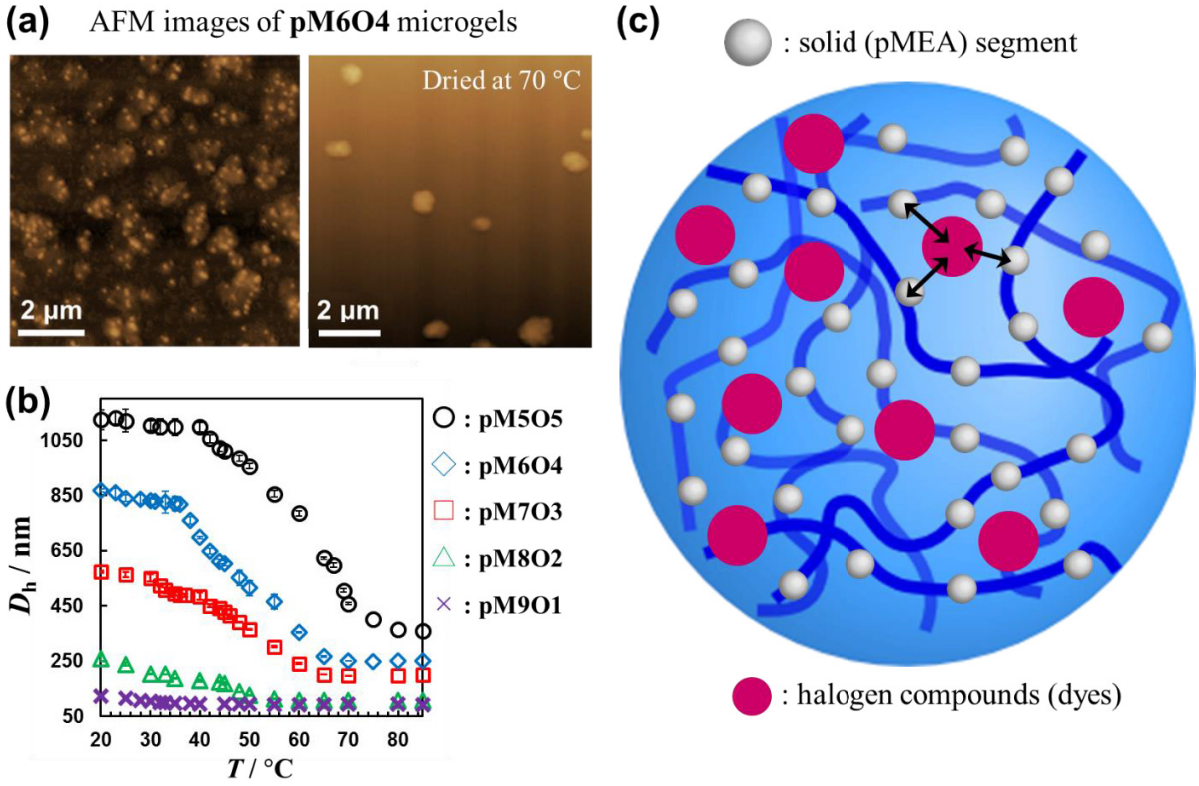

Figure 3.8. (a) AFM images of **pM6O4** microgels dried at 25 °C (left) and 70 °C (right). (b) The hydrodynamic diameter (D_h) of a series of p(MEA-*co*-OEG) microgels as a function of the temperature. The displayed sample code for each microgel corresponds to those listed in **Table 3.4**. (c) Schematic diagram of the swollen **pM6O4** nanocomposite microgels in the presence of halogen compounds.

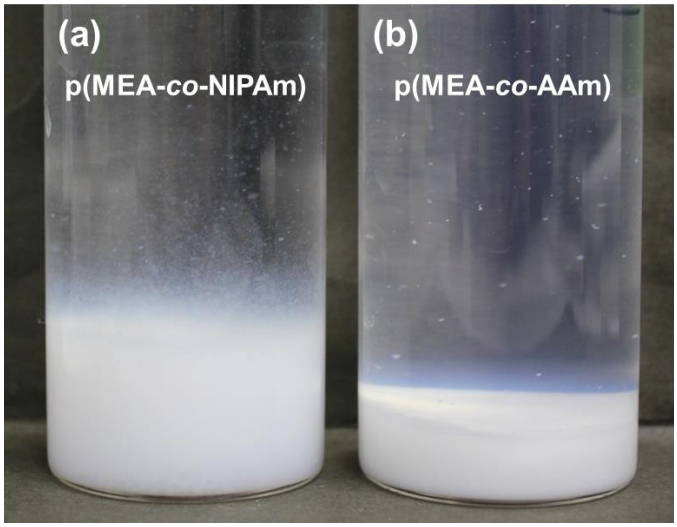

Figure 3.9 Photographs of samples obtained from precipitation copolymerization of MEA with (a) NIPAm or (b) AAm. When aggregates were observed during the polymerizations, stable microgels were not obtained.

However, the author expected **pM6O4** microgels to be suitable for the reversible selective adsorption and release of halogen compounds, given that their D_h values changed in a wide temperature range (**Figure 3.8b**), which allowed us to control the physical properties of the **pM6O4** microgels. In addition, different from poly(NIPAm-*co*-acrylic acid) microgels, which exhibited a decreased D_h as a result of the electrostatic interaction between the microgels and cationic dye molecules,[18] the D_h of the **pM6O4** microgels did not decrease in the presence of RB, and the swelling ratio was not significantly affected (**Figure 3.10**), which indicates that the pMEA domains suppress the loss of thermo-responsiveness of the entire microgels as intended. Here, although the hydrophobic MEA segments could be expected to suppress the swelling of composite microgels, the swelling ratios of **pM5O5** and **pM6O4** microgels were larger than those of pure pOEG microgels (**Table 3.4**). In addition, the quantities of RB that were adsorbed by a series of p(MEA-*co*-OEG) microgels for the same concentrations of microgel (0.1 wt%) and RB (1 mM) decreased with increasing monomer ratio of MEA during the copolymerization (**Figure 3.11**). These results suggest that the MEA segments act effectively as adsorption points due to the diffusion of RB into the inside of the nanocomposite microgels, and that the copolymerized MEA segments are dissolved in the microgels at the molecular level, which results in the increase of the effective adsorption area (**Figure 3.7c**).

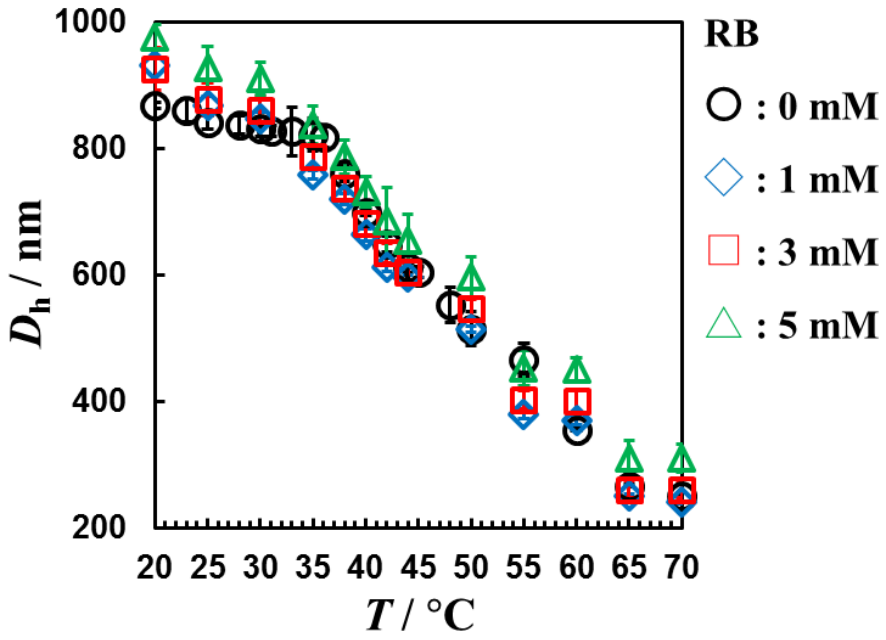

Figure 3.10 Hydrodynamic diameters (D_h) of **pM6O4** microgels (0.1 wt%) at various concentrations of RB: 0 mM (black circles), 1 mM (blue diamonds), 3 mM (red squares), and 5 mM (green triangles).

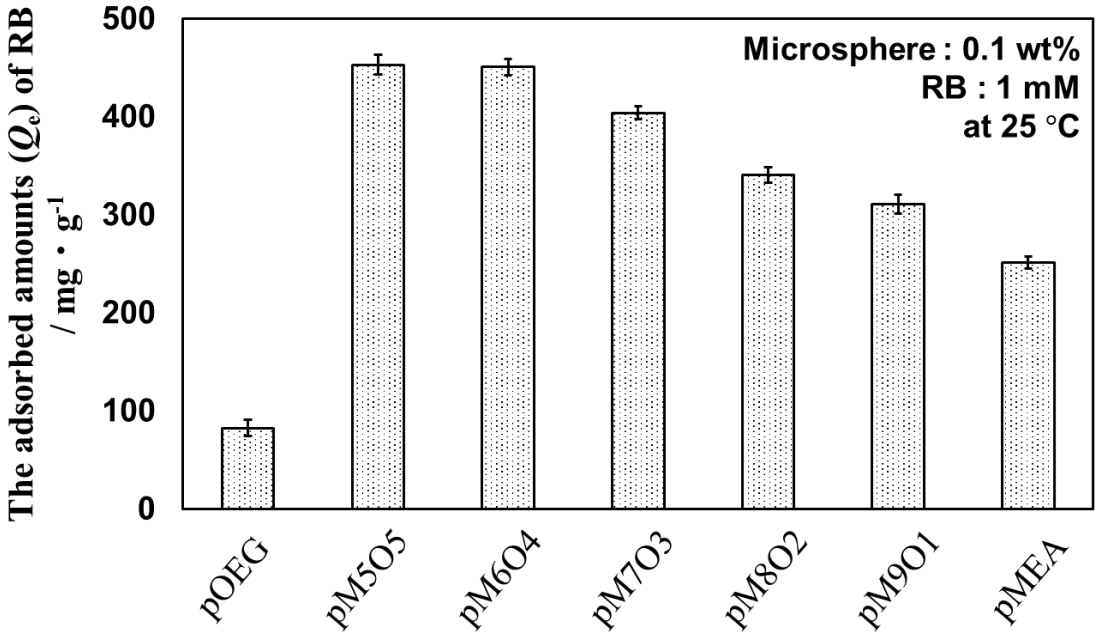

Figure 3.11 Quantities of RB adsorbed at 25 °C by a series of p(MEA-*co*-OEG) microgels at the same concentrations of microgel (0.1 wt%) and RB (1 mM). Each bar represents an average of three replicate experiments, and the error bars denote the standard deviations.

Even though the RB uptake in the **pM5O5** microgels was almost identical to that in **pM6O4**, the D_h did not change significantly upon increasing the temperature to 50 °C (**Figure 3.8b**), suggesting that the number of OEG segments was higher in **pM5O5** than in **pM6O4**, and that the volume transition temperature increased. As a result, the swelling ratio of **pM5O5** was slightly smaller than that of **pM6O4** (**Table 3.4**). It should also be noted that although the polymerization mechanisms of this series of p(MEA-*co*-OEG) microgels still remains unclear so far, the author observed excellent separation behavior towards halogen compounds for **pM6O4** microgels.

3.3.3. Adsorption Behavior of Halogen Compounds in Nanocomposite Hydrogel Microspheres

The dye-adsorption behavior of the **pO6M4** composite microgel was investigated in terms of its isotherm (**Figures 3.4a** and **3.5**), and the obtained isotherm parameters are shown in **Table 3.5** and **Table 3.3**. In this case, the Q_m values determined by the Langmuir model were also normalized as moles of dye per total volume of tested microsphere ($N_{m/v}$ in μmol/m^3) to avoid potential problems in those cases where it is impossible to determine the surface area of the pOEG and pM6O4 microgel adsorption behavior. Except for pMEA, pure pOEG microgels were able to adsorb higher quantities of the tested halide dyes per unit gram than the solid microspheres (**Figure 3.4a**), indicating that the

dyes, which were dissolved in water, diffused into the microgel network and adsorbed onto the microgels.

Among the tested microspheres, which include pure pMEA, the highest adsorption capacity (Q_m) for halide dyes was observed for **pM6O4** microgels (**Figure 3.4a** and **Table 3.5**), although the total size of the pMEA microspheres was smaller than that of **pM6O4** microgels in water (e.g. pMEA: D_h ~ 214 nm; **pM6O4**: D_h ~ 840 nm at 25 °C). This result suggests that the effective adsorption area of the copolymerized pMEA segment was larger than that of pure pMEA at the same weight (0.1 wt%). It is noteworthy that these dyes were adsorbed by the swollen, pOEG-rich domains in **pM6O4** similar to pure pOEG microgels, which resulted in an increased uptake. However, the R_L values for the halide dyes were close to those for pure pMEA (**Table 3.5**), which could be explained by the fact that the pMEA domain incorporated in the composite microgel inherits the properties of the pure pMEA microsphere.

Moreover, it seems that the crosslink density does not significantly affect the uptake and release behavior toward e.g. for RB, considering that highly crosslinked **pM6O4** microgels (**pM6O4E5**; constant 5 mol% EGDMA during the polymerization) exhibit a behavior similar to **pM6O4** microgels (**Figure 3.12**).

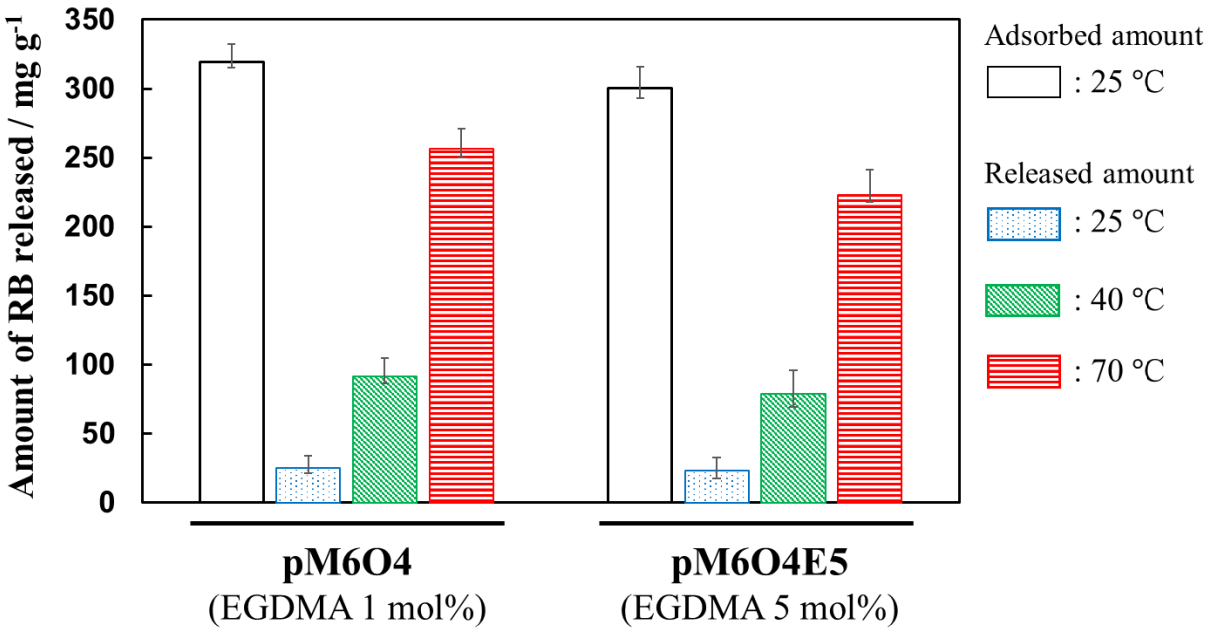

Figure 3.12 Adsorbed and released quantities of RB per unit gram of **pM6O4** and **pM6O4E5** microgels as a function of temperature. The white bars at the left of each dye and microgels represent the incorporated quantities of dye at 25 °C.

Table 3. Langmuir isotherm parameters for the adsorption of the tested anionic dyes on solid and hydrogel microspheres at 25 °C.

		Langmuir				
Dye	Adsorbent[a]	Q_m mg/g	$N_{m/v}$[b] μmol / m^3	b L/mg	R_L at 0.1mM	R^2
Rose bengal	pMEA	310	33.9	0.050	0.08	0.9928
	pOEG	95.1	20.2	0.006	0.80	0.9987
	pM6O4	475	101.3	0.039	0.14	0.9982
Phloxine B	pMEA	157	21.1	0.041	0.13	0.9989
	pOEG	91.9	24.0	0.003	0.98	0.9888
	pM6O4	328	86.0	0.034	0.18	0.9980
Erythrosine	pMEA	163	20.6	0.031	0.21	0.9994
	pOEG	65.7	16.2	0.008	0.76	0.9973
	pM6O4	337	83.1	0.030	0.21	0.9998
Eosin Y	pMEA	131	21.0	0.025	0.28	0.9991
	pOEG	80.4	25.2	0.005	0.94	0.9960
	pM6O4	211	66.4	0.028	0.26	0.9966
Orange II	pMEA	23.7	7.51	0.008	0.76	0.9976
	pSt	25.5	8.08	0.004	0.95	0.9660
	pOEG	75.8	46.9	0.007	0.82	0.9825
	pM6O4	64.2	39.7	0.008	0.76	0.9937
Tartrazine	pMEA	15.9	3.30	0.002	0.99	0.9872
	pSt	8.56	1.77	0.006	0.80	0.9937
	pOEG	56.6	22.9	0.004	0.95	0.9825
	pM6O4	64.2	26.0	0.008	0.76	0.9937

[a][microspheres] = 0.1 wt%.

[b]$N_{m/v}$ represents the adsorbed moles of dye per total volume of tested microsphere. The specific volume of the pOEG and pM6O4 microgels was calculated based on the assumption that the fully swollen microgels contain ~80% water.

3.3.4. Releasing Halogen Compounds from Nanocomposite Hydrogel Microspheres

Under the same conditions as for the pure pMEA microspheres, the **pM6O4** microgels also exhibited a controlled release of the halogen dyes (**Figure 3.6a**). The most strongly interacting dye with pMEA in this study is RB, and the released amounts of RB per unit gram are shown in **Figure 3.6b**. In the case of pOEG microgels, in the absence of halogen bonding, ~ 90% of the dyes were released by a single washing regardless of the release temperature.

Similar to pure pMEA microspheres, the release efficiency of RB from **pM6O4** was low (7%) at 25 °C, due to the strong interactions. Surprisingly, at 40 °C, where the **pM6O4** microgels are

partially deswollen (**Figure 3.8b**), the release efficiency of RB increased to 28% (**Figure 3.6b**), and a release efficiency of ~ 90% was achieved after four washings at 40 °C. Furthermore, at 70 °C, where the **pM6O4** microgels are drastically deswollen, the release efficiency reaches ~ 80% with a single washing, even though pure pMEA microspheres release the dyes only sparingly. Indeed, the deswollen pOEG domains in the nanocomposite microgels did not seem to hamper the release of RB upon increasing the temperature from 40 to 70 °C. Considering that the D_h of pOEG microgels decreases (**Table 3.4**), the amounts of RB adsorbed by pure pOEG should decrease accordingly (**Figure 3.13**). The release behavior will be discussed in **Chapter III** described below.

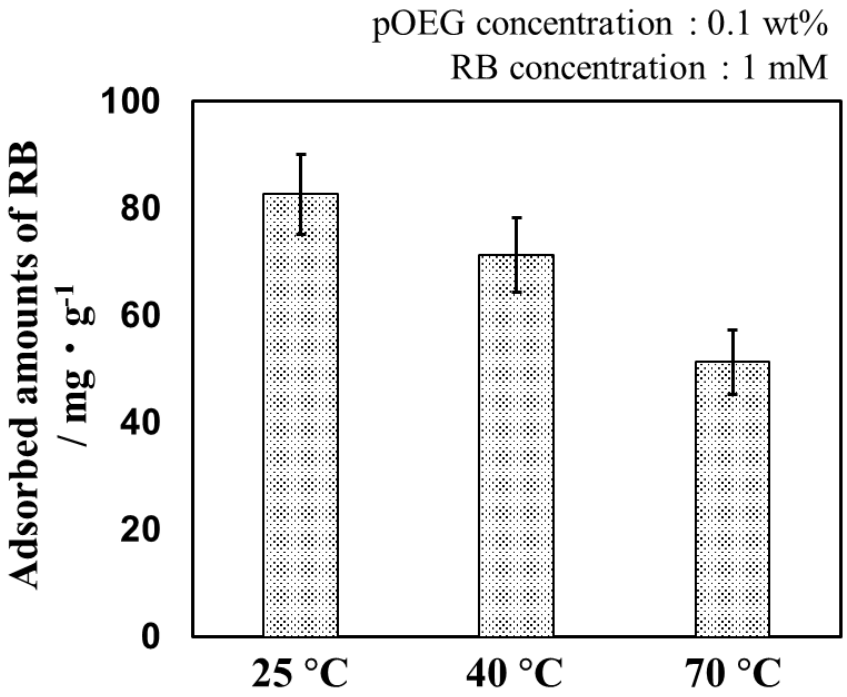

Figure 3.13 Quantities of RB adsorbed by pOEG microgels (0.1 wt%) at different temperatures ([RB] = 1 mM). Each value represents an average of three replicate experiments, and the error bars denote the standard deviations.

3.3.5. Selective Adsorption on Nanocomposite Hydrogel Microspheres and Applications

Halogen bonding in **pM6O4** microgels allows a selective separation of halide dyes in the presence of several other halogen-free anionic dyes. Anionic RB was selected as a target halide-containing dye, and anionic EoY, OrII, and Ttz were selected as competitive inhibitors for the uptake of RB (**Table 3.5**). The visible absorption spectrum of a mixture of these four dyes is shown in **Figure 3.14a**. It should be noted that the exact uptake of each dye cannot be quantified using the calibration

curve derived from the absorption spectrum of the dye mixture, due to the overlap of absorption peaks when Ery and PhB are employed.

Figure 3.15 shows the uptake rate of the tested dyes by **pM6O4** microgels (0.1 wt%), indicating that the adsorbed amount of RB was highest when the concentrations of all dyes were comparable. When each dye concentration is 2 mM, the uptake of RB accounts for ~ 91% of all dyes once the microgels reach the saturated adsorption state with respect to RB (**Figure 3.4a**). For low dye concentrations, the halide-containing dye EoY was also preferentially adsorbed on **pM6O4** compared to OrII and Ttz (e.g. EoY: ~ 23% at 0.1 mM and ~ 11% at 0.5 mM), suggesting that halogen bonding also occurs between EoY and the **pM6O4** microgels via the residues of the pMEA domain that are not involved in the adsorption of RB.

Finally, the author demonstrate an application by exploiting the high formability of **pM6O4** microgels: although the pure pOEG microgels cannot form the free-standing film, a free-standing **pM6O4** microgel film can be obtained by evaporating the water from a dispersion in the absence of a cross-linker for bonding between the microgels (**Figure 3.15b**). This result indicates that the interdiffusion between the soft and deformable pMEA domains serves as a physical cross-linking point for the whole film due to their rubber-like properties that are similar to pure pMEA microspheres as described in the **chapter I** (**Figure 2.11**). In addition to the formation of a film, a simplified column, packed with **pM6O4** microgel powder obtained from freeze drying in a Pasteur pipette, showed that RB can be removed effectively from a contaminated water sample (V = 2 mL; $[RB]_{initial}$ = 1 mM; $[RB]_{final} = 4.5 \times 10^{-5}$ mM; t = 5 min; **Figures 3.15c** and **3.14b**), despite the fact that this cannot be observed when using a pure pMEA microsphere column under identical conditions (**Figure 3.14c**). In contrast, when using pMEA powder, the flow of a similar RB solution was hampered and complete draining of the water required ~ 2 hours, while the efficiency of the removal of RB was decreased ($[RB]_{final}$ = ~ 0.4 mM). This result suggests that the specific adsorption area for RB in **pM6O4** is larger than that in the pMEA microspheres. Thus, it should be the hydrophilic gel domains that afford the benefits to the pMEA domains, i.e., stimuli-responsiveness, high dispersion stability, and water passage.

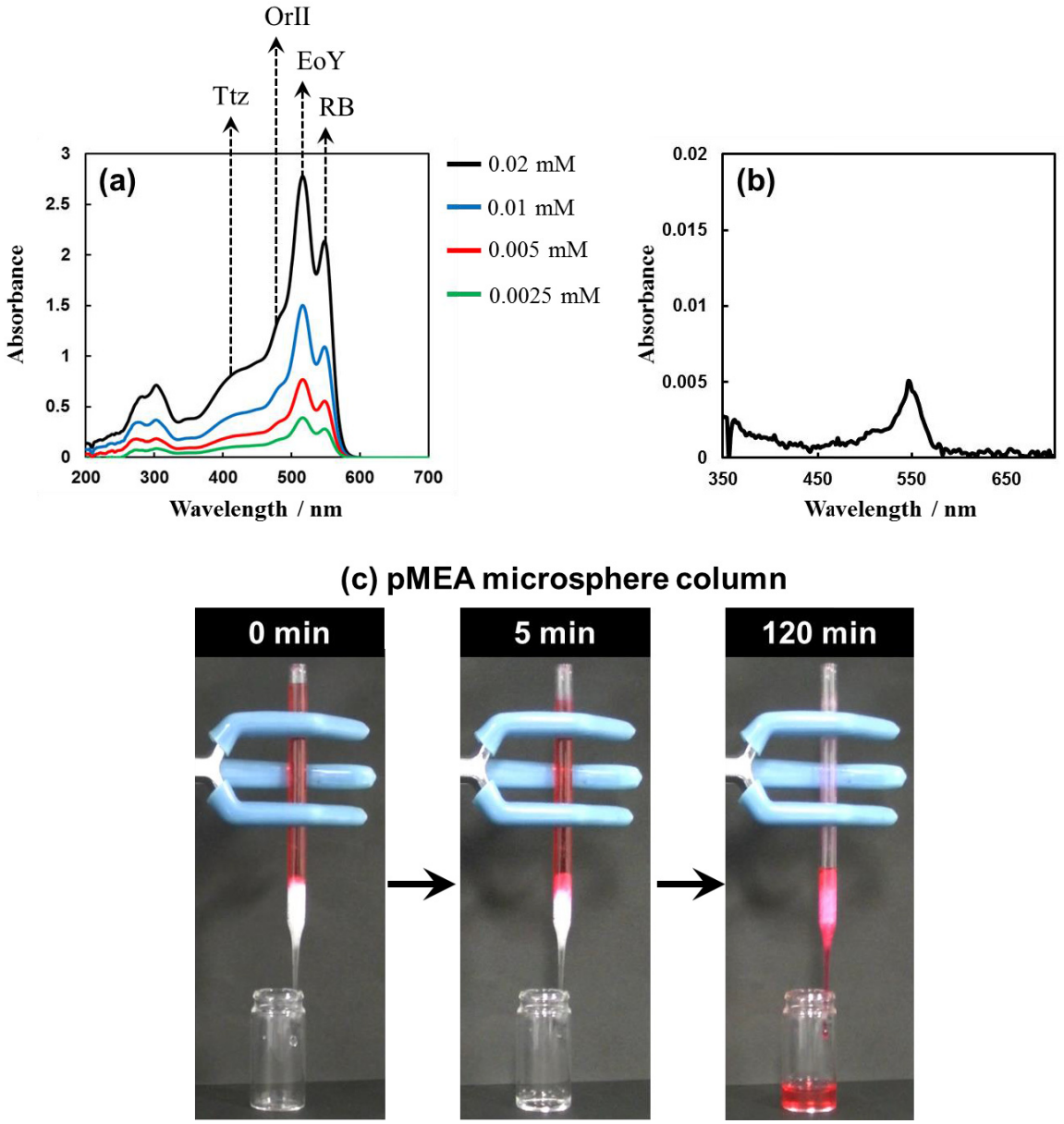

Figure 3.14 (a) UV-vis spectra of dye mixtures of RB, EoY, OrII, and Ttz at several concentrations in SPB buffer (pH = 7.0) measured at 25 °C for the calculation of the adsorbed quantities of dyes in the selective adsorption experiments. The arrows represent the maximum wavelength for each dye. (b) UV-vis spectra of the extracted water obtained from the column adsorption experiment (**Figure 3.15c**). The absorbance of RB measured by the UV-vis spectrophotometer is not clearly visible due to the detection limit, indicating that [RB] ≤ 4.5×10^{-5} mM. (c) The photographs of the column packed with the powder of pMEA microspheres (0.05 g) before and after the extraction of an RB solution (1 mM, 2 mL). The concentration of RB in the extracted water is ~ 0.4 mM.

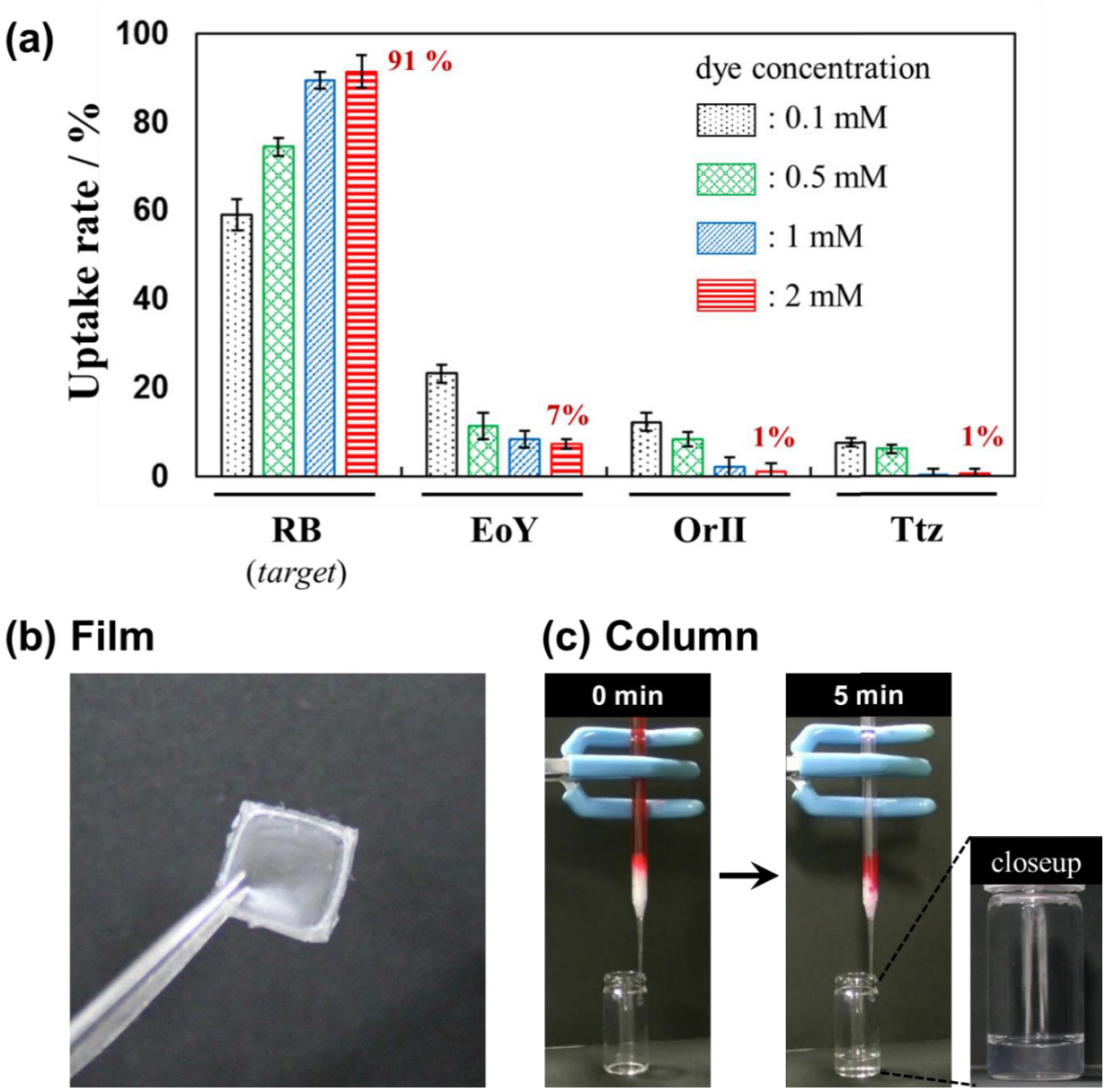

Figure 3.15 (a) Uptake rate for each dye by **pM6O4** microgels at different initial concentrations of dye mixtures at 25 °C. Photographs of (b) a **pM6O4** film (injection weight: 50 mg; template: 10 × 10 × 1 mm^3) after removal from the template, and (c) columns packed with **pM6O4** microgel powder before and after the extraction of an aqueous RB solution (1 mM).

3.4. Conclusions

The concept of halogen bonding was applied for the first time in polymer microsphere systems. Microspheres consisting of pMEA exhibited the capability of halogen bonding in water without the need for prior surface modifications. The adsorption isotherms of several anionic dyes showed that the methoxy groups in the pMEA side chains play an important role for the halogen bonding, resulting in strong adsorption of halide-containing dyes on the anionic pMEA microsphere surfaces. In addition, nanocomposite microgels with pMEA domains were prepared by precipitation copolymerization of MEA and OEG. The solid nanodomains suppressed deswelling in the presence of the target compounds, and control over the volume transition temperature of the whole microgels was possible upon copolymerization, which permitted a controlled release of the halide-containing dyes by changing the temperature. These nanocomposite microgels may thus be suitable for various applications, including the formation of microgel films and columns, due to the high formability and ease of handling. These results indicate that such nanocomposite microgels with solid domains as halogen bonding points should represent an important first step towards a new generation of separation materials for halogen-containing compounds.

3.5. References

1. Langmuir, I. THE CONSTITUTION AND FUNDAMENTAL PROPERTIES OF SOLIDS AND LIQUIDS. II. LIQUIDS. *J. Am. Chem. Soc.* **1917**, *39*, 1848-1906.
2. Weber, T. W.; Chakravarty, R. K. Pore and solid diffusion models for fixed-bed adsorbers. *Am. Inst. Chem. Eng. J*. **1974**, *20*, 228-238.
3. Freundlich, H. Über Die Adsorption in Lösungen Z. *Z. Phys. Chem*. **1906**, *57*, 385-470.
4. Tanaka, M.; Motomura, T.; Kawada, M.; Anzai, T.; Kasori, Y.; Shiroya, T.; Shimura, K.; Onishi, M.; Mochizuki, A. Blood compatible aspects of poly(2-methoxyethylacrylate) (PMEA)—relationship between protein adsorption and platelet adhesion on PMEA surface. *Biomaterials* **2000**, *21*, 1471-1481.
5. Tanaka, M.; Mochizuki, A. Clarification of the Blood Compatibility Mechanism by Controlling the Water Structure at the Blood–Poly(meth)acrylate Interface. *J. Biomater. Sci. Polym. Ed*. **2010**, *21*, 1849-1863.
6. Hirata, T.; Matsuno, H.; Kawaguchi, D.; Hirai, T.; Yamada, N. L.; Tanaka, M.; Tanaka, K. Effect of Local Chain Dynamics on a Bioinert Interface. *Langmuir* **2015**, *31*, 3661-3667.
7. Melle, A.; Balaceanu, A.; Kather, M.; Wu, Y.; Gau, E.; Sun, W.; Huang, X.; Shi, X.; Karperiend, M.; Pich, A. Stimuli-responsive poly(*N*-vinylcaprolactam-*co*-2-methoxyethyl acrylate) core–shell microgels: facile synthesis, modulation of surface properties and controlled internalisation into cells. *J. Mater. Chem. B* **2016**, *4*, 5127-5137.

8. Kureha, T.; Hiroshige, S.; Matsui, S.; Suzuki, D. Water-immiscible bioinert coatings and film formation from aqueous dispersions of poly(2-methoxyethyl acrylate) microspheres. *Colloid. Surf. B* **2017**, *155*, 166-172.
9. Lommerse, J. P. M.; Stone, A. J.; Taylor, R.; Allen, F. H. The Nature and Geometry of Intermolecular Interactions between Halogens and Oxygen or Nitrogen. *J. Am. Chem. Soc*. **1996**, *118*, 3108-3116.
10. Politzer, P.; Lane, P.; Concha, M. C.; Ma, Y.; Murray, J. S. An overview of halogen bonding. *J. Mol. Model*. **2007**, *13*, 305-311.
11. Erdélyi, M. Halogen bonding in solution. *Chem. Soc. Rev*. **2012**, *41*, 3547-3557.
12. Kureha, T.; Sato, T.; Suzuki, D. Relationship between Temperature-Induced Changes in Internal Microscopic Structures of Poly(*N*-isopropylacrylamide) Microgels and Organic Dye Uptake Behavior. *Langmuir* **2014**, *30*, 8717-8725.
13. Corradi, E.; Meille, S. V.; Messina, M. T.; Metrangolo, P.; Resnati, G. Halogen Bonding versus Hydrogen Bonding in Driving Self-Assembly Processes. *Angew. Chem*. **2000**, *112*, 1852-1856.
14. Sun, S.; Wu, P. On the Thermally Reversible Dynamic Hydration Behavior of Oligo(ethylene glycol) Methacrylate-Based Polymers in Water. *Macromolecules* **2013**, *46*, 236-246.
15. Smeets, N. M.; Bakaic, E.; Patenaude, M.; Hoare, T. Injectable and tunable poly(ethylene glycol) analogue hydrogels based on poly(oligoethylene glycol methacrylate). *Chem. Commun*. **2014**, *50*, 3306-3309.
16. Zhang, J.; Muirhead, B.; Dodd, M.; Liu, L.; Xu, F.; Mangiacotte, N.; Hoare, T.; Sheardown, H. An Injectable Hydrogel Prepared Using a PEG/Vitamin E Copolymer Facilitating Aqueous-Driven Gelation. *Biomacromolecules* **2016**, *17*, 3648-3658.
17. Maeda, Y.; Kubota, T.; Yamauchi, H.; Nakaji, T.; Kitano, H. Hydration Changes of Poly(2-(2-methoxyethoxy)ethyl Methacrylate) during Thermosensitive Phase Separation in Water. *Langmuir* **2007**, *23*, 11259-11265.
18. Kureha, T.; Shibamoto, T.; Matsui, S.; Sato, T.; Suzuki, D. Investigation of Changes in the Microscopic Structure of Anionic Poly(*N*-isopropylacrylamide-*co*-Acrylic acid) Microgels in the Presence of Cationic Organic Dyes toward Precisely Controlled Uptake/Release of Low-Molecular-Weight Chemical Compound. *Langmuir* **2016**, *32*, 4575-4585.
19. Brandrup, J.; Immergut, E. H.; Grulke, E. A. *Polymer Handbook*, 4th ed.; Wiley: New York, 1999; Vol. I, p193.

4. Chapter III

"Controlled Separation of Organoiodine Compounds using pMEA Analogue Microspheres"

*Part of this work was published in *ACS Omega*. Reprinted with permission from Kureha, T.; Nishizawa, Y.; Suzuki, D. Controlled Separation and Release of Organoiodine Compounds using Poly(2-methoxyethyl acrylate)-analogue Microspheres. *ACS Omega* **2017**, *2*, 7686−7694; copyright 2017, American Chemical Society.

4.1. Introduction

Chapter II reported that polymer microspheres selectively adsorb and release halogen compounds. These microspheres consist of hydrophobic pMEA and pOEG hydrogel matrix. In such microgels, the methoxy groups of the pMEA side chains are crucial for the halogen bonding. Consequently, halogen bonding in composite microgels leads to a strong adsorption of halogen compounds in the presence of other compounds under concomitant formation of strong atomic interactions and high selectivity.

Organoiodine compounds play an important role in everyday life. For example, functional iodine compounds have found applications as antibacterial and antiviral drugs, X-ray absorbers, and as components for food and cosmetics.[1-7] Especially, marine-derived organoiodine compounds are highly valuable, and they have received much attention due to their biological activity, which includes inhibitory activity against cancer and diabetes.[8-10] However, the variety and abundance of marine iodine compounds are much lower than those of the corresponding chlorine and bromine analogues.[9] Moreover, the organic syntheses of new iodine-containing drugs produces in many instances the corresponding iodine-free compounds in addition to the targeted organoiodines.[1] Thus, the selective recovery and reuse of the target iodine compounds as starting materials, catalysts, and synthesized products in aqueous solution should be highly desirable, irrespective of the concentration of these compounds in solution. On the other hand, the presence of mass-produced organoiodine compounds in industrial wastewater or natural water resources are of particular concern for safe drinking water, as organoiodine compounds can be toxic, mutagenic, or carcinogenic, and their removal from drinking water is highly important.[11]

However, for low concentrations of several compound mixture, where iodine-, bromine-chloride-, and halogen free-compounds coexist in water, the iodine-free compounds are usually also absorbed by the composite microgels (**Chapter II**, **Figure 3.15**), indicating that the selectivity of the

adsorption of iodine-containing compounds is still low. The very strong interactions between pMEA and halogen-containing compounds thus occur irrespective of the nature of the halogen atom, which stands in contrast to the behavior of halogen atoms with Lewis acids, wherein the strength of the donor-acceptor interaction depends on the polarizability of the halogen atom, which decreases in the order I > Br > Cl.[12-16]

A strategy that allows the highly selective adsorption of iodine-containing compounds at low cost and independent of time and place would be highly attractive for industrial (e.g., water treatment and iodine-recycling systems) and medical applications (drug development). With this objective in mind, the author changed the number and position of oxygen atoms, which are the Lewis-basic acceptors for the halogen bonds, in the polymer chain to control the strength of halogen bonding between the microspheres and the iodine-containing compounds. The induced dipole moment of oligo(ethylene glycol) depends on its molecular weight, and the polarizability of the polymer chain can thus be changed by the number of carbon-oxygen bonds.[17-19] The strength of halogen bonding relating to the polarizability should accordingly decrease with increasing number of carbon-oxygen bonds in the polymer side-chain. Therefore, the author hypothesized that pMEA analogues, which have more than two methoxy or ethoxy groups in their side-chains, should be able to interact specifically with the iodine compounds due to the decreased polarity. In this chapter, the author synthesized the first pMEA-analogue microspheres by free-radical polymerization in water, and subsequently examined their separation potential with respect to iodine-containing compounds.

4.2. Experimental Section

Materials

2-methoxyethyl acrylate (MEA, purity 98%), styrene (St, 99%), butyl acrylate (BA, 99%), potassium peroxodisulfate (KPS, 95%), sodium dodecyl sulfate (SDS, 95%), disodium hydrogenphosphate (99%), eosin Y (EoY, 95%), phloxine B (PhB, 98%), erythrosine (Ery, 95%), rose bengal (RB, 95%), orange II (OrII, 98%), tartrazine (Ttz, 98%), and ethanol (EtOH, 99.5%) were purchased from Wako Pure Chemical Industries and used as received. 2-(2-ethoxyethoxy) ethyl acrylate (ET2A, 98%), 4-methoxystyrene (MSt, 98%), *N*-isopropylacrylamide (NIPAm, 98%), and *N,N*'-methylenebis (acrylamide) (BIS, 97%) were purchased from Tokyo Chemical Industry and used as received. 2-(2-Methoxyetoxy) ethyl acrylate (ME2A, 95%) was purchased from Monomer-Polymer and Dajac Labs, Inc. 2-[2-(2-Methoxyethoxy) ethoxy]ethyl acrylate (Me3A, 98%) were kindly donated by Kyoeisha Chemical Co., Ltd. The cross-linker, ethylene glycol dimethacrylate (EGDMA, 98%) were purchased

from Sigma-Aldrich and used as received. Water used for microsphere preparations was distilled and then ion-exchanged (EYELA, SA-2100E1).

Synthesis of pMEA analogues and control microspheres

All microspheres were prepared via aqueous precipitation or emulsion polymerization using potassium peroxodisulfate (KPS). Polymerizations were performed in a three-necked round-bottom flask (300 mL) equipped with a mechanical stirrer, condenser, and nitrogen gas inlet. The initial total concentrations of each monomer for solid and hydrogel microspheres are listed in **Table 4.1**, respectively. For pNIPAm microgels, the initial total monomer concentration was held constant at 150 mM. Mixture of NIPAm (1.613 g, 95 mol%), BIS (0.116 g, 5 mol%), and SDS (2.8 mg, 0.1 mM) was prepared as the monomer solution. All monomer solutions were dissolved in water (95 mL) in the round-bottom flask and heated to 70 °C under constant stirring (250 rpm) and a stream of nitrogen. The solutions were allowed to stabilize for at least 30 min prior to initiation. Free-radical polymerizations were subsequently initiated using KPS (0.054 g) in water (5 mL). The solutions were stirred for 24 h (4 h for pNIPAm), and after the completion of the polymerizations, the obtained dispersions were cooled to room temperature. Each microsphere was purified via two cycles of centrifugation/re-dispersion in water using a relative centrifugal force (RCF) of 20000 × *g*, followed by dialysis for a week with daily water changes.

Characterization of the microspheres

The hydrodynamic diameter (D_h) of the microspheres was determined by DLS (Malvern Instruments Ltd., Zetasizer Nano S). The time-dependent scattering intensity was detected at a total scattering angle of 173°. D_h values of the microspheres were calculated from the measured diffusion coefficient using the Stokes–Einstein equation (Zetasizer software v6.12). The DLS experiments were conducted at a microsphere concentration of 0.001 wt%. The samples were allowed to thermally equilibrate at the desired temperature for 10 min prior to each measurement. The autocorrelation functions used an average of 15 intensity measurements (acquisition time: 30 s). The electrophoretic mobility (EPM) of the microspheres was measured using a Zetasizer Nano ZS instrument (Malvern) at a microsphere concentration of 0.001 wt%. Samples were allowed to thermally equilibrate at 25 °C for 10 min prior to each measurement. The zeta potential of the solid microspheres was calculated from the measured mobility using the Smoluchowski equation (Zetasizer software ver. 10.0). Atomic force microscopy (AFM) images were recorded under ambient conditions using an SPM-9500J3 microscope (Shimadzu,

Kyoto, Japan) operating in contact mode to visualize the microspheres deposited on circular mica substrates. For the sample preparation, microsphere dispersions (0.5 μL) at the required concentration were applied on freshly prepared mica substrates and dried for 60 min. AFM images were recorded using an Si_3N_4 probe (Olympus, OMCL-AC240FS; scanning speed = 0.2 Hz; operating voltage = 0.3 V).

Dye adsorption experiments

Stock solutions of anionic dyes (20 mM) in a sodium phosphate buffer (SPB; 80 mM, pH = 7.0) were prepared. The tested microsphere dispersions were poured into a vial. The final concentration of the microsphere was 0.1 wt% for all experiments. The microgel dispersions were allowed to thermally equilibrate at the desired temperature for 1 h under constant stirring (300 rpm) in an incubator (CN-25C, Mitsubishi Electric Engineering Co., Ltd.). After the solutions had stabilized in the incubator, the appropriate dye stock solutions were injected into the vials. The final dye concentrations were adjusted appropriately for the required conditions (0.1-2 mM). After 1 h of exposure, the mixtures were divided into three centrifuge tubes (SC-0200, Ina-Optika Co., Ltd). The mixtures were centrifuged (RCF; 20000 × *g*) to pack the microspheres at the bottom of each tube. The supernatants were carefully removed from the centrifuge tubes without disturbing the microsphere pellets at the bottom and the absorbance of each supernatant was measured using a UV–vis spectrophotometer (JASCO, V-630iRM).

Dye Release Experiments

The optimal conditions for RB adsorption were then used to prepare a mixture of the microspheres and RB in the same manner as described above. After the supernatant was removed from each centrifuge tube, each microgel pellet was redispersed in a different buffer solution at 25, 50, or 70 °C, and placed in the centrifuge tubes at the same concentration used in the adsorption experiment. Each dispersion was subsequently mixed using a thermomixer (Thermomixer R, Eppendorf) at 25, 50, or 70 °C for 1 h. Each mixture was then centrifuged at an RCF of 20000g, and the supernatants were removed from the centrifuge tubes. The absorbance of each supernatant was measured using a UV−vis spectrophotometer.

4.3. Results and Discussion

4.3.1. Synthesis and Characterization of pMEA Analogue Microspheres

The tested microspheres and their synthetic conditions used in this study were listed in **Table 4.1**. The atomic force microscopy (AFM) images and the chemical structures of the tested microspheres were shown in **Figure 4.1**. In this chapter, the initiator potassium persulfate (KPS), which lead to negatively charged surfaces, was used to start polymerizations in all cases because the effect of electrostatic attraction between the microspheres and the anionic halogen compounds can be ignored. The electrophoretic motilities (EPMs) of the tested microspheres were negative value (**Table 4.1**). Non-functionalized pMEA and pMEA analogue microspheres were prepared by soap-free precipitation polymerization, where these monomers were dissolved in water during the polymerizations and the resultant polymers were precipitated in water to form the microspheres. In order to compare the adsorption behavior of halogen compounds, the polystyrene (pSt), poly(butyl acrylate) (pBA) and poly(4-methoxy styrene) (pMSt) were selected as the solid control microspheres. Particularly, the methoxy groups in the pMSt microspheres act as the electron donating groups due to the resonance effect.[20] Thus, the difference of the dielectric polarization between the pMEA (analogues) and pMSt microspheres can be discussed.

Table 4.1. Synthesis conditions used and properties of the resulting microspheres.

Microsphere	Monomer concentration (mM)	[a] D_h (nm)	[a] EPM (10^{-8} m^2 V^{-1} s^{-1})
pMEA (solid)	100 (1.30 g)	214±5	-3.75±0.5
pET2A (solid)	100 (1.88 g)	453±6	-3.54±0.1
[b]pME2A (gel)	100 (1.65 g)	362±2	-1.44±0.2
[b]pME3A (gel)	100 (2.07 g)	284±5	-1.50±0.4
pMSt (solid)	100 (1.34 g)	168±5	-3.95±0.7
pSt (solid)	500 (5.21 g)	251±1	-4.17±0.2
pBA (solid)	500 (6.41 g)	414±3	-3.72±0.3

[a]Measurment for microspheres dispersed in sodium phosphate buffer at pH 7.
[b]The cross-linker EGDMA (5 mol%) was added to the polymerizations.

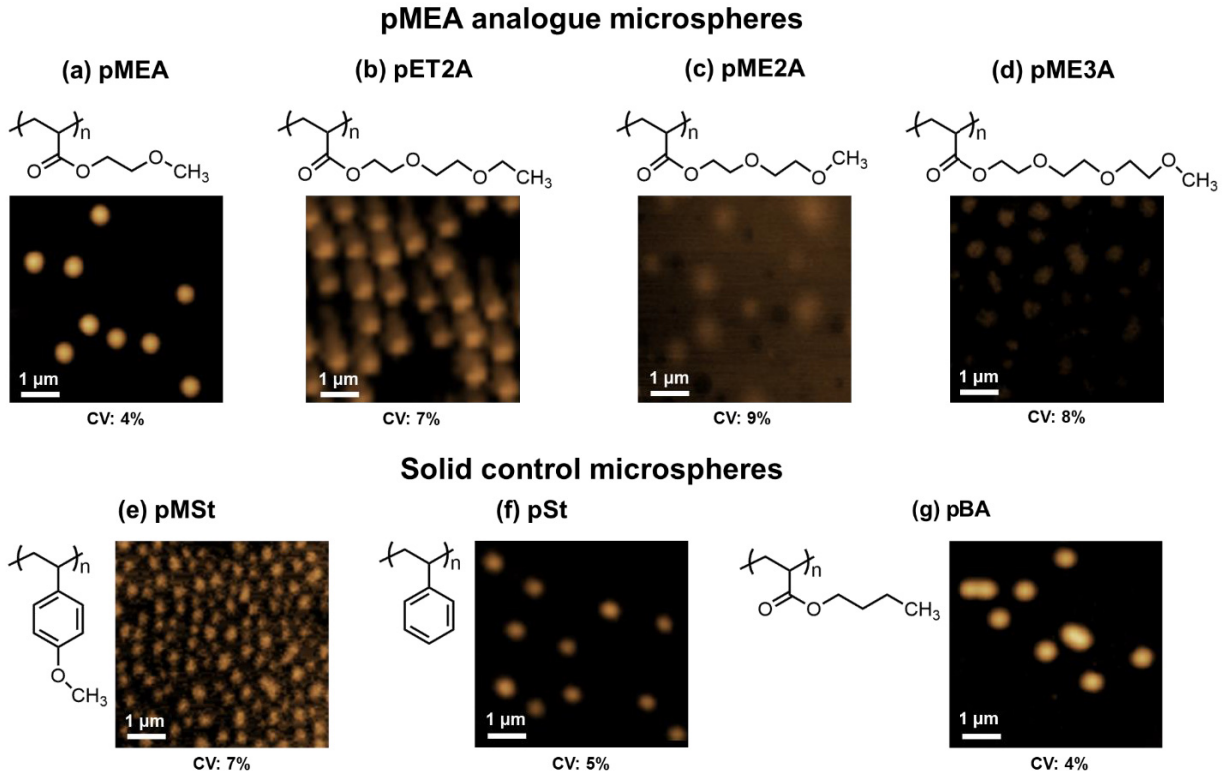

Figure 4.1. The represented atomic force microscopy (AFM) images and the chemical structures of the tested microspheres. The coefficients of variation (CV) for the microspheres are shown (N = 50).

Since poly(2-(2-ethoxyethoxy) ethyl acrylate) (pET2A) chains have lower critical solution temperature (LCST) ~ 15 °C,[21-23] the solid pET2A microspheres did no disintegrate at room temperature without adding of cross-linkers. On the other hand, poly(2-(2-Methoxyetoxy) ethyl acrylate) (pME2A) and poly(2-[2-(2-Methoxyethoxy) ethoxy]ethyl acrylate) (pME3A) microspheres were not obtained in the absence of cross-linkers during the polymerizations due to the fact that these polymers have LCST at ~ 43 °C for pME2A and ~ 63 °C for pME3A, respectively.[21-23] Thus, 5 mol.% of ethylene glycol dimethacrylate (EGDMA) cross-linker was added to the polymerizations, and thus the stable pME2A and pME3A microgels were successfully synthesized (**Table 4.1** and **Figure 4.1**). Here, they were thermo-responsive microgels because the hydrodynamic diameters (D_h) of pME2A and pME3A microgels were decreased with increasing temperature (**Figure 4.2**). The difference between the solid and hydrogel states of the microspheres also influenced the adsorption behavior of the low molecular compounds as discussed below.

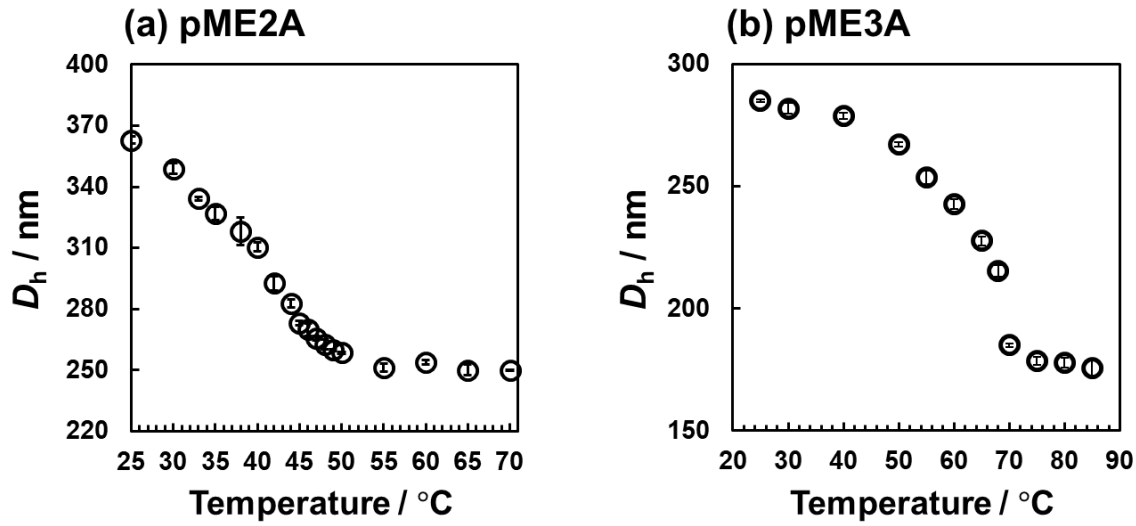

Figure 4.2. The hydrodynamic diameter (D_h) of (a) pME2A and (b) pME3A microgels as a function of temperature. For these measurements, microgels were dispersed in sodium phosphate buffer (pH = 7).

4.3.2. Halogen Compound Adsorption Behavior on pMEA Analogue Microspheres

To examine the origin of the halogen bonding, the anionic halide xanthene dyes, eosin Y (EoY), erythrosine (Ery), phloxine B (PhB), and rose bengal (RB) were selected as model halogen-containing compounds (**Figure 4.3**). Particularly, the iodine containing Ery and RB have been used in food and cosmetics.[1] In order to compare the halogen bonding with other, e.g. hydrophobic interactions, other anionic dyes that do not contain halogen atoms such as orange II (OrII) and tartrazine (Ttz) were also examined. **Figure 4.3** shows the adsorption isotherm for each dye for the tested microspheres at 25 °C. Langmuir (eq. 1) and Freundlich (eq. 3) models were applied to analyze the adsorption equilibrium data. These isotherms are shown in **Figure 4.4**. In all cases, the correlation coefficient (R^2) of the Langmuir model was close to 1 and much larger than that of the Freundlich model, indicating a good fit of the Langmuir model. **Table 4.2** shows the values of the Langmuir isotherm parameters, and all values are summarized in **Table 4.3**. Here, the adsorption capacity (Q_m) values determined by the Langmuir model were normalized as moles of dye per total surface area ($N_{m/s}$, μmol/m^2) and volume ($N_{m/v}$, μmol/m^3) of tested microsphere to compare the adsorption behavior considering the different size and state (e.g., solid or gel) of these microspheres and the different molecular weight of each dye. Furthermore, the essential characteristics of the Langmuir isotherm can be described by a separation factor (R_L) relating to Langmuir constant (b), which is defined by eq. 2 (**Tables 4.2** and **4.3**). The value

of R_L indicates the shape of the Langmuir isotherm and the nature of the adsorption process: irreversible ($R_L = 0$), favorable ($0 < R_L < 1$), linear ($R_L = 1$), or unfavorable ($R_L > 1$).[24]

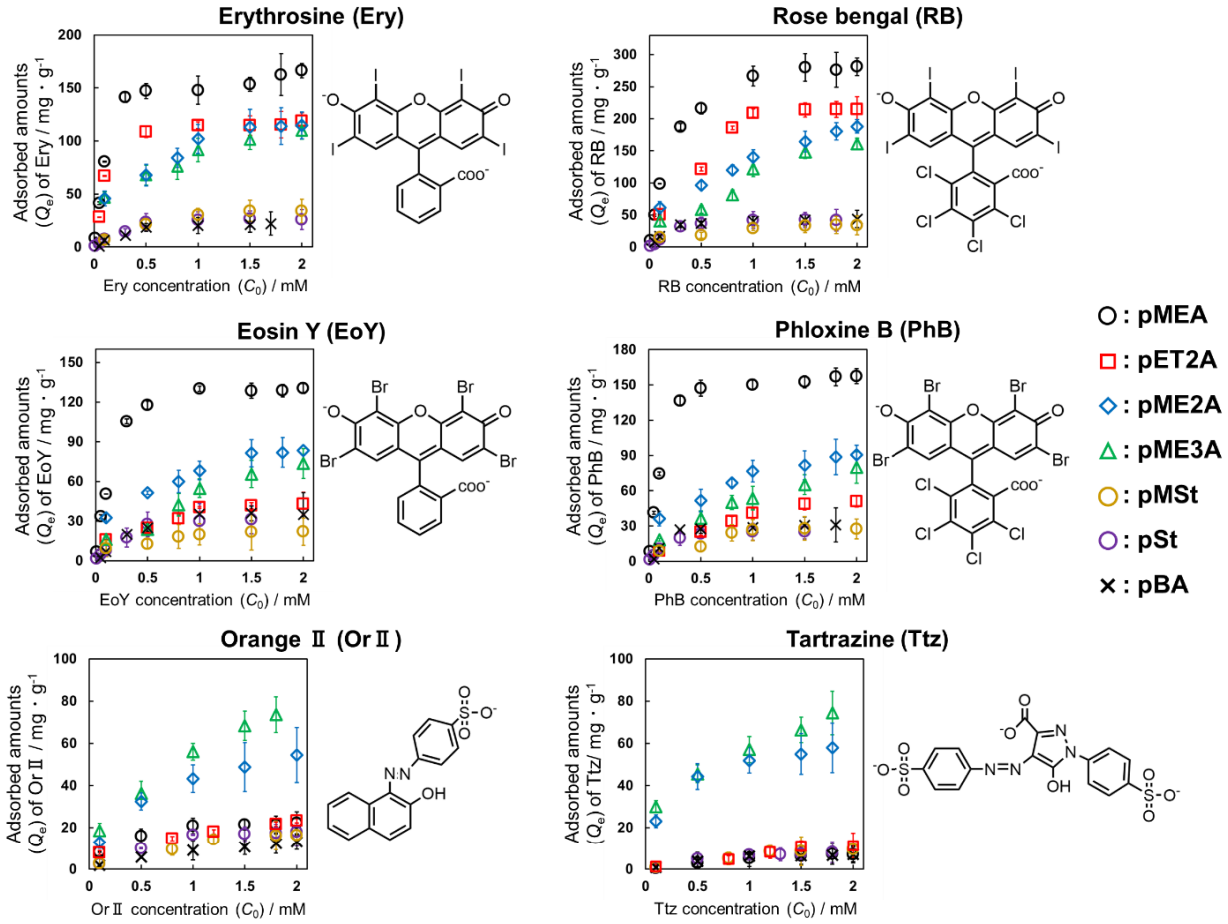

Figure 4.3. Adsorption isotherms for the tested dyes on each microsphere at 25 °C. Each point represents an average of three replicate adsorption experiments. The error bars denote the standard deviations.

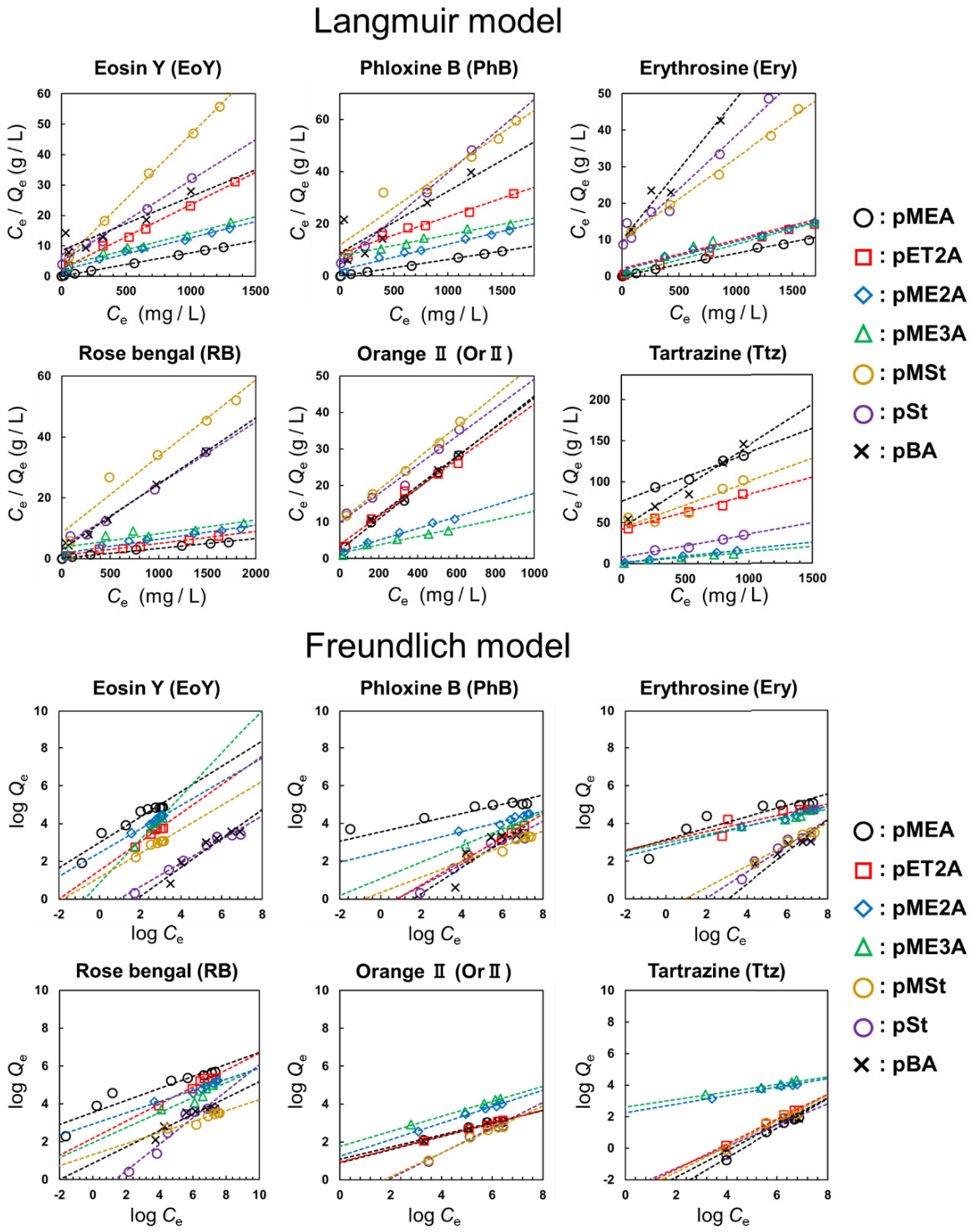

Figure 4.4. Langmuir (top) and Freundlich (bottom) isotherms for the adsorption of the tested dyes onto different microspheres (0.1 wt%) at different initial dye concentrations (25 °C).

Table 4.2. Langmuir isotherm parameters for the adsorption of the anionic dyes on the pMEA-, pMEA analogues, and control microspheres at 25 °C.

		Langmuir				
Dye	Adsorbent[a]	Q_m mg/g	$N_{m/s}$[b] µmol / m^2	$N_{m/v}$[c] µmol / m^3	b L/mg	R_L at 0.1mM
Erythrosine	pMEA	164	6.61	20.6	0.031	0.21
	pET2A	119	10.3	15.1	0.028	0.25
	pME2A	129	N.A.[d]	31.8	0.014	0.64
	pME3A	127	N.A.[d]	31.3	0.004	0.87
	pMSt	35.3	1.12	4.46	0.003	0.96
Rose bengal	pMEA	311	10.9	33.9	0.050	0.08
	pET2A	237	17.6	25.8	0.045	0.11
	pME2A	215	N.A.[d]	45.8	0.027	0.30
Eosin Y	pMEA	131	6.06	21.0	0.025	0.28
	pET2A	47.2	5.01	7.58	0.010	0.69
	pME2A	93.9	N.A.[d]	29.5	0.006	0.80
	pME3A	91.7	N.A.[d]	28.7	0.003	0.94
	pMSt	23.6	0.95	3.79	0.004	0.88
Phloxine B	pMEA	157	6.76	21.1	0.041	0.13
	pET2A	70.6	4.73	9.45	0.008	0.75
	pME2A	101	N.A.[d]	26.4	0.005	0.85
Tartrazine	pMEA	15.9	1.03	3.30	0.002	0.97
	pET2A	23.8	3.36	3.82	0.001	0.99
	pME2A	61.0	N.A.[d]	19.1	0.009	0.72
	pME3A	90.8	N.A.[d]	28.5	0.007	0.81
	pMSt	17.8	0.83	2.86	0.001	0.98

[a]microsphere concentration = 0.1 wt %.

[b]$N_{m/s}$ represents the adsorbed moles of dye per total surface area of the tested microspheres.

[c]$N_{m/v}$ represents the adsorbed moles of dye per total volume of tested microsphere. The specific volume of the pME2A and pME3A microgels was calculated based on the assumption that the fully swollen microgels contain ~80% water.

[d]$N_{m/s}$ could not be determined, as it is difficult to determine the surface area of the microgels.

Table 4.3. Langmuir and Freundlich isotherm parameters for the adsorption (25 °C) of the tested anionic dyes on all microspheres synthesized in this study.

		Langmuir						Freundlich		
Dye	Adsorbent[a]	Q_m mg / g	$N_{m/s}$[b] µmol / m^2	$N_{m/v}$[c] µmol / m^3	b L / mg	R_L at 0.1 mM	R^2	K_F L / mg	n	R^2
Eosin Y	pMEA	131	6.06	21.0	0.025	0.28	0.9991	20.1	3.38	0.9219
	pET2A	47.2	5.01	7.58	0.010	0.69	0.9966	33.3	1.32	0.9453
	pME2A	93.9	N.A.[d]	29.5	0.006	0.80	0.9877	29.3	1.60	0.9766
	pME3A	91.7	N.A.[d]	28.7	0.003	0.94	0.9835	7.20	0.87	0.9795
	pMSt	23.6	0.95	3.79	0.004	0.88	0.9993	14.4	1.57	0.9468
	pSt	29.8	1.88	4.78	0.005	0.85	0.9864	0.47	1.48	0.9862
	pBA	39.7	4.21	6.37	0.003	0.97	0.9811	0.16	1.15	0.9297
Phloxine B	pMEA	157	6.76	21.1	0.041	0.13	0.9989	32.9	0.18	0.8810
	pET2A	70.6	4.73	9.45	0.008	0.75	0.9981	0.31	1.60	0.9724
	pME2A	101	N.A.[d]	26.4	0.005	0.85	0.9754	31.1	3.69	0.9568
	pME3A	97.0	N.A.[d]	25.4	0.002	0.96	0.9921	9.73	2.10	0.9274
	pMSt	34.8	1.18	4.66	0.002	0.97	0.9335	2.15	2.45	0.9288
	pSt	30.1	1.58	4.03	0.007	0.82	0.9937	0.51	1.58	0.9511
	pBA	32.5	2.88	4.35	0.012	0.68	0.9996	0.27	1.40	0.7264
Erythrosine	pMEA	164	6.61	20.6	0.031	0.21	0.9994	23.4	3.40	0.8222
	pET2A	119	10.3	15.1	0.028	0.25	0.9994	20.4	7.82	0.9401
	pME2A	129	N.A.[d]	31.8	0.014	0.64	0.9778	61.3	3.78	0.9436
	pME3A	127	N.A.[d]	31.3	0.004	0.87	0.9397	14.7	5.54	0.9139
	pMSt	35.3	1.12	4.46	0.003	0.96	0.9687	0.28	1.74	0.9687
	pSt	32.2	1.60	4.06	0.004	0.95	0.9865	0.21	1.32	0.9719
	pBA	27.3	2.27	3.45	0.008	0.76	0.9989	0.67	2.19	0.9873
Rose bengal	pMEA	311	10.9	33.9	0.050	0.08	0.9928	35.1	3.21	0.8881
	pET2A	237	17.6	25.8	0.045	0.11	0.9849	20.5	2.34	0.9450
	pME2A	215	N.A.[d]	45.8	0.027	0.30	0.9765	80.2	3.40	0.9465
	pME3A	209	N.A.[d]	44.5	0.013	0.71	0.9979	23.0	3.20	0.8653
	pMSt	39.7	1.98	4.33	0.003	0.96	0.9668	21.4	3.46	0.9113
	pSt	48.6	2.09	5.30	0.008	0.76	0.9888	0.11	1.43	0.9273
	pBA	47.4	3.42	5.17	0.011	0.70	0.9972	1.62	2.05	0.9353
Orange Ⅱ	pMEA	23.7	2.42	7.51	0.008	0.76	0.9976	8.54	3.11	0.9720
	pET2A	26.0	5.60	4.18	0.009	0.72	0.9974	8.56	2.91	0.9775
	pME2A	62.2	N.A.[d]	19.5	0.008	0.77	0.9925	17.8	2.30	0.9870
	pME3A	86.5	N.A.[d]	27.1	0.007	0.81	0.9844	58.1	2.53	0.9480
	pMSt	23.2	0.85	3.83	0.004	0.95	0.9963	0.06	1.60	0.9778
	pSt	25.5	3.18	8.08	0.004	0.95	0.9660	0.05	1.47	0.9607
	pBA	23.9	4.02	7.58	0.011	0.70	0.9952	7.98	2.88	0.9780
Tartrazine	pMEA	15.9	1.03	3.30	0.002	0.97	0.9872	0.01	1.06	0.9601
	pET2A	23.8	3.36	3.82	0.001	0.99	0.9944	0.02	1.27	0.9610
	pME2A	61.0	N.A.[d]	19.1	0.009	0.72	0.9973	18.5	3.70	0.9824
	pME3A	90.8	N.A.[d]	28.5	0.007	0.81	0.9702	31.3	3.62	0.9685
	pMSt	17.8	0.83	2.86	0.001	0.98	0.9552	0.01	1.23	0.8533
	pSt	8.56	0.71	1.77	0.006	0.81	0.9937	0.03	1.19	0.9110
	pBA	9.94	1.31	2.06	0.002	0.97	0.9642	0.21	1.46	0.9620

[a][Microspheres] = 0.1 wt %. [b]$N_{m/s}$ represents the adsorbed moles of dye per total surface area of the tested microspheres. [c]$N_{m/v}$ represents the adsorbed moles of dye per total volume of tested microsphere. The specific volume of the pME2A and pME3A microgels was calculated based on the assumption that the fully swollen microgels contain ~ 80% water. [d]$N_{m/s}$ could not be determined, as it is difficult to determine the surface area of the microgels.

First of all, the significance of the polarization for these polymer side-chain contributing to halogen bonding was discussed. Different from pMEA, the methoxy group in pMSt acts as an electron donating group, i.e., Lewis acid, due to resonance effect.[20] The adsorbed amounts of halogen containing dyes on pMSt microspheres were much lower than that of pMEA microspheres, and were close to those on pSt and pBA microspheres (**Figure 4.3** and **Table 4.2**). In addition, pMSt paste were not stained with e.g. the red color of Ery and EoY after centrifugation, although facile staining of the pMEA pastes were observed (**Figure 4.5**), indicating that the inductive effect due to permanent dipole for the methoxy groups in pMEA is important factor for halogen bonding. As reported in the **Chapter II**, the hydrophobic interactions should occur between the tested solid microspheres and the dyes because the tested dyes were also adsorbed on the control pMSt, pSt, and pBA microspheres, resulting in $R_L < 1$ (**Tables 4.2** and **4.3**). Indeed, the quantity of the hydrophilic dye Ttz, which exhibits the lowest octanol-water partition coefficient (log K_{ow}), adsorbed on the solid microspheres was smaller than those of the other dyes (**Figure 4.3**). A similar behavior was also observed for OrII adsorption (**Table 4.3**).

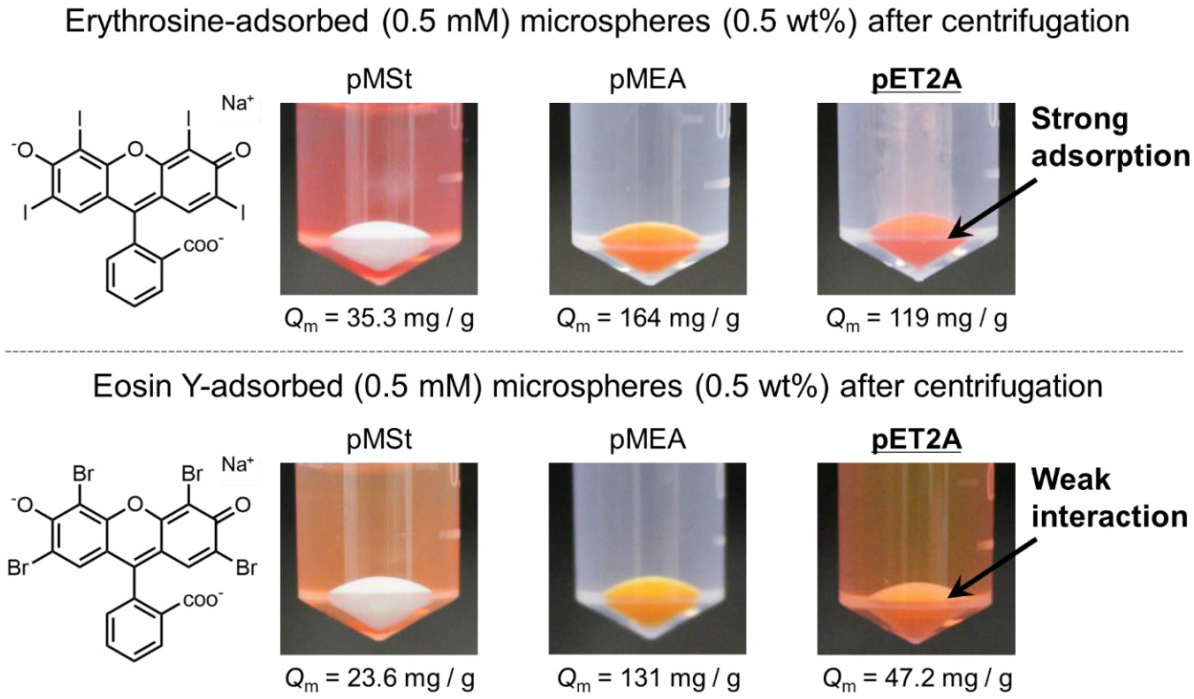

Figure 4.5. Photographs of solid pMSt, pMEA, and pET2A microsphere (0.5 wt %) after centrifugation in the presence of erythrosine (top) and eosin Y (bottom) at 0.5 mM and 25 °C. The displayed values of adsorption capacity, Q_m (mg/g), of each microsphere were obtained from the isotherm analysis (**Table 2**).

In the case of solid ET2A microspheres, where the number of oxygen atom in the side-chains is two-times more than that of pMEA (**Figure 4.1**), the adsorbed amounts of iodine containing dyes, Ery and RB, per unit gram of pET2A were close to those of pMEA microspheres (**Figure 4.3**), although the hydrodynamic diameter (D_h) of pMEA is smaller than that of pET2A microspheres (e.g., D_h = 214 nm for pMEA and D_h = 453 nm for pET2A; **Table 4.1**). As a result, $N_{m/s}$ of Ery and RB for pET2A were bigger than those for pMEA, and R_L values of Ery and RB is close to those for pMEA (**Table 4.2**), suggesting that the halogen bonding occurred in pET2A microsphere system. Assuming that the numbers of each side-chain per surface area of pMEA and pET2A microspheres are the same, the number of halogen bonding site (oxygen atom) of pET2A is larger than that of pMEA microspheres, which results the increase in adsorbed amounts of iodine compounds.

On the other hand, in the case of pME2A microgels, where the number of oxygen atom is the same with pET2A side-chain (**Figure 4.1**), the Langmuir constant values of Ery and RB were lower than those for pMEA and pET2A microspheres (**Table 4.2**), indicating that the strength of halogen bonding between the pME2A and iodine dyes was lower than those for pMEA and pET2A. Notable, the saturated adsorption amounts of Ery and RB per unit gram of pME2A microgels were close to those of the solid pMEA and pET2A microspheres (e.g., Q_m = 119 mg/g for pET2A and Q_m = 129 mg/g for pME2A in the case of Ery adsorption; **Table 4.2**), suggesting that the swollen microgels can take the low-molecular weight compounds in their inside due to the osmotic pressure.[25,26] It is supported by the results that the halogen-free dyes Ttz and OrII were also taken up by the pME2A and pME3A microgels (**Figure 4.3**), i.e., the $N_{m/v}$ values of Ttz and OrII for these microgels were higher than those for the control solid microgels (**Table 4.3**).

The reason for this result that the Langmuir constants (or R_L values) of iodine compounds were different between the pET2A and pME2A cannot be explained easily as there are several possible factors: i) the ethoxy groups in the pET2A side-chain terminal can aid the polarization more than the methoxy group in the pME2A side-chain terminal, resulting in the increase in vectorial sum of dipole moment in pET2A. This surmise is proposed based on the results that the polarizabilities of oligo ethylene glycol molecules were different from the conformer and the number of ethylene glycol unit,[18] suggesting that the polarizability also changes with the number of carbon atoms, e.g., methoxy and ethoxy groups; ii) the hydrophobic interaction between solid pET2A microspheres and the dyes supports the adsorption on the surface, which is hard to occur between water-swollen pME2A microgels and the dyes. Furthermore, the Langmuir constants of Ery and RB for pME3A microgels, where the number of oxygen-carbon bonds increased more than pME2A side-chain (**Figure 4.1**), were

smaller than those for pMEA, pET2A and pME2A (**Table 4.2**). Therefore, the author concluded that the polarizability of whole polymer side-chain contributing to halogen bonding and hydrophobic interaction are important factor for the strong adsorption of iodine compounds.

Conversely, the adsorbed amounts of iodine-free compounds, including bromine containing dyes (EoY and PhB), on the pET2A microspheres were smaller than those of iodine containing dyes (**Figure 4.3**), although the pET2A microspheres have the halogen bonding capacity for iodine compounds. Consequently, R_L values of EoY and PhB were close to 1 compared to those for pMEA (e.g., $R_L \sim 0.69$ for pET2A and $R_L \sim 0.28$ for pMEA at 0.1 mM EoY, **Table 4.2**), suggesting that the strength of halogen bonding at the one adsorption site in pET2A side-chain was decreased compared to that of pMEA. The results caused that the iodine-containing Ery was adsorbed on the pET2A microspheres, showing the transparent supernatant, although the EoY was also present in the supernatant (**Figure 4.5**). The author infers that the polarizability for pET2A was smaller than that for pMEA due to the fact that the dipole moment at pET2A side-chain act to compensate with each other. Therefore, the pET2A microspheres exhibit the halogen bonding ability for iodine compounds, while do not have the ability for bromine compounds significantly. This trend was also observed in the cases of pME2A and pME3A microgels (e.g., for pME2A, $R_L \sim 0.64$ of Ery and $R_L \sim 0.80$ of EoY, **Table 4.2**).

4.3.3. Selective Adsorption and Release of Iodine Compounds

To achieve the high selective adsorption of iodine compounds on the microspheres, the author selected the pET2A microspheres, which have the suitable halogen bonding ability for the adsorption of iodine compounds more than pMEA microspheres. In the same manner as the **Chapter II**, anionic RB was selected as a target iodine-containing dye, and iodine-free EoY, OrII, and Ttz were selected as competitive inhibitors for the adsorption of RB. **Figure 4.6** shows the adsorption occupancy of each tested dyes on the pMEA and pET2A microspheres (0.1 wt.%), indicating that the adsorbed amounts of RB on both microspheres were highest when the concentrations of all dyes were comparable. However, at low dye concentrations (e.g., 0.1 mM), the bromine containing EoY was preferentially adsorbed on pMEA microspheres compared to OrII and Ttz (e.g. EoY: ~ 35% at 0.1 mM and ~ 28% at 0.5 mM; **Figure 4.6a**), suggesting that halogen bonding also occurs between EoY and the pMEA via the residues of the methoxy groups that are not involved in the adsorption of RB. This phenomenon cause the decrease in the RB adsorption rate, regardless of dye concentrations.

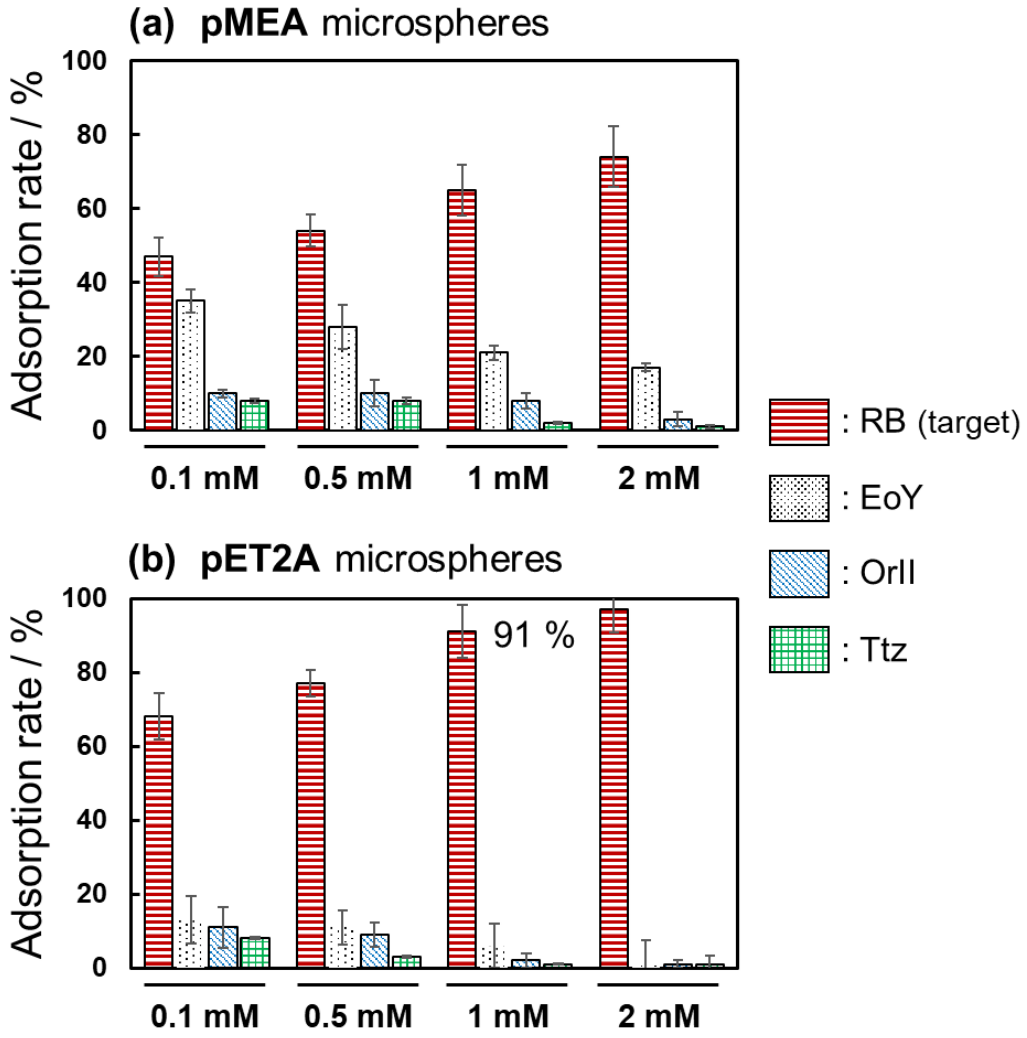

Figure 4.6. Adsorption rate for each dye by (a) pMEA and (b) pET2A microspheres at different initial concentrations of dye mixtures at 25 °C.

On the other hand, in the case of pET2A microspheres, the adsorption of RB accounts for ~ 70% of all dyes even when each dye concentration is 0.1 mM (**Figure 4.6b**). In addition, the maximum adsorption rate of RB reached ~ 91% at 1 mM, although the maximum rate of RB adsorbed on pMEA reached only 65 % at the same dye concentrations. As intended, the pET2A microspheres have the high affinity for the iodine compounds, while do not high affinity for the iodine-free compounds. The selectivity of iodine compound adsorption can be improved by using the pET2A microspheres.

Finally, the author achieved the release of the adsorbed iodine compounds by using pME2A microgels. Similar to the pMEA microsphere case (**Chapter II**, **Figure 3.6**), the adsorbed iodine compounds RB on the solid pET2A microspheres were not desorbed easily as evident from the

quantities of released RB as a function of temperature (**Figure 4.7**). Note that as maximum adsorption was observed at 25 °C in the presence of 1 mM of RB, the pET2A microspheres (0.1 wt%) were subjected to these conditions prior to evaluating the desorption behavior. The result indicates that the RB remained strongly attached to the pET2A surfaces, even at 70 °C. Here, the thermo-responsive pME2A microgels were selected to release RB because the D_h of pME2A microgels was decreased with increasing temperature up to 50 °C (**Figure 4.2a**). Indeed, the released quantity of RB was increased when the temperature increased to 50 °C, and then their release behavior did not dramatically change even at 70 °C (**Figure 4.7**). In **Chapter II**, the pMEA composite microgels, where the pOEG with an ethylene oxide chain length of 5 or 6 played the role of the thermo-responsive gel matrix, also showed the controllable release of RB by rising temperature (**Chapter II**, **Figure 3.6**).

However, these scenarios are different from the thermo-responsive poly(*N*-isopropyl acrylamide) (pNIPAm) microgel case,[25,26] where the isopropyl groups form the hydrophobic domains, and the uptake of the Ery increases as the temperature increases. The anionic pNIPAm microgels did not significantly release the RB when the pNIPAm microgels were highly deswollen at high temperature (**Figures 4.7** and **4.8**). Note that the amount of RB taken up by the pNIPAm microgels, which did not have the halogen bonding site, was smaller than that by the pME2A microgels at 25 °C (e.g., Adsorbed amount, Q_e, of RB at 1 mM is ~ 140 mg/g for pME2A and Q_e is ~ 70 mg/g for pNIPAm microgels; **Figure 4.7**).

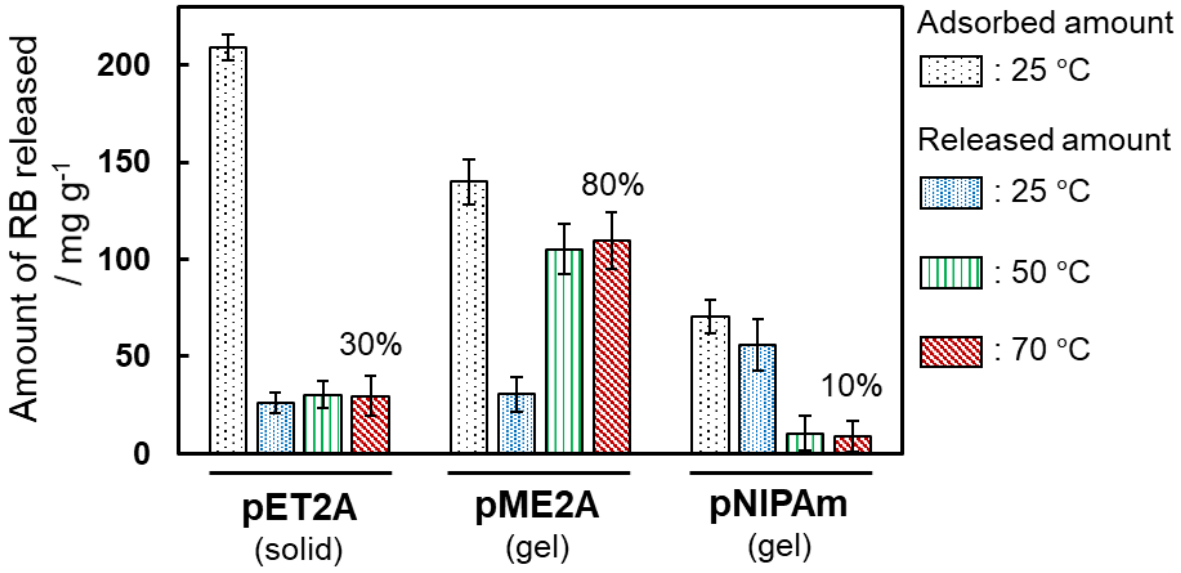

Figure 4.7. Released amounts of RB per unit gram of pET2A, pME2A, and pNIPAm microspheres as a function of temperature. The white dot bars at the left of each microsphere represent the adsorbed amounts of RB at 25 °C. The anionic pNIPAm microgels were cross-linked by *N,N'*-methylenebis acrylamide (5 mol%).

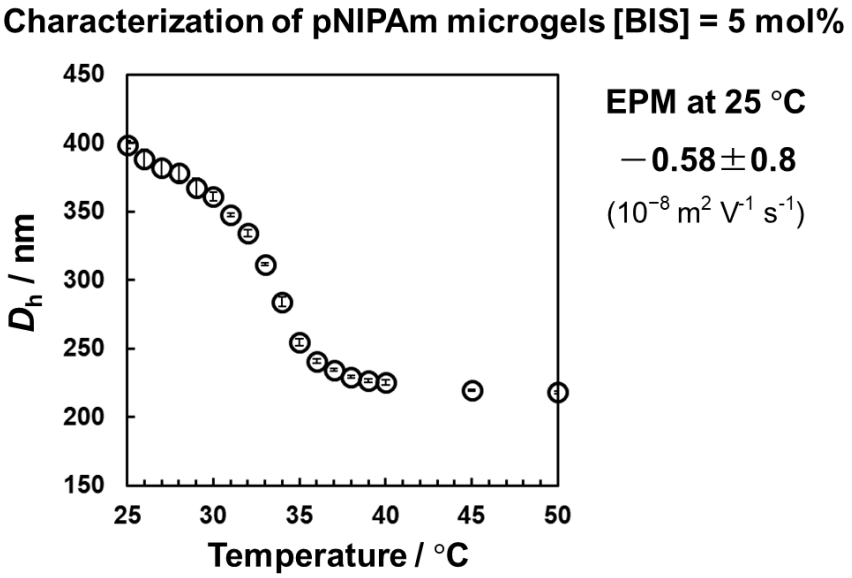

Figure 4.8. The hydrodynamic diameter (D_h) as a function of temperature, together with the electrophoretic mobility (EPM) at 25 °C of pNIPAm microgels cross-linked by BIS (5 mol%).

The unique release behavior of pME2A microgels may be due to the fact that the thermo-responsive behavior is different between the pNIPAm and the polymer containing oligo(ethylene glycol) side-chains. Lutz, J. F. et. al., proposed the mechanism for explaining the thermo-responsive behavior of pOEG-based polymer and gel;[27] above their LCSTs, the hydrogen bond cleavage between the ethylene glycol units and water was the driving force for the phase transition. The dehydrated oligo (ethylene glycol) chains were folded along the apolar backbone due to the hydrophobic interaction, because there was no strong hydrogen bond donors in the pOEG-based polymer, i.e., the interaction between the oligo(ethylene glycol) side-chains was hard to occur, which were characterized by ^{1}H NMR spectra and dynamic light scattering method. On the other hand, above the LCST of pNIPAm, the local packing of isopropyl groups of two neighboring chains and/or hydrogen bonds between amide groups promoted the formation of small hydrophobic nanopockets, where the association of isopropyl groups minimized the exposed surface area.[28] Thus, the formation of hydrophobic isopropyl domains in the pNIPAm microgels inhibited the release of organic dyes, whereas the deswollen pME2A microgels did not hamper the release of RB at high temperature (**Figure 4.7**).

4.4. Conclusions

The high selective adsorption and controlled release of iodine compounds were achieved by using the pMEA analogue microspheres, where their side-chains exhibited the capability of specialized

halogen bonding towards iodine compounds in water. The two ethoxy groups in the pET2A side-chains have the moderate strength of halogen bonding corresponding to polarizability, and thus the iodine compounds can be adsorbed, although the bromine compounds were not adsorbed significantly, which were characterized by the adsorption isotherms of several anionic dyes. These results lead to the high selectivity of iodine compound adsorption in the presence of iodine-free compounds: the target iodine containing dye RB accounts for above 90 % of all adsorbed dyes. Moreover, the pME2A microgels allow the controlled release of iodine dyes due to their thermo-responsive swell/deswell transition. Therefore, these findings should represent an important first step towards the selective separation of iodine compounds associated with e.g., the recovely of valuable drug, the reuse of iodine containing catalyst, and the removal of harmful iodine compounds in wastewater that need to separate with high selectivity.

4.5. References

1. Kaiho, T. Ed., Iodine Chemistry and Application, *John Wiley & Sons, Inc. Hoboken.* **2014**
2. Zhdankin, V. V.; Stang, P. J. Recent Developments in the Chemistry of Polyvalent Iodine Compounds. *Chem. Rev.* **2002**, *102*, 2523-2584.
3. Cloete, T. E. Resistance mechanisms of bacteria to antimicrobial compounds. *Int. Biodeter. & Biodeg*. **2003**, *51*, 277-282.
4. Yeung, C. S.; Dong, V. M. Catalytic Dehydrogenative Cross-Coupling: Forming Carbon-Carbon Bonds by Oxidizing Two Carbon-Hydrogen Bonds. *Chem. Rev.* **2011**, *111*, 1215-1292.
5. Biondi, B.; Wartofsky, L. Treatment With Thyroid Hormone. *Endoc. Rev*. **2014**, *35*, 433-512.
6. Miller, K. D.; Siegel, R. L.; Lin, C. C.; Mariotto, A. B.; Kramer, J. L.; Rowland, J. H.; Stein, K. D.; Alteri, R.; Jemal, A. Cancer Treatment and Survivorship Statistics, 2016. *CA. Cancer J. Clin*. **2016**, *66*, 271-289.
7. Peng, H.; Chen, C.; Cantin, J.; Saunders, D. M. V.; Sun, J.; Tang, S.; Codling, G.; Hecker, M.; Wiseman, S.; Jones, P. D.; Li, A.; Rockne, K. J.; Sturchio, N. C.; Cai, M.; Giesy, J. P. Untargeted Screening and Distribution of Organo-Iodine Compounds in Sediments from Lake Michigan and the Arctic Ocean Untargeted Screening and Distribution of Organo-Iodine Compounds in Sediments from Lake Michigan and the Arctic Ocean. *Environ. Sci. Technol*. **2016**, *50*, 10097−10105.
8. Küpper, F. C.; Carpentere, L. J.; McFiggans, G. B.; Palmer, C. J.; Waite, T. J.; Boneberg, E. M.; Woitsch, S.; Weiller, M.; Abela, R.; Grolimund, D.; Potin, P.; Butler, A.; Luther, G. W.; Kroneck, P. M. H.; Meyer-Klauckel, W.; Feiters, M. Iodide accumulation provides kelp with an inorganic antioxidant impacting atmospheric chemistry. *Proc. Natl. Acad. Sci. USA* **2008**, *105*, 6954-6958.

9. Wang, L.; Zhou, X.; Fredimoses, M.; Liao, S.; Liu, Y. Naturally occurring organoiodines. *RSC Adv*. **2014**, *4*, 57350-57376.
10. Fuge, R.; Johnson, C. C. Iodine and human health, the role of environmental geochemistry and diet, a review. *Appl. Geochem*. **2015**, *63*, 282-302.
11. Guidelines for Drinking-water Quality, 4th ed. WHO Press, *World Health Organization*: Geneva, Switzerland, **2011**.
12. Murray-Rust, P.; Motherwell, W. D. S. Computer retrieval and analysis of molecular geometry. 4. Intermolecular interactions. *J. Am. Chem. Soc*. **1979**, *101*, 4374-4376.
13. Politzer, P.; Lane, P.; Concha, M. C.; Ma, Y.; Murray, J. S. An overview of halogen bonding. *J. Mol. Model*. **2007**, *13*, 305-311.
14. Erdélyi, M. Halogen bonding in solution. *Chem. Soc. Rev*. **2012**, *41*, 3547-3557.
15. Beale, T. M.; Chudzinski, M. G.; Sarwar, M. G.; Taylor, M. S. Halogen bonding in solution: thermodynamics and applications. *Chem. Soc. Rev*. **2013**, *42*, 1667-1680.
16. Robertson, C. C.; Wright, J. S.; Carrington, E. J.; Perutz, R. N.; Hunter, C. A.; Brammer, L. Hydrogen bonding vs. halogen bonding: the solvent decides. *Chem. Sci*. **2017**, *8*, 5392-5398.
17. Zaslavsky, B. Y.; Miheeva, L. M.; Masimov, E. A.; Djafarov, S. F.; Reichardt, C. Solvent polarity of aqueous polymer solutions as measured by the solvatochromic technique. *J. Chem. Soc., Faraday Trans*. **1990**, *86*, 519-524.
18. Wang, R. L. C.; Kreuzer, H. J.; Grunze, M.; Pertsin, A. J. The effect of electrostatic fields on an oligo(ethylene glycol) molecule: dipole moments, polarizabilities and field dissociation. *Phys. Chem. Chem. Phys*. **2000**, *2*, 1721-1727.
19. He, X.; Lopes, P. E. M.; MacKerell Jr., A. D. Polarizable Empirical Force Field for Acrclic Polyalcohols Based on the Classical Drude Oscillator. *Biopolymers* **2013**, *99*, 724-738.
20. Domenicano, A.; Murray-Rust, P. Geometrical substituent parameters for benzene derivatives: inductive and resonance effects. *Tetrahedron Lett*. **1979**, *20*, 2283-2286.
21. Sato, K.; Kobayashi, S.; Kusakari, M.; Watahiki, S.; Oikawa, M.; Hoshiba, T.; Tanaka, M. The Relationship Between Water Structure and Blood Compatibility in Poly(2-methoxyethyl Acrylate) (PMEA) Analogues. *Macromol. Biosci*. **2015**, *15*, 1296-1303.
22. Hoshiba, T.; Nemoto, E.; Sato, K.; Orui, T.; Otaki, T.; Yoshihiro, A.; Tanaka, M. Regulation of the Contribution of Integrin to Cell Attachment on Poly(2-Methoxyethyl Acrylate) (PMEA) Analogous Polymers for Attachment-Based Cell Enrichment. *PloS One* **2015**, *10*, e0136066.
23. Hoshiba, T.; Nemoto, E.; Sato, K.; Maruyama, H.; Endo, C.; Tanaka, M. Promotion of Adipogenesis of 3T3-L1 Cells on Protein Adsorption-Suppressing Poly(2-methoxyethyl acrylate) Analogs. *Macromolecules* **2016**, *17*, 3808-3815.

24. Weber, T. W.; Chakravarty, R. K. Pore and solid diffusion models for fixed-bed adsorbers. *Am. Inst. Chem. Eng. J*. **1974**, *20*, 228-238.
25. Kureha, T.; Sato, T.; Suzuki, D. Relationship between Temperature-Induced Changes in Internal Microscopic Structures of Poly(*N*-isopropylacrylamide) Microgels and Organic Dye Uptake Behavior. *Langmuir* **2014**, *30*, 8717-8725.
26. Kureha, T.; Shibamoto, T.; Matsui, S.; Sato, T.; Suzuki, D. Investigation of Changes in the Microscopic Structure of Anionic Poly(*N*-isopropylacrylamide-*co*-Acrylic acid) Microgels in the Presence of Cationic Organic Dyes toward Precisely Controlled Uptake/Release of Low-Molecular-Weight Chemical Compound. *Langmuir* **2016**, *32*, 4575-4585.
27. Lutz, J. F.; Weichenhan, K.; Akdemir, Ö.; Hoth, A. About the Phase Transitions in Aqueous Solutions of Thermoresponsive Copolymers and Hydrogels Based on 2-(2-methoxyethoxy)ethyl Methacrylate and Oligo(ethylene glycol) Methacrylate. *Macromolecules* **2007**, *40*, 2503-2508.
28. Ahmed, Z.; Gooding, E. A.; Pimenov, K. V.; Wang, L.; Asher, S. A. UV Resonance Raman Determination of Molecular Mechanism of Poly(*N*-isopropylacrylamide) Volume Phase Transition. *J. Phys. Chem. B* **2009**, *113*, 4248−4256.

5. Summary

In this thesis, pMEA, pMEA composite microgels, and pMEA-analogue microspheres were used for the selective separation and release of halogen-containing compounds. The delivery and/or removal of halogen-containing compounds is of particular importance in the context of drug delivery or the decontamination of drinking water. For the latter, metallic materials, such as layered double hydroxides (LDHs), are usually employed, even though this method is not without flaws, as the adsorbed halide anions need to be released from the LDHs prior to the reduction of the anions, which is accompanied by a release of chloride anions.

The results of the present study demonstrate a controlled way to separate and release halogen-containing compounds independent of time and locus, using commercially available polymers. Especially noteworthy is the development of a new concept that is based on pMEA and its analogues as the halogen-bonding acceptor. Methoxy and ethoxy groups in the side-chains of the microspheres are suitable for the bonding site to adsorb the targeted halogen compounds. In addition, the side-chains in the pMEA-analogue microspheres exhibit adequate affinity that is selective for organoiodine compounds. As a result, pMEA-analogue microspheres exhibit a high selectivity for the adsorption of iodine-containing compounds in the presence of iodine-free compounds, which is important considering that iodine-containing dyes account for > 90% of all adsorbed dyes.

Moreover, water-immiscible pMEA was incorporated in swollen poly(oligo ethylene glycol methacrylate) hydrogels in order to increase the specific adsorption volume and dispersion stability. Due to the properties of the soft and swellable microgels, it was possible to control the amount of adsorbed halogen-containing compounds that was released, even though the gel network retained the benefits to the solid pMEA components, i.e., stimuli-responsiveness, high dispersion stability, and increase of effective adsorption volume.

The results of the present thesis should be highly attractive for scientists concerned with microgel research, and also for those engaging in applications that include water treatment and medical technologies.

List of Publicatons

1. **Takuma Kureha**, Seina Hiroshige, Shusuke Matsui, Daisuke Suzuki*
"Water-immiscible bioinert coatings and film formation from aqueous dispersions of poly(2-methoxyethyl acrylate) microspheres"
Colloids and Surfaces B: Biointerfaces, Elsevier, 155, pp166-172 (2017)

2. **Takuma Kureha**, Yuichiro Nishizawa, Daisuke Suzuki*:
"Controlled Separation and Release of Organoiodine Compounds using Poly(2-methoxyethyl acrylate)-analogue Microspheres"
ACS Omega, American Chemical Society, 2, pp7686-7694 (2017)

3. **Takuma Kureha**, Daisuke Suzuki*:
"Nanocomposite Microgels for the Selective Separation of Halogen Compounds from Aqueous Solution"
Langmuir, American Chemical Society, 34, pp837-846 (2018)

Other Publicatons

1. Daisuke Suzuki*, Yasuhisa Nagase, **Takuma Kureha**, and Takaaki Sato:
"Internal Structures of Thermosensitive Hybrid Microgels Investigated by Means of Small-Angle X-ray Scattering"
The Journal of Physical Chemistry B, American Chemical Society, 118, pp2194-2204 (2014)

2. **Takuma Kureha**, Takaaki Sato, and Daisuke Suzuki*:
"Relationship between Temperature-Induced Changes in Internal Microscopic Structures of Poly(*N*-isopropylacrylamide) Microgels and Organic Dye Uptake Behavior"
Langmuir, American Chemical Society, 30, pp8717-8725 (2014)

3. Shusuke Matsui, **Takuma Kureha**, Yasuhisa Nagase, Kosuke Okeyoshi, Ryo Yoshida,
Takaaki Sato, and Daisuke Suzuki*:
"Small-angle X-ray Scattering Study on Internal Microscopic Structures of Poly(*N*-isopropylacrylamide-*co*-tris(2,2'-bipyridyl))ruthenium(II) Complex Microgels"
Langmuir, American Chemical Society, 31, pp7228-7237 (2015)

4. Chiaki Kobayashi, Takumi Watanabe, Kazuyoshi Murata, **Takuma Kureha**, and Daisuke Suzuki*:
"Localization of Polystyrene Particles on the Surface of Poly(*N*-isopropylacrylamide-*co*-methacrylic acid) Microgels Prepared by Seeded Emulsion Polymerization of Styrene"
Langmuir, American Chemical Society, 32, pp1429-1439 (2016)

5. **Takuma Kureha**, Takahisa Shibamoto, Shusuke Matsui, Takaaki Sato, and Daisuke Suzuki*:
"Investigation of Changes in the Microscopic Structure of Anionic Poly(*N*-isopropylacrylamide-*co*-Acrylic acid) Microgels in the Presence of Cationic Organic Dyes toward Precisely Controlled Uptake/Release of Low-molecular-weight Chemical Compound"
Langmuir, American Chemical Society, 32, pp4575-4585 (2016)

6. Takumi Watanabe, Chiaki Kobayashi, Chihong Song, Kazuyoshi Murata, **Takuma Kureha**, and Daisuke Suzuki*:
"Impact of Spatial Distribution of Charged Groups in Core Poly(*N*-isopropyl acrylamide)-Based Microgels on the Resultant Composite Structures Prepared by Seeded Emulsion Polymerization of Styrene"
Langmuir, American Chemical Society, 32, pp12760-12773 (2016)

7. Seina Hiroshige, **Takuma Kureha**, Daichi Aoki, Jun Sawada, Daisuke Aoki, Toshikazu Takata*, and Daisuke Suzuki*:
"Formation of Tough Films by Evaporation of Water from Dispersions of Elastomer Microspheres Crosslinked with Rotaxane Supramolecules"
Chemistry - A European Journal, Wiley-VCH, 23, pp8405-8408 (2017)

8. Shusuke Matsui, **Takuma Kureha**, Seina Hiroshige, Mikihiro Shibata, Takayuki Uchihashi* and Daisuke Suzuki*:
"Fast Adsorption of Soft Hydrogel Microspheres on Solid Surfaces in Aqueous Solution" *Angewandte Chemie International Edition*, Wiley-VCH, 56, pp12146-12149 (2017)

9. **Takuma Kureha**, Daichi Aoki, Seina Hiroshige, Keisuke Iijima, Daisuke Aoki, Toshikazu Takata* and Daisuke Suzuki*:
"Decoupled Thermo- and pH-responsive Hydrogel Microspheres Cross-linked by Rotaxane Networks"
Angewandte Chemie International Edition, Wiley-VCH, 56, pp15393-15396 (2017)

10. Haruka Minato, Masaki Murai, Takumi Watanabe, Shusuke Matsui, Masaya Takizawa, **Takuma Kureha*** and Daisuke Suzuki*:
"The Deformation of Hydrogel Microspheres at the Air/Water Interface"
Chemical Communications, Royal Society of Chemistry, 54, pp932-935 (2018)

Reviews

1. 鈴木大介*、**呉羽拓真**
ソフトヒドロゲル微粒子の表面・内部構造と機能」
高分子　高分子科学最新の進歩、65 巻 1 月号、pp30-34 (**2016**)

2. **呉羽拓真**、鈴木大介*
「ヒドロゲル微粒子の微細構造変化と分子内包機能の相関」
色材協会誌、リキッドマーブルとカプセル化技術の進展と応用、89 巻 3 月号、pp70-74 (**2016**)

3. Daisuke Suzuki*, **Takuma Kureha** and Koji Horigome:
"Functional Hydrogel Microspheres"
Encyclopedia of Biocolloid and Biointerface Sciences (Ohshima Ed.),
Wiley Inter. Science, pp554-569 (**2016**) Book ISBN:9781118485590

4. Daisuke Suzuki*, Koji Horigome, **Takuma Kureha**, Shusuke Matsui, and Takumi Watanabe:
"Polymeric hydrogel microspheres: design, synthesis, characterization, assembly and applications"
Polymer Journal, Nature Publishing Group, 49, pp695-702 (**2017**)

Oral Presentation (National conference)

1. **呉羽拓真**、堀込幸司、小林勇志、佐藤高彰、鈴木大介:
「ゲル微粒子界面動電現象の新解釈」
第 17 回高分子ミクロスフェア討論会、東北大学、宮城、11 月　(2012)

2. **Takuma Kureha**, Takaaki Sato and Daisuke Suzuki:
"Electrodynamic Phenomenon of Temperature-responsive Microgels"
62th SPSJ Annual Meeting (Kyoto, Japan) May 30th 2L09 (2013)　口頭英語(1G30)

3. **呉羽拓真**、青木大地、佐藤高彰、鈴木大介
「高分子鎖の形態変化に伴うヒドロゲル微粒子の界面動電現象」
第 62 回高分子討論会、金沢大学、金沢、9 月 13 日　(2013)、発表番号 3I08

4. **呉羽拓真**、青木大地、佐藤高彰、鈴木大介:
「高分子鎖の形態変化に伴うヒドロゲル微粒子の動電挙動」
第 64 回コロイドおよび界面化学討論会、名古屋工業大学、名古屋、9 月 20 日　(2013)、発表番号 3H08

5. **Takuma Kureha**, Takaaki Sato and Daisuke Suzuki:
"Temperature Dependent Behavior Of Hydrogel Particles As Separation Carriers Of Organic Dyes"
63th SPSJ Annual Meeting (Nagoya, Japan) May 29th (2014) oral (2M25)

6. **呉羽拓真**、佐藤高彰、鈴木大介
「小角Ｘ線散乱法による温度応答性ヒドロゲル微粒子の内部微細構造の評価」
第 63 回高分子討論会、長崎大学、長崎、9 月 24 日(2014)、発表番号 1S17

7. **呉羽拓真**、青木大地、佐藤高彰、鈴木大介
「温度応答性ゲル微粒子の内部微細構造と有機染料分離挙動の関係」
第 18 回高分子ミクロスフェア討論会、福井大学、福井、11 月 6 日(2014)、
発表番号 39A　**※学生優秀発表賞受賞**

8. **呉羽拓真**、青木大地、佐藤高彰、鈴木大介
「温度応答性ゲル微粒子の内部微細構造変化と分子分離挙動の関係」
第 26 回高分子ゲル研究討論会、東京大学、東京、1 月 20 日(2015)、発表番号 26

9. **呉羽拓真**、佐藤高彰、鈴木大介
「高分子電解質ゲル微粒子の有機染料分離機能」
第 64 回高分子学会年次大会、札幌コンベンションセンター、札幌、5 月 27 日(2015)、発表番号 1J25

10. **呉羽拓真**、佐藤高彰、鈴木大介
「標的分子が誘起するヒドロゲル微粒子のミクロ構造変化と分子分離特性」
第 64 回高分子討論会、東北大学、宮城、9 月 16 日(2015)、発表番号 2L12

11. **呉羽拓真**、佐藤高彰、鈴木大介
「刺激応答性ゲル微粒子の分子分離挙動とミクロ構造変化の関係」
第 27 回ゲル研究討論会、東京大学、東京、1 月 18 日(2016)、発表番号 12

12. **Takuma KUREHA**、Takaaki SATO、Daisuke SUZUKI
「Impact of Microscopic Structural Changes in Stimuli-responsive Hydrogel Particles on Molecular Separation Behavior」
第 65 回高分子年次大会、神戸国際会議場・展示場、兵庫、5 月 25 日(2016)、
口頭英語、発表番号 1L11

13. **呉羽拓真**、鈴木大介
「選択的分子吸着能を有する血液適合性ナノ粒子複合ゲル微粒子の創製」
第 65 回高分子討論会、神奈川大学、神奈川、9 月 16 日(2016)、発表番号 3W01

14. **呉羽拓真**、広重聖奈、松井秀介、鈴木大介
「血液適合性ポリ(2-メトキシエチルアクリレート)複合ゲル微粒子の特異的な分子分離機能」
第 66 回高分子学会年次大会、幕張メッセ、千葉、5 月 29 日(2017)、発表番号 1H08

15. 呉羽拓真
「刺激応答性ヒドロゲル微粒子の分子分離機能の追求」
第 161 回東海高分子研究会講演会、西浦温泉ホテルたつき、愛知、9 月 2 日(2017)、
※招待講演

16. 呉羽拓真、柴本貴央、酒井嵩匡、鈴木大介
「モデルソフト微粒子を用いた界面動電現象の検討」
第 68 回コロイドおよび界面化学討論会、神戸大学、兵庫、9 月 7 日(2017)、
発表番号 2D09

17. 呉羽拓真、鈴木大介
「ナノコンポジットゲル微粒子の高選択的なハロゲン分子吸脱着特性」
第 68 回コロイドおよび界面化学討論会、神戸大学、兵庫、9 月 6 日(2017)、
発表番号 1F15

18. 呉羽拓真、鈴木大介
「難水溶性ドメインが網目に複合したヒドロゲル微粒子の分子分離機能」
第 66 回高分子討論会、愛媛大学、愛媛、9 月 22 日(2017)、発表番号 3V01

Poster Presentation (National conference)

1. ○呉羽拓真、佐藤高彰、鈴木大介
「体積相転移を示すゲル微粒子の界面動電現象」
第 24 回高分子ゲル研究討論会、東京大学、東京、1 月　(2013)

2. ○呉羽拓真、佐藤高彰、鈴木大介
「刺激応答性ゲル微粒子の界面動電現象」
第 62 回高分子学会年次大会、京都国際会館、京都、5 月 31 日　(2013)、発表番号 3Pc111

3. ○呉羽拓真、青木大地、佐藤高彰、鈴木大介
「形態が変化するヒドロゲル微粒子の界面動電現象」
第 62 回高分子討論会、金沢大学、金沢、9 月 13 日　(2013)、発表番号 3Pd026

4. ○呉羽拓真、青木大地、佐藤高彰、鈴木大介
「形態が変化するヒドロゲル微粒子界面の動電挙動」
第 64 回コロイドおよび界面化学討論会、名古屋工業大学、名古屋、9 月 20 日　(2013)、発表番号 P173

5. ○呉羽拓真、佐藤高彰、鈴木大介
「体積相転移を示すヒドロゲル微粒子の有機染料分離挙動」
第 63 回高分子学会年次大会、名古屋国際会議場、名古屋、5 月 28 日 (2014)、
発表番号 1Ph118

6. ○呉羽拓真、佐藤高彰、鈴木大介
「温度応答性ヒドロゲル微粒子の内部微細構造と機能との関係」
第 63 回高分子討論会、長崎大学、長崎、9 月 25 日(2014)、発表番号 2Pd068

7. ○呉羽拓真、佐藤高彰、鈴木大介
「多刺激応答性ゲル微粒子の内部微細構造と分子分離挙動の関係」
第 64 回高分子学会年次大会、札幌コンベンションセンター、札幌、5 月 27 日(2015)、発表番号 1Pg051

8. ○呉羽拓真、佐藤高彰、鈴木大介
「標的分子存在下におけるヒドロゲル微粒子の微細構造変化と分子分離挙動」
第 153 回東海高分子研究会講演会(2015 年夏季合宿)、サンパーク犬山、愛知、9 月 4 日(2015)、発表番号 P14-D
※東海高分子研究会学生研究奨励賞受賞

9. ○呉羽拓真、佐藤高彰、鈴木大介
「刺激応答性ゲル微粒子の微細構造変化が分子分離機能へ与える影響」
第 64 回高分子討論会、東北大学、宮城、9 月 17 日(2015)、発表番号 3Pc033
※公益社団法人高分子学会優秀ポスター賞

10. ○呉羽拓真、佐藤高彰、鈴木大介
「小角・広角 X 線散乱による高分子ゲル微粒子の微細な網目構造解析」
精密ネットワークポリマー研究会 第 9 回若手シンポジウム、兵庫県立大学、兵庫、
3 月 4 日(2016)、発表番号 P9
※ベストポスター賞

11. ○呉羽拓真、佐藤高彰、鈴木大介
「環境応答性ヒドロゲル微粒子の微細構造変化と標的分子分離能」
第 65 回高分子年次大会、神戸国際会議場・展示場、兵庫、5 月 26 日(2016)、
発表番号 2Pa060

12. ○呉羽拓真、佐藤高彰、鈴木大介
「ヒドロゲル微粒子の内部微細構造と分子分離能の関係」
第 62 回高分子研究発表会(神戸)、兵庫県民会館、兵庫、7 月 15 日(2016)、
発表番号 Pa-30

13. ○呉羽拓真、広重聖奈、青木大地、飯島圭裕、青木大輔、高田十志和、鈴木大介
「架橋点が超分子構造から成るソフトゲル微粒子の創製」
第 157 回東海高分子研究会講演会(岐阜)、長良川観光ホテル石金、岐阜、9 月 2 日(2016)、発表番号 P01-D

14. ○呉羽拓真、鈴木大介
「Poly(2-methoxyethyl acrylate)複合ゲル微粒子の選択的分子吸着挙動」
第 65 回高分子討論会、神奈川大学、神奈川、9 月 16 日(2016)、発表番号 3Pa021

15. ○呉羽拓真、蓬生健介、柴本貴央、鈴木大介
「血液適合性 poly(2-methoxyethyl acrylate)ナノコンポジットゲル微粒子の分子分離能」
第 6 回 CSJ 化学フェスタ 2016、タワーホール船掘、東京、11 月 14 日(2016)、
発表番号 P3-112
※優秀ポスター発表賞

16. ○呉羽拓真、蓬生健介、柴本貴央、鈴木大介
「ヒドロゲル微粒子のミクロ構造が分子分離能に与える影響」
第 28 回高分子ゲル研究討論会、東京大学、東京、1 月 16 日(2017)、発表番号 P13

17. ○呉羽拓真、鈴木大介
「血液適合性ナノ粒子複合ゲル微粒子の分子分離挙動」
第 28 回高分子ゲル研究討論会、東京大学、東京、1 月 16 日(2017)、発表番号 P14
※優秀ポスター賞

18. ○**呉羽拓真**、広重聖奈、松井秀介、鈴木大介
「生体不活性な難水溶性ポリマー複合ヒドロゲル微粒子の選択的な低分子内包挙動」
第 66 回高分子学会年次大会、幕張メッセ、千葉、5 月 30 日(2017)、発表番号 2Pe067

19. ○**呉羽拓真**、鈴木大介
「難水溶性ナノドメイン複合ゲル微粒子の創製と分子分離機能」
第 68 回コロイドおよび界面化学討論会、神戸大学、兵庫、9 月 8 日(2017)、
発表番号 P128

20. ○**呉羽拓真**、鈴木大介
「疎水性／親水性ポリマーコンポジット微粒子の分子内包・放出挙動」
第 66 回高分子討論会、愛媛大学、愛媛、9 月 22 日(2017)、発表番号 3Pa075

21. ○**呉羽拓真**、鈴木大介
「ハロゲン結合能を有するナノコンポジットゲル微粒子の分子分離機能」
平成 29 年度高分子ゲル研究会ゲルワークショップ、愛媛大学、愛媛、9 月 22 日(2017)、発表番号 No.19

Oral Presentation (International conference)

1. **Takuma Kureha** and Daisuke Suzuki:
"Synthesis of Poly (2-methoxyethyl acrylate)-based Hydrogel Particles for Bio-Coatings and Carriers"
253rd ACS National meeting & Exposition, COLL 694, (San Francisco) April 5th (2017)

2. **Takuma Kureha** and Daisuke Suzuki:
"Hydrogel Microspheres for Selective Separation of Halogen Compounds"
255th ACS National meeting & Exposition, COLL, (New Orleans) March 22nd (2018)

Poster Presentation (International conference)

1. ○**Takuma Kureha** and Daisuke Suzuki:
"Electrodynamic Phenomenon of Thermo-responsive Microgels"
ICBS2013 (Tsukuba, Japan) Mar (2013)

2. ○**Takuma Kureha**, Takaaki Sato and Daisuke Suzuki:
"Internal Microscopic Structures of Thermosensitive Hydrogel Particles"
Polymer Networks Group Meeting & Gel Symposium 2014 (Tokyo, Japan) November 12th (2014) Poster (PST11c)

3. ○**Takuma Kureha**, Takaaki Sato and Daisuke Suzuki:
"Relationship between Temperature-Induced Changes in Internal Structures of Hydrogel Particles and Low Molecular Uptake Behavior"
The 3rd International Symposium on Dynamical Ordering of Biomolecular Systems for Creation of Integrated Functions (Mie, Japan) January 10th (2015) Poster (P010)

4. ○**Takuma Kureha**, Takaaki Sato and Daisuke Suzuki:
"Microscopic Structural Changes in Hydrogel Particles in the presence of Target Molecules investigated by Small- and Wide-Angle X-ray Scattering"
The 4th International Symposium on Dynamical Ordering of Biomolecular Systems for Creation of Integrated Functions (Fukuoka, Japan) November 22th (2015) Poster (P093)

5. ○**Takuma Kureha**, Shusuke Matsui, Takahisa Shibamoto, Takumi, Watanabe, Takaaki Sato and Daisuke Suzuki:
"Small-angle X-ray scattering studied on thermoresponsive microgels"
PACHIFICHEM2015 (Hawaii, USA) December 17th (2015) Poster (MACR 585)

6. ○**Takuma Kureha** and Daisuke Suzuki:
"Investigation of Changes in the Microscopic Structure of Hydrogel Microspheres toward Controlled Uptake/Release of Functional Molecular"
3rd International Conference on Biomaterials Science (Tokyo, Japan) November 28-30th (2016) Poster(P109)

7. ○**Takuma Kureha** and Daisuke Suzuki
"Poly(2-methoxyethyl acrylate) Composite Hydrogel Microspheres for Bio-Coating and Carriers"
The 5th International Symposium on Dynamical Ordering of Biomolecular Systems for Creation of Integrated Functions (Tokyo, Japan) January 21th (2017) Poster (P069)

8. ○**Takuma Kureha** and Daisuke Suzuki:
"Selective Adsorption of Halide Compounds from Aqueous Solution by Poly(2-methoxyethyl acrylate)-based Hydrogel Microspheres"
11th internatinal Gel Symposium (Chiba, Japan) March 7th (2017) Poster (F-4)
***Soft Matter Awards**

Patent

1. 鈴木大介、**呉羽拓真**
「高分子粒子およびその製造方法」
特願 2016-162554、出願日 8 月 23 日 (**2016**)

Awards

1. 第 18 回高分子ミクロスフェア討論会　**学生優秀発表賞** (2014 年)
2. 第 153 回東海高分子研究会講演会　**東海高分子研究会学生研究奨励賞** (2015 年)
3. 第 64 回高分子討論会　**公益社団法人高分子学会優秀ポスター賞** (2015 年)
4. 第 9 回シンポジウム精密ネットワークポリマー研究会　**優秀ポスター賞** (2016 年)
5. 第 6 回 CSJ 化学フェスタ　**優秀ポスター発表賞** (2016 年)
6. 第 28 回高分子ゲル研究討論会　**優秀ポスター賞** (2017 年)
7. 11th International Gel Symposium　**RSC Soft Matter Awards** (2017 年)
8. 第 27 回日本 MRS 年次大会　**奨励賞** (2017 年)

6. Acknowledgements

First of all, I would like to express my sincerest gratitude and appreciation to my supervisor Prof. Dr. Daisuke Suzuki (Shinshu University) for all the kind help and support, as well as for introducing me to the world of science as a researcher. The opportunities that he has offered me, including a research visit to the RWTH Aachen (Germany), are invaluable. I would also like to express my utmost respect for Prof. Suzuki, who embodies the phrase "*discoveries are buried deeply*", which has motivated me to pursue science at a very high level. Overall, it is difficult to express my appreciation in words.

I would also like to thank Prof. Dr. Naoki Asao (Shinshu Univ.), Prof. Dr. Mizuo Maeda (Shinshu Univ.; RIKEN), Prof. Dr. Hiroshi Moriwaki (Shinshu Univ.), Prof. Dr. Yoshitake Akiyama (Shinshu Univ.), and Prof. Dr. Shinichi Yusa (Univ. of Hyogo) for the examination of this thesis and the corresponding discussions.

Moreover, I would like to thank Prof. Dr. Walter Richtering (RWTH Aachen) for accepting my research visit (04/05 2015). In his group, I have learned a lot on how to grow as a researcher.

I would also like to thank Prof. Dr. Toshikazu Takata and Prof. Dr. Daisuke Aoki (Tokyo Institute of Technology) for the fruitful discussions and their assistance regarding rotaxane cross-linkers.

Furthermore, I would like to extend my gratitude to Emeritus Prof. Haruma Kawaguchi (Keio Univ.), Prof. Dr. L. A. Lyon (Georgia Instit. of Technology), Prof. Dr. Mitsuhiro Shibayama (Tokyo Univ.), Prof. Dr. Hiroyuki Ohshima (Tokyo Univ. of Science), Prof. Dr. Kenji Urayama (Kyoto Instit. of Technology), Prof. Dr. Takamasa Sakai (Tokyo Univ.), Prof. Dr. Syuji Fujii (Osaka Instit. of Technology), Prof. Dr. Takashi Miyata (Kansai Univ.), Prof. Dr. Akifumi Kawamura (Kansai Univ.), Prof. Dr. Takaaki Sato (Shinshu Univ.), Prof. Dr. Kosuke Okeyoshi (Japan Advanced Instit. of Science and Technology), Prof. Dr. Haruyuki Ishii (Tohoku Univ.), Prof. Dr. Yukiya Kitayama (Kobe Univ.) and Prof. Dr. Michinari Kohri (Chiba Univ.) for useful discussions on gel and colloid science.

I am most thankful for financial support from a JSPS Research Fellowship for Young Scientists (15J11533) and from the Interdisciplinary Graduate School of Science and Technology (Shinshu Univ.).

Of course, I cannot miss the opportunity to thank the Suzuki lab members, who have always influenced me positively and contributed to a great working atmosphere in the lab and to my daily life. I wish all the Suzuki lab members many more successful years to come.

Finally, I would like to thank my family Hiroaki, Mika, Megumi, and Taiyou. Thank you for everything you have done for me; I can never thank you enough.

Takuma Kureha